

Towards fundamental understanding of interlaminar ply delamination growth under mode II and mixed-mode loading

Amaral, Lucas

DOI

[10.4233/uuid:1e20169a-6179-47f8-b70d-452cd3e11460](https://doi.org/10.4233/uuid:1e20169a-6179-47f8-b70d-452cd3e11460)

Publication date

2018

Document Version

Final published version

Citation (APA)

Amaral, L. (2018). *Towards fundamental understanding of interlaminar ply delamination growth under mode II and mixed-mode loading*. [Dissertation (TU Delft), Delft University of Technology].
<https://doi.org/10.4233/uuid:1e20169a-6179-47f8-b70d-452cd3e11460>

Important note

To cite this publication, please use the final published version (if applicable).
Please check the document version above.

Copyright

Other than for strictly personal use, it is not permitted to download, forward or distribute the text or part of it, without the consent of the author(s) and/or copyright holder(s), unless the work is under an open content license such as Creative Commons.

Takedown policy

Please contact us and provide details if you believe this document breaches copyrights.
We will remove access to the work immediately and investigate your claim.

Towards fundamental understanding of
interlaminar ply delamination growth under
mode II and mixed-mode loading

Dissertation
for the purpose of obtaining the degree of doctor
at Delft University of Technology
by the authority of the Rector Magnificus, Prof.dr.ir. T.H.J.J. van
der Hagen
Chair of the Board for Doctorates
to be defended publicly on
Tuesday 16 October 2018 at 10:00 o'clock
by

Lucas AMARAL

Master of Science in Mechanical Engineering,
Universidade Federal do ABC,
born in São Bernardo do Campo, Brazil

This dissertation has been approved by the promotor

Composition of the doctoral committee:

Rector Magnificus
Dr. ir. R. C. Alderliesten
Prof. dr. ir. R. Benedictus

Chairperson
Delft University of Technology
Delft University of Technology

Independent members:
Prof.dr.ir. S. van der Zwaag
Prof. Dr. G. Pinter
Prof.dr.ir. L. E. Govaert
Dr. A.J. Brunner
Dr. C. Kassapoglou

Delft University of Technology
University of Leoben, Austria
University of Twente, Netherlands
Empa, Switzerland
Delft University of Technology



The fear of the Lord is the beginning of wisdom, and knowledge of the Holy One is understanding

Proverbs 9:10, New International Version

SUMMARY

In a context of many studies addressing delamination growth in laminated composites, this thesis provides understanding of the underlying physics of this phenomenon. The models currently used to assess delamination growth are phenomenological in nature and rely almost solely on curve fittings and experimental data. These empirical models are used to predict delamination growth rather than aid in understanding it.

This lack of knowledge on the physics of delaminations causes problems for both academia and industry. From the perspective of academia, science needs to be built upon fundamental understanding. However, this is currently not the case for delamination growth. Phenomenological trends, for which the reasons are not yet clear, are assumed as fact, and science tries to advance building on these trends. Meanwhile, from the perspective of industry, engineers compensate for the lack of fundamental understanding with conservativeness, overdesign and a great amount of tests, yielding extra costs.

Therefore, the present thesis seeks to understand the fundamentals of delamination growth by physically characterising it. This characterisation is performed relating the strain energy dissipated in delamination growth with the delamination growth rate and the damage mechanisms encountered on the fracture surfaces. To this aim, carbon-epoxy unidirectional laminated specimens were manufactured and tested under mode II and mixed-mode static and fatigue loading. Fracture surfaces were analysed on a Scanning Electron Microscope, and the damage mechanisms were identified and correlated to the strain energy dissipated.

The actual strain energy dissipated in crack growth was observed to depend heavily on fracture and not on the loading condition per se (static or fatigue loading). The Strain Energy Release Rate (SERR) for fatigue and quasi-static loading conditions were correlated. The lower limit is given by the SERR under fatigue loading at low crack growth rates, while the upper limit is given by the SERR under quasi-static fracture.

For mode II delaminations, damage was observed to propagate ahead of the main crack tip in a process zone, which dissipates energy that should be accounted for when characterizing delamination growth. Therefore, the definition of a crack tip should be redefined in mode II delamination growth. This was also observed to be the case for mixed-mode delaminations under 80% of mode II loading.

Furthermore, for mixed-mode delaminations, no dependence on the displacement ratio was observed when relating crack growth rate and energy dissipation per cycle under a given mode mixity. The importance of the damage mechanisms acting in fracture was highlighted once more. What causes a delamination extension under a specific loading mode to consume more energy per area of crack created are the different damage and dissipation mechanisms that might be activated under certain loading parameters.

When relating different loading modes (I, II and mixed-mode I/II), the Strain Energy Density (SED) was found to be a key parameter. The onset of crack growth occurs when the SED in the vicinity of the crack tip reaches a critical value. This critical SED for the onset of crack growth is constant and independent of the loading mode. Hence, it gives a physical basis for a relationship between the onset of crack growth under different loading modes.

In conclusion, strain energy dissipation and damage mechanisms acting in fracture were found to be the key parameters when characterising delamination growth. The physical characterisation of mode II and mixed-mode delamination under static and fatigue loading enabled developing better understanding of these phenomena. More research will be necessary to properly define the magnitude of fracture including the damage on the process zone. Besides, the hypothesis that this critical SED also defines the observed fatigue threshold in delamination growth should be tested.

SAMENVATTING

Binnen de context van vele studies naar delaminatiegroei van gelamineerde composieten, biedt deze thesis begrip van de onderliggende fysica van dit fenomeen. De modellen die momenteel worden gebruikt om delaminatiegroei te beoordelen zijn fenomenologisch van aard en steunen bijna volledig op het trekken van curven door data en experimentele data. Deze empirische modellen worden gebruikt om delaminatiegroei te voorspellen in plaats van bij te dragen aan het begrijpen ervan.

Dit gebrek aan kennis betreffende de fysica van delaminaties zorgt voor problemen voor zowel de academische wereld als de industrie. Vanuit het perspectief van de academische wereld moet wetenschap worden gebaseerd op fundamenteel begrip. Echter, dit is momenteel niet het geval voor delaminatiegroei. Fenomenologische trends, waarvoor de redenen nog onduidelijk zijn, worden als feit aangenomen en wetenschap probeert verder te ontwikkelen gebaseerd op deze trends. In de tussentijd, vanuit industrie bezien, compenseren ingenieurs voor het gebrek aan fundamenteel begrip met conservatisme, overdimensioneren en veel testwerk, wat zorgt voor extra kosten.

De huidige thesis streeft er derhalve naar om de grondbeginselen van delaminatiegroei te begrijpen door deze fysische te karakteriseren. Deze karakterisering is uitgevoerd door het relateren van de gedissipeerde rek-energie bij delaminatiegroei aan de delaminatiegroeisnelheid en de schademechanismen aanwezig op het scheuroppervlak. Om dit te bereiken werden koolstof-epoxy unidirectionele gelamineerde proefstukken geproduceerd en getest in modus II en in gecombineerde belastingmodi onder statische en cyclische belasting. Scheuroppervlakken werden geanalyseerd met een elektronenmicroscopie en de schademechanismen werden geïdentificeerd en gecorreleerd aan de gedissipeerde rekenergie.

De werkelijke rek-energie gedissipeerd gedurende de scheurgroei, bleek sterk af te hangen van het breukproces en niet van de belastingconditie als zodanig (statische of cyclische belasting). The Strain Energy Release Rate (SERR) voor cyclische en quasi-statische belastingcondities werden gecorreleerd. The ondergrens is gegeven door de SERR van cyclische belasting bij lage scheurgroeisnelheden, terwijl de bovengrens is gegeven door de SERR behorende bij quasi-statische breuk, wat de grootste SERR geeft.

Voor delaminaties onder modus II belasting, werd waargenomen dat schade voor het hoofd scheurfront uit groeit waarbij energie dissipeert, waarmee rekening moet worden gehouden bij het karakteriseren van delaminatiegroei. Daarom dient de definitie voor een scheurfront geherdefinieerd te worden bij modus II belasting. Hetzelfde werd waargenomen voor delaminaties onder gecombineerde belastingmodi bij 80% modus II belasting.

Verder werd er voor delaminaties bij combineerde belastingmodi geen afhankelijkheid van de verplaatsingsratio waargenomen bij het relateren van de scheurgroeisnelheid en de energiedissipatie per cyclus onder een bepaalde combinatie van belastingmodi. Het belang van de bij breuk actieve schademechanismen werd nogmaals onderstreept. De oorzaken van een verhoogde energieconsumptie per eenheid van toegenomen scheuroppervlak bij delaminatiegroei onder een bepaalde belastingwijze zijn de verschillende schade- en dissipatiemechanismen die geactiveerd zouden kunnen worden onder bepaalde belastingparameters.

Bij pogingen om verschillende belastingmodi (I, II en gecombineerd I/II) te relateren bleek de Strain Energy Density (SED) een bepalende parameter. De aanvang van scheurgroei vindt plaats wanneer de SED in de buurt van het scheurfront een kritieke waarde bereikt. Deze kritische SED voor de aanvang van scheurgroei is constant en onafhankelijk van de belastingwijze. Vandaar dat het een fysische basis geeft voor een relatie tussen de aanvang van scheurgroei onder verschillende belastingmodi.

Samenvattend, dissipatie van rek-energie en bij breuk actieve schademechanismen werden bepalend geacht bij het karakteriseren van delaminatiegroei. De fysische karakterisering van delaminatie in modus II en gecombineerde belastingmodi onder statische en cyclische belasting maakt meer begrip van deze fenomenen mogelijk. Meer onderzoek zal nodig zijn om de omvang van breuk inclusief schade in de proceszone goed te definiëren. Daarnaast dient de hypothese dat deze kritische SED ook de geobserveerde ondergrens van delaminatiegroei onder cyclische belasting definieert te worden getest.

Contents

1	Introduction	17
1.1	Composite materials and the aerospace industry	18
1.2	Fatigue delamination growth and the similitude principle	19
1.3	Scope of the thesis	20
1.4	Outline	21
1.5	References	21
2	SERR in Quasi-static and Fatigue Delamination Growth	23
2.1	Introduction	24
2.2	Problem Statement.....	24
2.3	Hypotheses	25
2.3.1	Analysing quasi-static data as low-cycle fatigue data	25
2.3.2	da/dN versus dU/dN : a physical SERR	26
2.3.3	The SERR and the fracture surfaces.....	27
2.3.4	The micro and the macro scales in the context of the present thesis 28	
2.4	Data integration	29
2.5	Linking quasi-static and fatigue SERR	32
2.6	Conclusions	39
2.7	References	40
3	Energy dissipation in mode II crack growth.....	43
3.1	Introduction	44
3.1.1	Problem Statement.....	44
3.1.2	Hypothesis	45
3.2	Methodology.....	45
3.2.1	Static and fatigue set-up	45
3.2.2	Phased-Array	48
3.2.3	Acoustic Emission	48

3.3	Results and Discussion	49
3.3.1	Phased-Array: estimating the crack tip position	49
3.3.2	Process zone detection in quasi-static crack-growth	50
3.3.3	The similitude problem solved: using the physical SERR G^*	52
3.3.4	Compliance Calibration	61
3.4	Conclusions	62
3.5	References	63
4	Mixed-Mode fatigue delamination growth	65
4.1	Introduction	66
4.1.1	Problem Statement and Research Objectives	67
4.2	Methodology.....	68
4.2.1	Relating applied work to energy dissipation	68
4.2.2	The Mixed-Mode Bending Test	70
4.2.3	Material and specimen preparation.....	70
4.2.4	Calculating the physical SERR G^*	73
4.3	Results and Discussion	74
4.3.1	Process zone effects on mode II dominated fracture	75
4.3.2	Effects of applied maximum displacement on delamination growth 79	
4.3.3	Damage mechanisms: the key for understanding energy dissipation in fatigue delamination growth.....	82
4.3.4	Breakage and pull-out of bridging fibres: changing the damage mechanisms	84
4.3.5	The “stress ratio effect”	86
4.4	Conclusion.....	88
4.5	References	88
5	A physics-based relationship for crack growth under different loading modes 91	
5.1	Introduction	92

5.1.1	Motivation	92
5.1.2	Objectives	93
5.1.3	Methodology.....	93
5.2	Hypotheses	93
5.2.1	Fracture and Energy.....	93
5.2.2	Saint-Venant's principle	94
5.2.3	Pure mode I fracture	95
5.3	Rail Shear Tests	95
5.4	The critical Strain Energy Density	96
5.4.1	Isotropic Materials	96
5.4.2	Orthotropic Materials	98
5.4.3	Strain Energy Density and Potential energy in the system	100
5.5	Results and Discussion	101
5.5.1	Brittle Isotropic Materials.....	101
5.5.2	Orthotropic Composite Laminates.....	104
5.5.3	The fundamental relationship between pure mode I and pure mode II crack growth	115
5.6	Conclusions	119
5.7	References	119
6	Conclusions and recommendations	123
6.1	Conclusions	124
6.1.1	Quasi-static and fatigue delamination growth	124
6.1.2	The influence of process zone in mode II strain energy dissipation	124
6.1.3	Effect of mode mixities and loading parameters in energy dissipation.....	124
6.1.4	A physics-based relationship between different fracture modes ..	125
6.1.5	General conclusions.....	125
6.2	Recommendations	126

Epilogue.....	127
Acknowledgements	129
Curriculum Vitae	131
List of Publications.....	133

Nomenclature

A	Delamination area [m^2]
a	delamination length [m]
V	Volume [m^3]
$w_i(V)$	Strain energy evaluated in an arbitrary volume [J]
s_i	critical strain energy density that causes the onset of crack growth [J/m^2]
\mathcal{G}	Shear modulus [GPa]
G_i	Strain Energy Release Rate [J/m^2]
E	Elastic modulus [GPa]
K_i	Stress Intensity Factor [$\text{Pa}\cdot\text{m}^{1/2}$]
P	Potential energy per unit volume [J/m^3]
U	Strain Energy per unit volume [J/m^3]

Acronyms

SED	Strain Energy Density
SIF	Stress Intensity Factor
SERR	Strain Energy Release Rate
ENF	End-Notch Flexure
DCB	Double Cantilever Beam
MMB	Mixed-Mode Bending

Greek symbols

ν	Poisson's ratio
-------	-----------------

θ_0 Angle at which the Strain Energy Density reaches a minimum value

Subscripts

crit Critical

i=I, II, III, I/II Crack opening mode

SED Value calculated using the SED approach

experimental Value obtained via experiments

ENF Value obtained via End-Notch Flexure specimens

min minimum

max maximum

on onset

1 Introduction

1.1 Composite materials and the aerospace industry

Laminated composites are attractive for aerospace applications because of their high specific strength and stiffness [1]. This makes composites a potential lighter alternative to the traditional aluminium structures in aircraft. A lighter aircraft would reduce fuel consumption and enlarge the efficiency of the flight, bringing potential environmental and economic advantages. An example of the use of composite materials in aircraft is the Boeing 787, which is 50% composite by weight. Figure 1.1 highlights, in black, the composite parts manufactured from carbon fibre laminates.

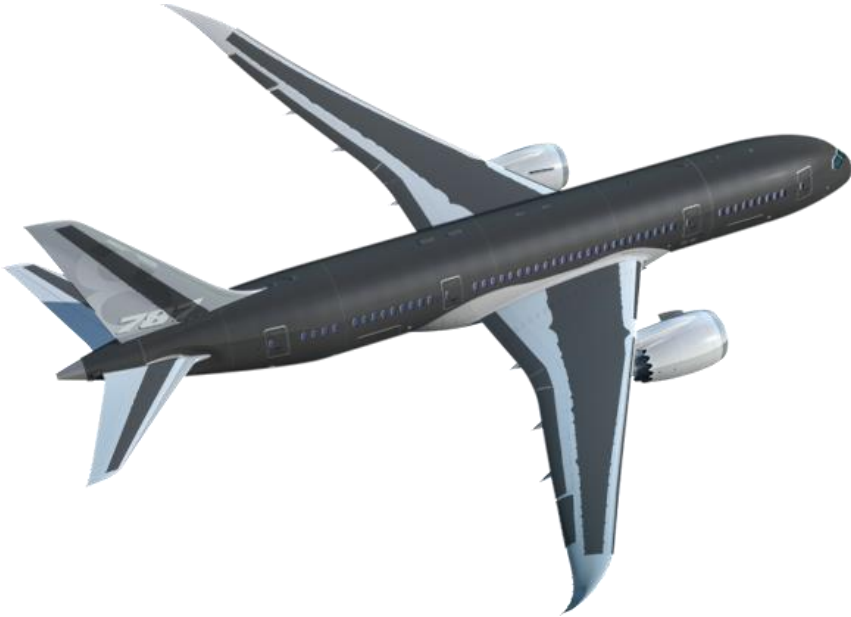


Figure 1.1. Boeing 787 is 50% composite material by weight – the parts in black are carbon fibre laminates [2]

However, laminated composites have poor interlaminar strength, which makes them susceptible to delaminations. Delamination is the most observed damage mode in laminated composites [3], and it is defined as decohesion of plies or lamina, under tensile peel loading, shear loading or combinations thereof. This phenomenon was often observed to initiate due to stress concentrations at material discontinuities such as illustrated in Figure 1.2, or at locations of impact damage due to, for example, tool drop during maintenance [4, 5].

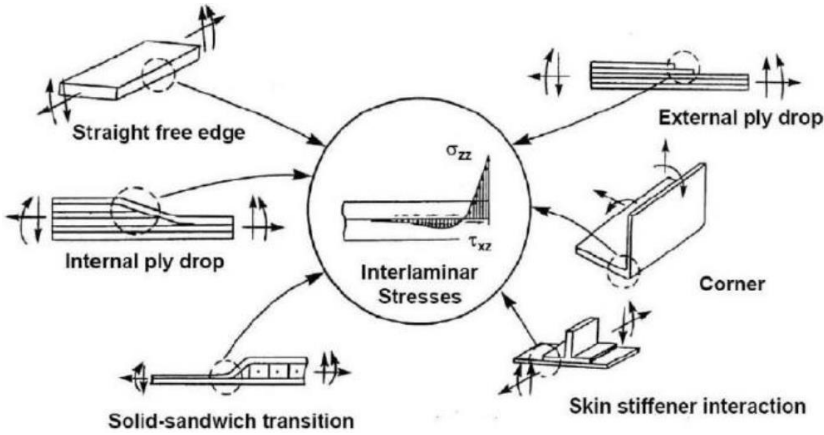


Figure 1.2. Example of sources of interlaminar stresses (reproduced from [6])

The models currently used to assess fatigue delamination growth are phenomenological in nature and not based on the physics of the problem. They rely almost solely on curve fittings of experimental data [7]. These empirical models do provide input for engineering applications, but they do not provide understanding of the phenomena and the parameters of influence. This leads to a vast amount of data and empirical models, without progressing the understanding on the fracture phenomena and principles. Because of this, certification of composite structures for aircraft is primarily based on full scale component testing rather than on in-depth and physics-based evaluation and prediction methodologies. In addition, due to this lack of fundamental knowledge of the physics underlying delamination growth and the scatter usually observed on composites data, composite structures in aircraft, as well as metals, are overdesigned in order to safeguard the structural integrity of the airplane [8, 9]. Such an overdesign hampers further weight reductions, decreasing the advantages of using composite structures in aircraft.

Besides, academia has been performing science based on these phenomenological models, which were not developed for that purpose. Therefore, understanding the underlying physics of fatigue delamination growth is necessary for building knowledge on this topic on solid foundations. This might set the path towards reliably designing lighter load-bearing composite structures for aircraft.

1.2 Fatigue delamination growth and the similitude principle

Delaminations can grow under quasi-static or fatigue loading. When considering delamination growth under fatigue loading, no agreement has been reached on which parameter should be used to describe similitude appropriately [7, 8]. Some authors use the maximum Strain Energy Release Rate (SERR) G_{\max} [10], while others prefer the SERR range $\Delta G = G_{\max} - G_{\min}$ [11], although $\Delta\sqrt{G} = (\sqrt{G_{\max}} - \sqrt{G_{\min}})^2$ was discussed as a parameter that would correctly apply the similitude principle [8, 12]. None of these parameters, however, describes uniquely a load cycle, which also leads to the observation of an artificial stress ratio dependence [7]. Furthermore, these parameters describe an artificial SERR that can be calculated even when there is no crack growth. This concept of

SERR has been developed assuming fixed grip conditions, which do not apply under fatigue loading [13].

Notable in this context is the work performed in [13-17], in which a physical SERR, derived from the crack extension and based on physical principles, is used to characterize fatigue crack growth. This approach focuses on characterising fatigue crack growth according to the work input in the structure and the actual strain energy dissipated in crack growth. The use of this physical SERR has enabled a better understanding of the physics underlying fatigue delamination and disbond growth under mode I fatigue loading. Furthermore, the use of the physical SERR enabled the correlation of the damage mechanisms encountered on the fracture surfaces with the actual energy dissipated in the process.

Given the relatively successful characterization of mode I crack growth based on strain energy dissipation, the same approach should be employed to characterize mode II and mixed-mode (I/II) delamination growth. Once this characterization is established, a physics-based relationship between different loading modes should be uncovered. This will enable a deeper understanding of the physics behind delamination growth in composites, setting the path towards reliable, physics-based prediction models. Physics-based prediction models might then lead to less over-designed composite structures and lighter aircraft.

1.3 Scope of the thesis

The aforementioned lack of fundamental understanding on delamination growth is a drawback in the optimal use of laminated composites in aircraft structures. Although literature shows a vast amount of empirical prediction models, there is very little understanding on the physical principles of delamination growth. It is not uncommon to find studies filled with unexplained phenomena and, sometimes, contradicting results, which are discussed in further chapters. Since the physics of mode I delamination growth could be characterized through an energy-based approach, the main research question addressed in this thesis is:

How can delamination growth under mode II and mixed-mode (I/II) loading in unidirectional composites be characterized through an energy-based approach?

Considering this main research question, the following sub-questions are also addressed in the present thesis:

- What is the relation between the energy dissipation in quasi-static and fatigue delamination growth?
- What is the influence of the process zone ahead of the crack tip in the strain energy dissipated in mode II fatigue delamination?
- What are the effects of different mode mixities and loading conditions to energy dissipation in delamination growth?
- What is the physics-based relationship between different fracture modes?

1.4 Outline

Chapter 2 presents a discussion on the relationship between delamination growth under quasi-static and fatigue loading. Energy dissipation and the influence of a fracture process zone in delamination growth under mode II fatigue loading are discussed in Chapter 3. Chapter 4 discusses the effects of different mode mixities and loading parameters in delamination growth. A physics-based relationship for delamination growth under different loading modes is presented in Chapter 5. Chapter 6 presents a discussion on the importance of understanding the underlying principles of delamination growth, and chapter 7 summarises the conclusions of this thesis.

1.5 References

- [1] Khan R. Delamination Growth in Composites under Fatigue Loading [PhD Thesis]. Delft: Delft University of Technology; 2013.
- [2] Boeing. <http://www.boeing.com/commercial/787/by-design/#/advanced-composite-use>. 2017.
- [3] Hojo M, Ando T, Tanaka M, Adachi T, Ochiai S, Endo Y. Modes I and II interlaminar fracture toughness and fatigue delamination of CF/epoxy laminates with self-same epoxy interleaf. *International Journal of Fatigue*. 2006;28:1154-65.
- [4] Alderliesten RC. Towards structural fatigue evaluation in composite structures. *JEC Composites Magazine* 2012. p. 46 - 50.
- [5] Azouaoui K, Rechak S, Azari Z, Benmedakhene S, Laksmi A, Pluvineau G. Modelling of damage and failure of glass/epoxy composite plates subject to impact fatigue. *International Journal of fatigue*. 2001;23:877-85.
- [6] Krueger R. Computational fracture mechanics for composites. State of the art and challenges, NAFEMS Nordic seminar: prediction and modelling of failure using FEA, Copenhagen/Roskilde, Denmark 2006.
- [7] Pascoe JA, Alderliesten RC, Benedictus R. Methods for the prediction of fatigue delamination growth in composites and adhesive bonds - A critical review. *Engineering Fracture Mechanics*. 2013;112-113:72-96.
- [8] Jones R, Kinloch AJ, Hu W. Cyclic-fatigue crack growth in composite and adhesively-bonded structures: The FAA slow crack growth approach to certification and the problem of similitude. *International Journal of Fatigue*. 2016;88:10-8.
- [9] Jones R, Kinloch A, Michopoulos J, Brunner AJ, Phan N. Delamination Growth in Polymer-Matrix Fibre Composites and the Use of Fracture Mechanics Data for Material Characterisation and Life Prediction. *Composite Structures*. 2017.
- [10] Roderick GL, Everett RA, Crews Jr JH. Debond Propagation in Composite Reinforced Metals. Hampton, VA: NASA; 1974.
- [11] Mostovoy S, Ripling EJ. Flaw Tolerance of a Number of Commercial and Experimental Adhesives. In: Lee L-H, editor. *Adhesion Science and Technology*. New York: Plenum Press; 1975. p. 513-62.
- [12] Rans C, Alderliesten RC, Benedictus R. Misinterpreting the results: How similitude can improve our understanding of fatigue delamination growth. *Composites Science and Technology*. 2011;71:230-8.
- [13] Alderliesten RC. How proper similitude can improve our understanding of crack closure and plasticity in fatigue. *International Journal of Fatigue*. 2016;82, Part 2:263-73.
- [14] Pascoe JA, Alderliesten RC, Benedictus R. Towards Understanding Fatigue Disbond Growth via Cyclic Strain Energy. *Procedia Materials Science* 2014;3 (ECF-20):610-5.

- [15] Pascoe JA, Alderliesten RC, Benedictus R. On the relationship between disbond growth and the release of strain energy. *Engineering Fracture Mechanics*. 2015;133:1-13.
- [16] Yao L, Alderliesten RC, Zhao M, Benedictus R. Discussion on the use of the strain energy release rate for fatigue delamination characterization. *Composites Part A: Applied Science and Manufacturing*. 2014;66:65-72.
- [17] Yao L, Alderliesten R, Benedictus R. Interpreting the stress ratio effect on delamination growth in composite laminates using the concept of fatigue fracture toughness. Submitted to *Composites: Part A*. 2015.

2 SERR in Quasi-static and Fatigue Delamination Growth

This work proposes to use an average Strain Energy Release Rate (SERR) to characterize fatigue and quasi-static delamination growth with the same method. Mode I quasi-static and fatigue tests were performed. The quasi-static crack extension was considered as a low-cycle fatigue process, discretized to different levels and its energy dissipation was correlated to the energy dissipation under fatigue. Fracture surfaces were analysed and damage mechanisms were related to average SERRs for each case. The strain energy released in crack extension showed to be dependent on the decohesion mechanisms, and it is demonstrated how the values of the SERR for fatigue and quasi-static loading can be linked through physical principles.

2.1 Introduction

The appropriate similitude parameter that should be used for the assessment of fatigue delamination is still under discussion [1]. Amongst the propositions in literature, some authors propose obtaining an actual SERR from measured data only, and not from a theoretical model. The procedure consists in measuring during a fatigue test the crack length a , the displacement δ , the force P and the number of cycles N . With these data it is possible to obtain a graph, plotting da/dN versus dU/dN , where U is the potential strain energy, defined as $U=1/2P\delta$. In this presentation of the data, the SERR dU/dA is obtained from the inverse of the slope of the curve that connects the origin and each data point, defined by Equation (2.1), where b is the width of the specimen. It is notable that this procedure is based on an energy balance, and it accounts for the stress ratio in its definition, often collapsing fatigue curves for different stress ratios [2-5].

$$G^* = \frac{1}{b} \frac{dU/dN}{da/dN} = \frac{dU}{dA} \quad (2.1)$$

In general, fatigue and quasi-static delamination growth are evaluated with different methods. For quasi-static delamination growth, the SERR is calculated just before the crack propagates [6]. This value is generally referred to as the onset value G_{on} . Meanwhile, fatigue delamination is usually assessed through the relation of a SERR based parameter (G_{max} , ΔG or $\Delta\sqrt{G}$) with da/dN , or via delamination resistance curves [7-15]. Although several studies have performed both quasi-static and fatigue tests [16-21], a clear relation between what is done for both loading conditions does not seem to be available. Moreover, although the energy balance introduced by Griffith [22] proposed a release of strain energy per unit area of crack independently of the load, the SERR parameter that is used nowadays to assess crack extension seems to be regarded as being dependent on the loading condition.

2.2 Problem Statement

The question that arises is where do these quasi-static and fatigue SERR definitions meet? These different approaches to assess fatigue and quasi-static delamination complicate the establishment of a correlation between the energy released by crack growth in both loading conditions. Moreover, some authors [10] normalize the SERR used to characterise fatigue delamination data with a critical SERR calculated from quasi-static tests. This seems to imply that there is a straightforward correlation between the crack growth resistance in fatigue and in quasi-static loading. However, the exact nature of such correlation has not been established yet. Thus, the questions that need to be answered are: what are the differences in the energy dissipation in delamination growth in quasi-static and fatigue loading, and to which mechanisms should such differences be attributed?

For that reason it is proposed here to analyse the quasi-static data with the same procedure as proposed in [3], described by Equation (2.1). Assessing both quasi-static and fatigue delamination data with the same procedure may shed light on how these parameters of similitude may correlate. Thus, the objective of this study is to correlate quasi-static and fatigue loading using identical energy balance principles. To this end, the difference in the energy released in both fatigue and quasi-static loading conditions is characterised and related to fracture surfaces observed with microscopy.

2.3 Hypotheses

2.3.1 Analysing quasi-static data as low-cycle fatigue data

A schematic load-displacement curve is shown in Figure 2.1 (a) for a typical mode I quasi-static test performed on a CFRP double cantilever beam (DCB) specimen in displacement controlled conditions, according to ASTM D5528-01 standard [6]. In this illustration, Point 1 represents the conditions just before the test starts. When the applied force P is increased to a critical value, Point 2, crack growth occurs, which under displacement control condition causes a decrease in the applied force. The system is thus taken to Point 3, because the machine keeps imposing a displacement upon the test specimen and the crack propagation is not perfectly continuous. Subsequently, there is additional work applied to the specimen with the test machine, which increases the applied force P once more. In the illustration this is represented by moving from Point 3 to Point 4. This incremental decrease in force by crack extension and increase in force by application of additional work to the specimen is repeated continuously in a gradual negative slope of the curve. In this regard it is important to note that for different materials the load-displacement curve may be different. Particularly, the alternation seen in these experiments between increase and decrease in load, during quasi-static crack extension, may be attributed to the slip-stick phenomenon observed in toughened composites. Nevertheless, the energy dissipation during quasi-static crack extension can still be compared to the unit crack growth observed in the test specimen in a consistent manner.

Therefore, the quasi-static test seems to allow representation of the data as low-cycle fatigue behaviour. For example, each drop and increase in the load can be considered a cycle N , and a strain energy release dU can be associated with each N , as illustrated in Figure 2.1 (b).

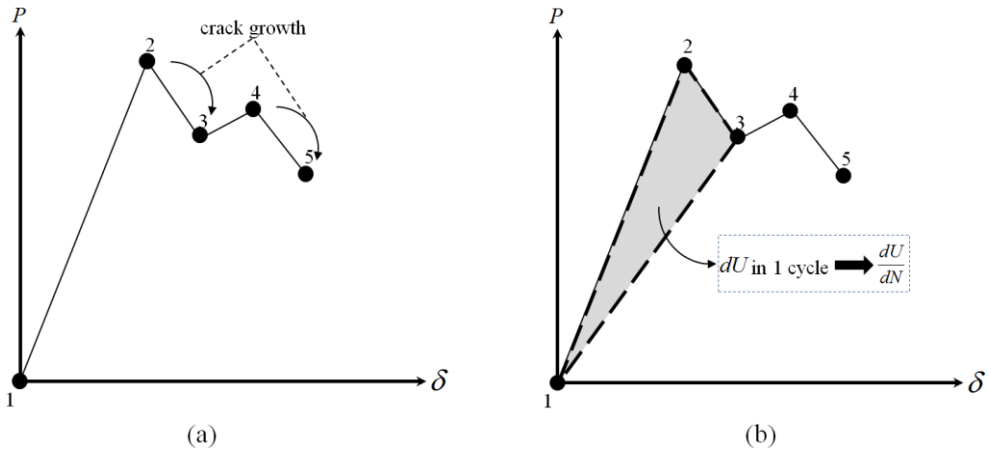


Figure 2.1. (a) Illustration of a quasi-static force-displacement curve and (b) determination of dU in a quasi-static test increment

2.3.2 da/dN versus dU/dN : a physical SERR

Such as introduced in Section 2.1, measuring the crack length a , the displacement δ , the force P and the number of cycles N allows to plot a graph between the crack growth rate and the change in strain energy with the number of cycles: da/dN versus dU/dN . Fatigue data has been shown to align approximately linearly in this type of presentation of data, under different stress ratios [2, 3]. Suppose a straight line is fit to this data in a linear scale, such as illustrated in Figure 2.2. The SERR of a crack extension is obtained by Equation (2.1). Therefore, the crack extension can be characterized by a single physical parameter, the average SERR over the cycle, G^* . One should note that G^* is a parameter of a different nature than G_{\max} and ΔG . The maximum SERR and the SERR range describe a theoretical energy release that can be calculated even if there is no crack extension. If there was no crack extension, what SERR are we calculating? Meanwhile, G^* is a parameter that describes the energy released by crack growth and is calculated from crack extensions.

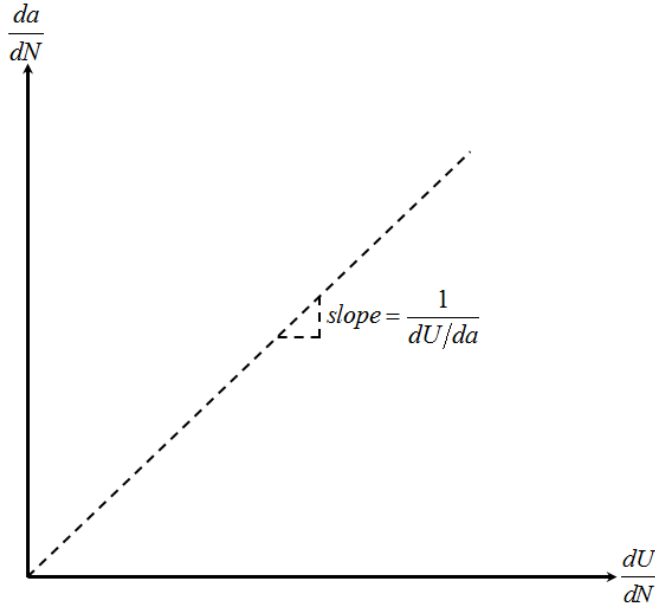


Figure 2.2. da/dN versus dU/dN : illustration of a straight line adjusted to the data in a linear scale

The basic assumption in the da/dN versus dU/dN plot is that when data are aligned along the same slope in a linear plot, this means they have the same release of strain energy per crack increment, dU/da . Thus, the same amount of energy dissipation corresponds to the same amount of crack growth or crack surface.

Regarding this point, it is worth noting that the physical SERR works as a fundamental parameter to characterize delamination growth and not as a prediction model. This means that the physical SERR is used to characterize delamination growth behaviour, but not to predict it. Prediction models, based on G_{\max} , ΔG or $\Delta\sqrt{G}$ give an estimation of the crack

growth rate for a given load cycle, but they do not explain crack growth, as they do not have a physics-based theory behind them. Meanwhile, a fundamental theory allows the understanding of crack propagation based on physical principles, but does not necessarily allow the prediction of the crack growth rate. Therefore, once this fundamental theory is formulated, efforts shall be directed to developing prediction models based on this theory.

In addition, the reader should note that in Equation (2.1), the crack length a is not a continuous function. The crack extends on a given discrete moment. After that, the crack might stay for cycles without any observed growth. In a similar manner, the number of cycles N is also not continuous. Instead, the number of cycles is an integer. Therefore, one might argue that the derivatives in Equation (2.1) are only valid for continuous functions. However, the concept in Equation (2.1) for d/dN is an average over the time scale. This is a simplification. The complete physical description of the problem would require the derivatives to be taken in relation to time, d/dt , through the entire cycle. Nevertheless, d/dN is used as an engineering simplification of the crack growth problem.

Furthermore, considering another simplifying assumption that the composite material used in this study presents neither relevant plasticity nor other significant energy dissipation mechanisms, any curve adjusted to the data in the da/dN versus dU/dN plot is assumed to go through the origin, because it is deemed impossible to dissipate energy without extending a crack. Other energy dissipation mechanisms such as vibration of the loading fixture, friction unrelated with crack growth or specimen heating were not considered, once none of these energy dissipation mechanisms were observed during the tests.

2.3.3 The SERR and the fracture surfaces

The energy released per unit area in crack growth is related to the amount of damage created. Decohesion implies breaking bonds, which requires energy. If more decohesion happens, more energy is released per unit area. Thus, the fracture surface generated in a crack extension and the strain energy released during this crack extension are related. Therefore, as data aligned on the same slope in the da/dN versus dU/dN plot present the same amount of energy dissipation per area, they are expected to present similar fracture surfaces as well. Any clear differences in the fracture surfaces, such as rougher or smoother features, would indicate a change in the damage state.

A change in the damage state indicates that more, or less energy, is consumed during crack surface extension. This would be equivalent to data located on a different trend in the da/dN versus dU/dN plot. Fracture surfaces obtained from quasi-static and fatigue mode I crack extensions usually present as characteristic features: matrix cleavage, fibre imprints, fibre bridging, broken fibres and shear cusps [23]. Each one of these features is considered to contribute with the release of energy during crack extension. Thus, the fracture surfaces that present more of these features are expected to relate with higher values of dU/dA . In case of the comparison between two fracture surfaces with the same damage features, for example presenting only fibre imprints, the roughness of the fracture surface is expected to relate to the energy release.

As an example consider Figure 2.3, which illustrates a straight line that fits linearly a set of data. Data located to the right of this straight line would represent crack extensions that consumed more energy per crack area, and are thus expected to present rougher fracture

surfaces or more damage features. Data located to the left of this straight line would represent crack extensions that consumed less energy per crack area, assumed equivalent to smoother fracture surfaces or less damage features.

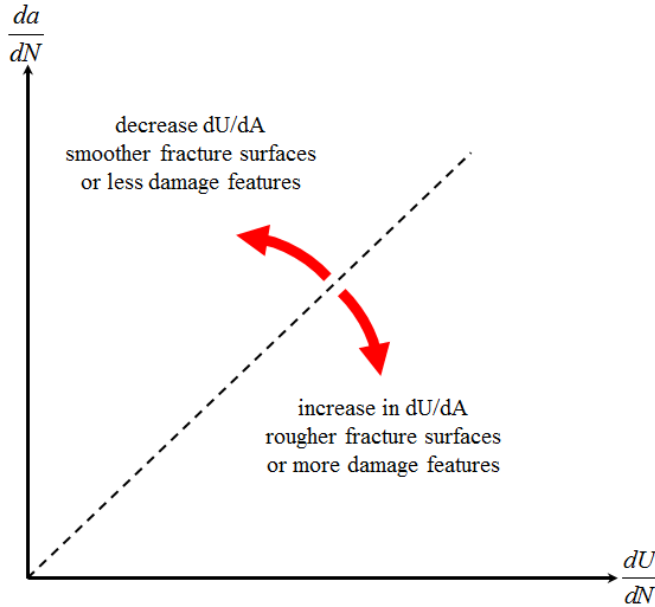


Figure 2.3. Illustration of linear fit. Data to the right of the fit consumed more energy per crack area

2.3.4 The micro and the macro scales in the context of the present thesis

The present thesis discusses, in the current and following chapters, the connection between the micro-mechanisms acting in fracture and the macroscopic description of delamination. Literature fails to give a proper description of what exact size micro and macro mechanisms actually refer to. Therefore, this section aims at providing a semi-quantitative qualification of macro and microscopic damage within the context of this thesis.

From a qualitative perspective, macroscopic damage refers to damage that can be observed by naked eye or with the help of a simple video camera, such as macroscopic crack propagation. Meanwhile, microscopic damage refers to damage which is difficult or not possible to be observed by the naked eye, requiring the use of microscopes. An example of such damage is the formation of cracks in the process zone, discussed in further chapters. In order to quantify these damage descriptions within this thesis' context, consider microscopic damage to be of the order of 200 μm of length. For the macroscopic damage growth, a crack length of the order of 0.5 mm or larger is considered.

2.4 Data integration

Five mode I quasi-static tests were performed in CFRP DCB specimens. All test specimens were unidirectional and manufactured from the same material batch (M30SC-150-DT 120-34 F) with 32 layers. A 13 μm Polytetrafluoroethylene (PTFE) film was used as initial crack. The tests were reported in [2, 24].

Each of the five sets of quasi-static data was discretized in order to calculate dU/dN . This discretization was performed as illustrated in Figure 2.4 (a), in which each shaded area is considered a dU in one cycle. Because the quasi-static data is treated as a low-cycle fatigue, each shaded area in Figure 2.4 (a) can then be considered a dU/dN .

As an outcome of this discretization, a cloud of points was obtained when plotting the results in terms of da/dN versus dU/dN . This is shown by the blue markers in Figure 2.5. The average of these points, in da/dN and dU/dN , resulted in one point in the graph plotting da/dN versus dU/dN , shown by the red marker in Figure 2.5. However, this result is not enough to enable full understanding of the trend of dU/da with respect to an increasing da/dN , because a single data point contains no information on the slope. In which fashion would this point move if da/dN was increased or decreased?

Thus, analysing the same data with different discretization levels was necessary. Therefore, in order to analyse the trend of the data properly, each of the five sets of data was discretized in four different levels. The data was discretized to different levels, considering different number of cycles for the same crack growth, such as illustrated in Figure 2.4 (a) to (d). In Figure 2.4 (a), for example, 3 cycles were considered, and thus 3 values of dU/dN and da/dN were calculated. Meanwhile, the exact same crack was considered to be grown in 6 cycles in Figure 2.4 (b), resulting in 6 values of dU/dN and da/dN . In each of these integrations what differs is the step da in crack growth that is used to calculate dU/dN . In this illustration each shaded area limited by dashed lines represents a dU/dN . In Figure 2.4 (b) and (c), for example, the steps da are smaller than in Figure 2.4 (a). Meanwhile, in Figure 2.4 (d), the step in da is bigger than in Figure 2.4 (a).

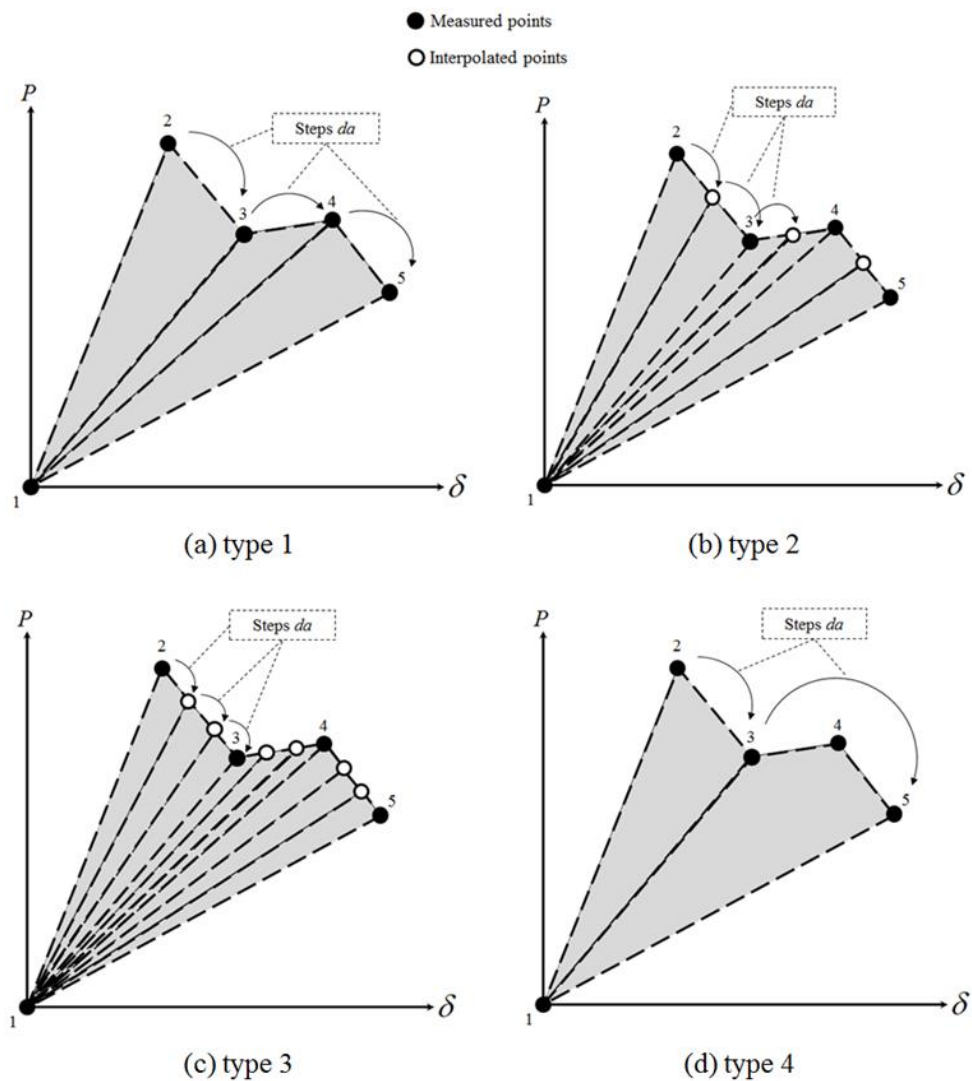


Figure 2.4. Integration of the quasi-static data as low-cycle fatigue data – each shaded area delimited by dashed lines is considered a dU/dN

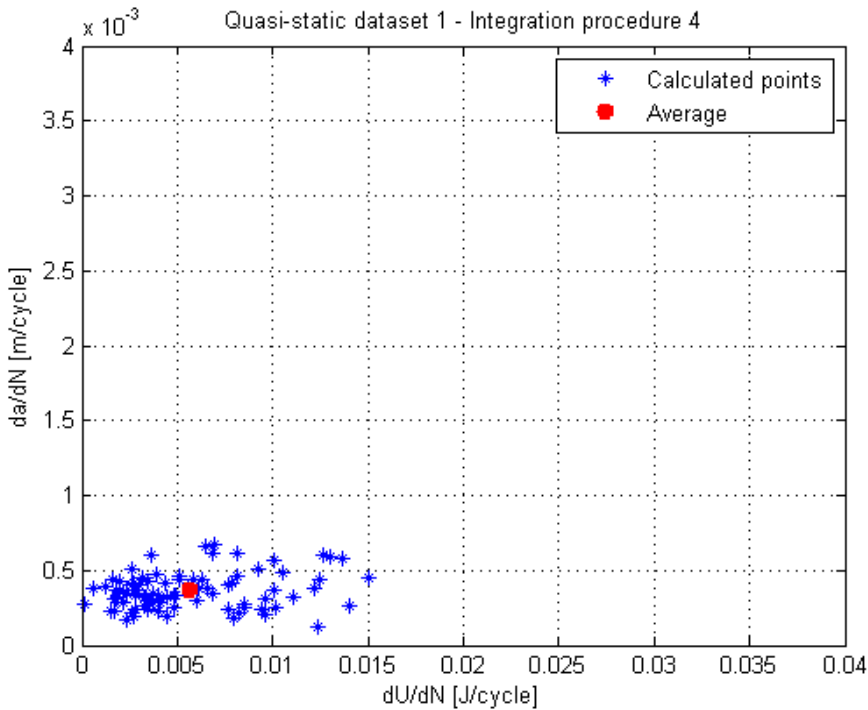


Figure 2.5. Quasi-static dataset 1: the blue markers show the points that resulted from the integration procedure 4, and the red marker shows the average

It is important to note that, although each set of data is discretized at four different levels, each set still represents the same crack extension. In other words, the fracture surface and the energy spent in creating this fracture surface quasi-statically is the same, independently of the way dU/dN was calculated. This is observed by the fact that all integration procedures, for a given test specimen, yield the same value for the sum of the individuals dU/dN . This can be easily observed in Figure 2.4: the sum of the shaded areas always results the same total area. This shows that the procedure is consistent, because the total energy spent in extending the crack is the same for a given dataset.

Therefore, the average values of dU/dN and da/dN were calculated with these discretization procedures and plotted together. Data obtained from five specimens were discretized in four different increments, yielding 20 points in the da/dN versus dU/dN plot. These points were plotted together, and a linear regression was used to produce the best linear fit by the minimization of the sum of the square of the error. The result, presented in Figure 2.6, shows a good correlation (i.e. coefficient of determination $R^2 = 0.9894$). This graph shows that a quasi-static test can be analysed as low-cycle fatigue in a consistent manner, and the SERR can be easily calculated from the slope of the linear fit, which is $1/(dU/da)$. Therefore, the actual SERR in the mode I quasi-static fracture is given by Equation (2.2).

$$G_{quasi-static}^* = 611.6 \text{ J} / \text{m}^2 \quad (2.2)$$

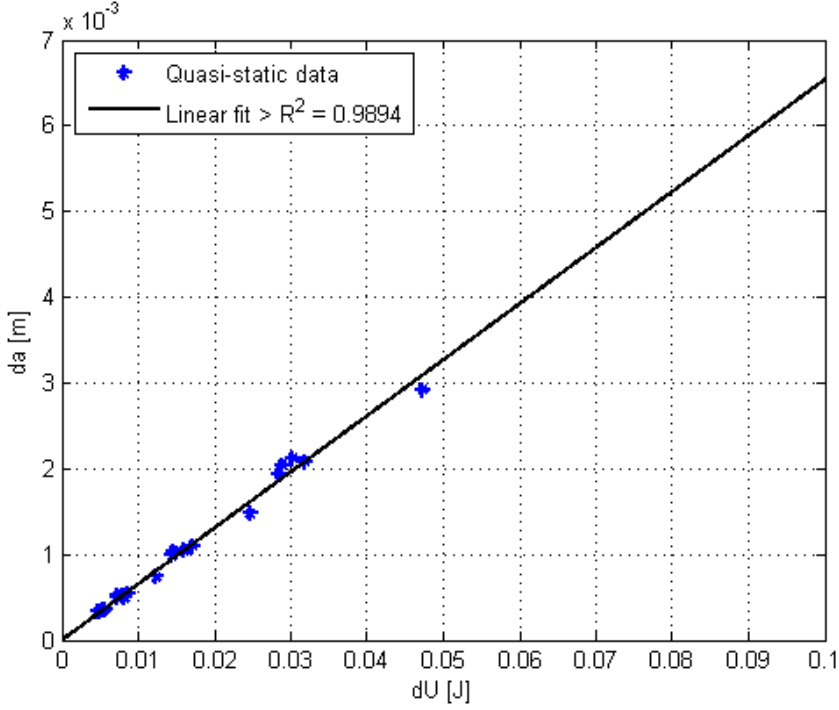


Figure 2.6. Linear fit through the average values of dU/dN and da/dN obtained by the integration of the 5 sets of data with 4 different procedures

2.5 Linking quasi-static and fatigue SERR

Considering the quasi-static test as a low-cycle fatigue has the advantage of enabling the presenting of data from both fatigue and quasi-static tests in the same format, i.e. the da/dN versus dU/dN plot. In this plot the SERR can be easily calculated from the slope of the curve, as explained in the previous section for the quasi-static SERR. It is important to note that with this procedure a real physical SERR is obtained directly from measured data and not from a theoretical model [3].

Fatigue tests were performed at three stress ratios (0.1, 0.5 and 0.7) on DCB specimens made from the same material and with the same dimensions as the ones used in the quasi-static tests. These were reported in [2].

The fatigue data is also fitted by a linear function in a da/dN versus dU/dN plot. Figure 2.7 (a) shows the plot of both quasi-static and fatigue linear fits. The common procedure at this moment would be to fit both fatigue and quasi-static datasets with the same linear function. However, as explained in Section 2.3.3, the functions that fit the data must start at

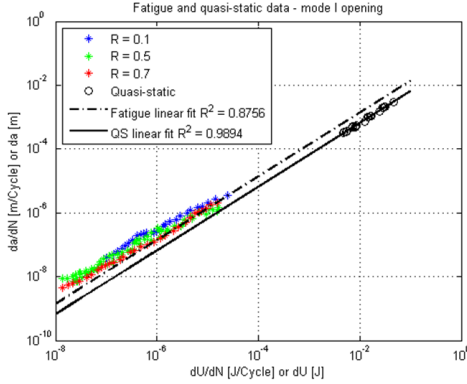
the origin of axes, because it is deemed impossible to dissipate energy without extending a crack.

In Figure 2.7 it is notable that the quasi-static data is shifted to the right of the fatigue data. This indicates more energy is dissipated per area in the quasi-static crack growth. In other words, less energy is required for the same amount of crack growth in fatigue than under quasi-static loading. A reason for this lower energy dissipation during fatigue crack growth may be attributed to the frequent change in the local delamination fronts under repeated cycles, so that the crack growth takes the least resistant path. Thus, it can be argued that growing a crack in fatigue is more efficient than growing it quasi-statically, as it is shown by Equation (2.4).

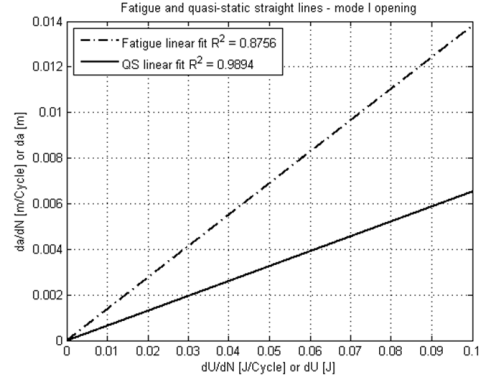
In addition, this difference in the energy released during crack extension implies that different mechanisms of decohesion contributed to the energy dissipation, as seen in Figure 2.8. Scanning Electron Microscopy (SEM) was performed after the tests, and the results are reported here. The fracture surface corresponding to the fatigue loading presents less damage features than the quasi-static one, resulting in less energy consumption per crack extension, i.e. smaller dU/dA . This is shown in Figure 2.8 (b). The main features visible on the fracture surface of the fatigue specimen are fibre imprints and cusps. Although cusps are typical features of mode II crack extension, they are commonly observed in mode I fracture surfaces and they occur due to the local shear induced by fibres being pulled from the surfaces during crack opening [23].

Meanwhile, the fracture surface that is the result of quasi-static crack extension, shown in Figure 2.8(a), presents broken fibres, matrix cleavage, fibre imprints and cusps. The fibre-bridging process plays an important role in the energy consumption in crack extension and, consequently, in the fracture surface appearance. For the tests performed, fibres would bridge throughout several different crack growth rates. However, it was observed that at low values of da/dN these bridging fibres do not break. Therefore, as they remain in their elastic behaviour, there is no energy release [2]. Meanwhile, at large values of da/dN , going towards the quasi-static failure, the bridging fibres break, releasing energy. Thus, the broken fibres and the matrix cleavages are the reason for the higher energy consumption in quasi-static crack extension. These decohesion mechanisms explain why the quasi-static crack extension requires a larger dU/dA .

The crack growth resistance is not the same under fatigue and quasi-static loading conditions, as shown in Figure 2.7 (b). However, normalising the fatigue SERR by a SERR obtained quasi-statically is still possible, if this normalisation is performed with parameters obtained by identical energy balance principles. G_{\max} and G_{on} , or G_{crit} for the case of the maximum SERR at quasi-static failure, are different parameters that do not describe the same physical process. Meanwhile, the average SERR G^* is an identical parameter for both quasi-static and fatigue crack extensions, and allows such normalisation.

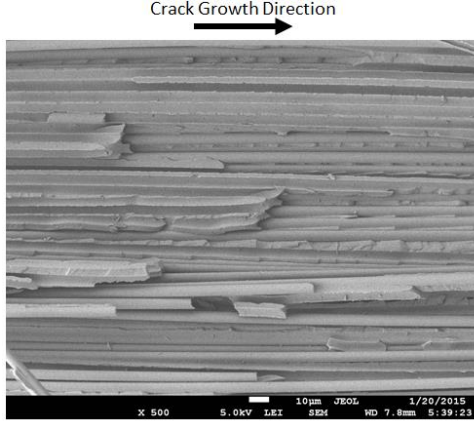


(a) log scale plot



(b) Linear scale plot

Figure 2.7. Relation between fatigue and quasi-static conditions: (a) log scale and (b) linear scale



(a) Quasi-static fracture surface

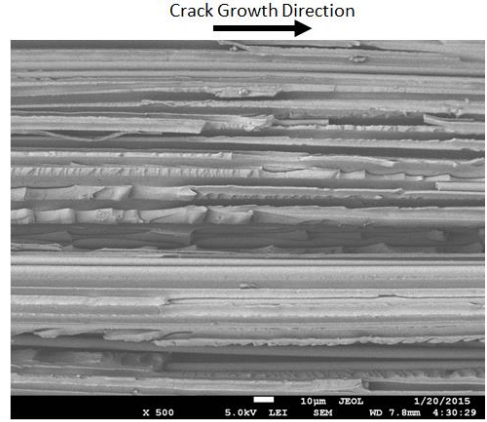
(b) Fatigue fracture surface
 $da/dN = 10^{-6} \text{ m/cycle}$

Figure 2.8. Quasi-static and fatigue fracture surfaces: roughness pattern

Characterising the difference in the energy released in quasi-static and fatigue loading allows the calculation of the actual SERR for each case. From the linear fit of the fatigue data it is possible to calculate that:

$$G_{fatigue}^* = 289.7 \text{ J} / \text{m}^2 \quad (2.3)$$

$$\frac{G_{quasi-static}^*}{G_{fatigue}^*} = 2.1 \quad (2.4)$$

Equation (2.4) shows that to extend a crack by a unit area dA in fatigue releases approximately half the strain energy to extend a crack by the same dA quasi-statically. This

shows there is crack growth in fatigue at values of SERR lower than the critical SERR calculated in quasi-static tests. Therefore, one should not just fit a single curve through both fatigue and quasi-static datasets, but characterise the offset from fatigue to quasi-static crack extension from an energy point of view, taking into account the damage mechanisms associated with the fractured material.

The linear slope of the fatigue fit seems to correlate to lesser extent with the data at low values of da/dN . As it is observed in Figure 2.9, the points are slightly shifted to the left of the theoretical straight line. This indicates that less energy was released per crack extension under fatigue loading at low values of da/dN . Thus, a smoother fracture surface is expected to be obtained from these data points. This suggests the release of strain energy during fatigue crack growth is not really constant. This is discussed further in the work of Yao et al. [25] and in Chapter 4 of the present thesis.

The fracture surfaces generated under fatigue loading at low values of crack growth rate are shown in Figure 2.10 (a). When fracture surfaces obtained at a low crack growth rate are compared with fracture surfaces obtained at a high crack growth rate one observes a difference in the roughness pattern. The fracture surfaces at low crack growth rates are smoother, and present basically fibre imprints as the main features. Meanwhile, the fracture surfaces at higher crack growth rates, where the linear fit presents a better correlation with the data, are rougher and present more damage features, such as fibre-imprints and cusps. Therefore, the difference in the SERR due to the mechanism of cusps formation, at higher values of da/dN , causes fatigue data to correlate to lesser extent with the linear fit at low values of crack growth rate.

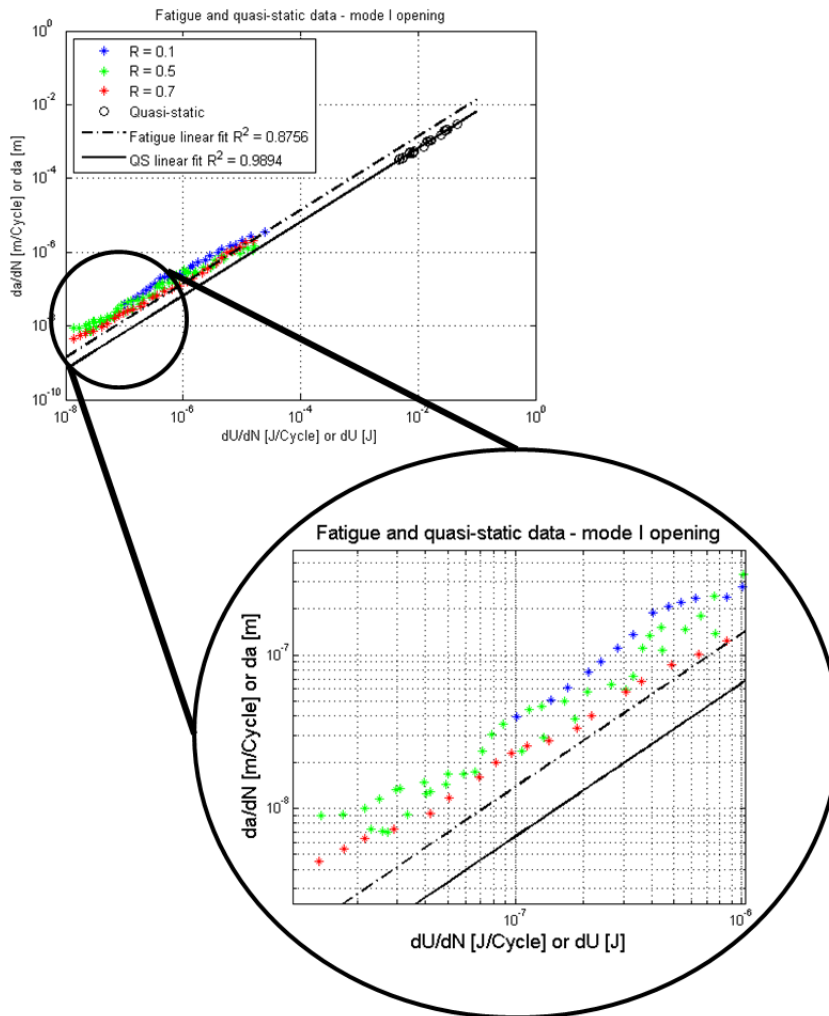


Figure 2.9. Fatigue data at lower crack growth rate: less energy spent due to non-damaged fibre bridging

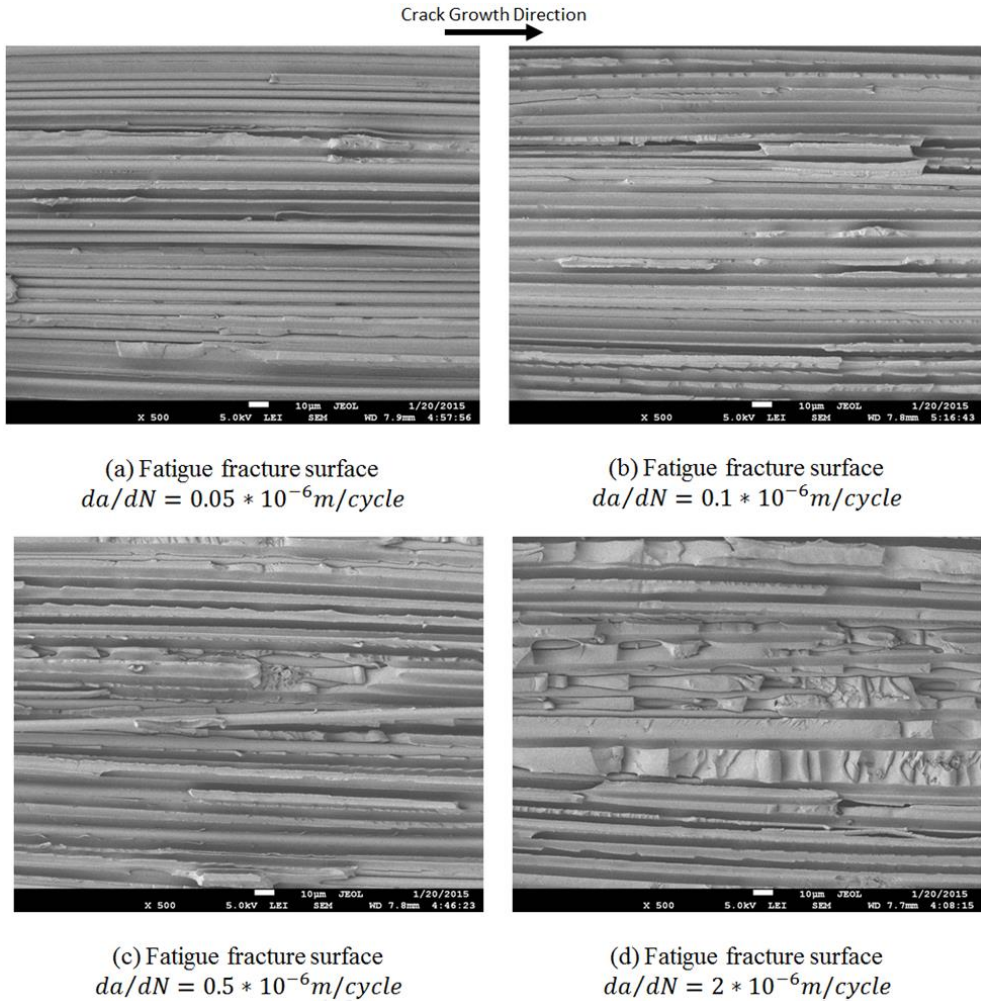
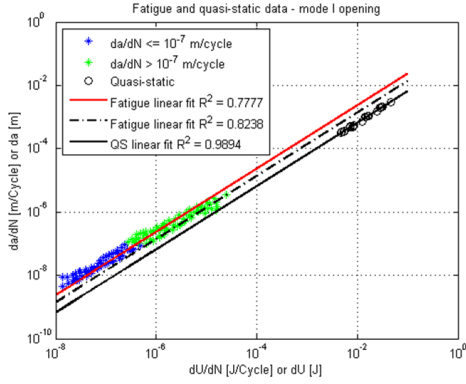


Figure 2.10. Fracture surfaces at different crack growth rates. Roughness and number of damage features increase for higher crack growth rates da/dN , indicating larger energy release

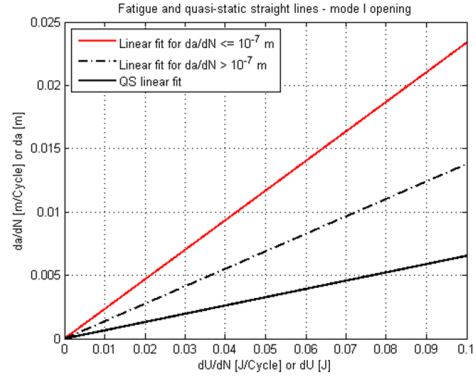
Following this trend, the fatigue data was then divided into two groups, according to similarities encountered on their fracture surfaces. Data below a crack growth rate around $10^{-7} m/cycle$ presented similar smooth fracture surfaces, dominated by fibre imprints, as in Figure 2.10 (a) and (b). Data above this crack growth rate presented similar rough fracture surfaces, dominated by features as fibre imprints and cusps, as in Figure 2.8 (b) and Figure 2.10 (c) and (d).

Data with a crack growth rate below $10^{-7} m/cycle$ can be fitted by a different linear function, as shown in Figure 2.11. The data with a crack growth rate above $10^{-7} m/cycle$ can still be fitted by the same linear function as before. Therefore, from the linear fit in Figure 2.11 (b), the SERR for the fatigue data with crack growth rates below $10^{-7} m/cycle$ is given by Equation (2.5).

$$G^*_{\frac{da}{dN} \leq 10^{-7} \text{ m/cycle}} = 171.2 \text{ J / m}^2 \quad (2.5)$$



(a) log scale plot



(b) Linear scale plot

Figure 2.11. Relation between fatigue and quasi-static loading conditions: divided fatigue data - (a) log scale and (b) linear scale

From the analyses of the SEM pictures it becomes obvious that the energy released by a crack extension relates to the roughness pattern and the damage features that appear on the fracture surface. This is shown in Figure 2.12. This picture brings together the fracture surfaces presented in this work, starting from the smoother in Figure 2.12 (a), at low crack growth rates, and increasing in the number of fractographic features until the quasi-static fracture surface, shown in Figure 2.12 (f). It is observed that mode I crack extensions start with cohesive fracture and smooth fracture surfaces, and other features as cusps, fibre breakage and matrix cleavage appear as the crack growth rate increases towards a quasi-static failure. The decohesion mechanisms of fibre breakage and matrix cleavage, encountered on the quasi-static fracture surface, are the dominant energy dissipation mechanisms.

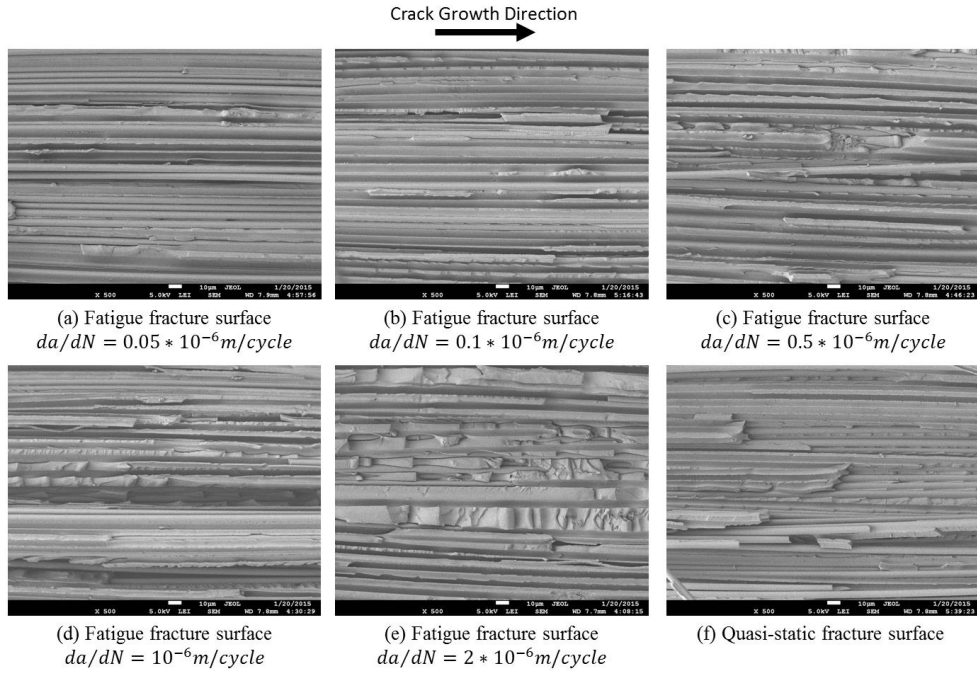


Figure 2.12. Fracture surfaces: from the smoother to the rougher - an indication of the energy released

The fatigue data may, indeed, be divided in other intermediate groups, according to small differences encountered in their fracture surfaces. Although these groups of data may be fitted with higher coefficients of determination, they will follow a pattern of increasing roughness with increasing crack growth rate, until a new microscopic feature can be observed on the fracture surface.

2.6 Conclusions

Quasi-static data was consistently treated as low-cycle fatigue, which allowed a comparison between mode I crack extensions in fatigue and quasi-static loading. A real physical SERR can be consistently obtained from a da/dN versus dU/dN plot, for both loading conditions. The average SERR over a cycle, G^* , obtained by energy balance principles, can be used to characterise fatigue and quasi-static crack extensions. The SERR range or the maximum SERR are parameters that do not maintain the similitude principle. Although these parameters can give a crude estimation of the crack growth rate that is expected from a certain load, for materials where the relation with the crack growth rate was established, the discussion about which of them should be used can be misleading. They do not describe uniquely the load cycle and are not based on the physics of the problem. Thus, once the physical SERR describes the crack growth as a basis theory, efforts shall now be directed to developing a prediction model based on this theory.

Furthermore, the SERR depends on the damage state of the fracture surface. Therefore, the energy released during crack growth is a characteristic of the damage mechanisms observed on the fracture surface, and not of the loading condition. The values of the SERR for

fatigue and quasi-static loading conditions can be linked. The lower limit is given by fatigue loading at low da/dN values, which present the lowest SERR and, consequently, the smoother fracture surfaces. As the crack growth rate increases, the damage mechanism starts to change, and more energy is released in fracture. The upper limit is given by the quasi-static fracture, which presents the largest SERR due to matrix cleavage and fibre breakage.

2.7 References

- [1] Pascoe JA, Alderliesten RC, Benedictus R. Methods for the prediction of fatigue delamination growth in composites and adhesive bonds - A critical review. *Engineering Fracture Mechanics*. 2013;112-113:72-96.
- [2] Yao L, Alderliesten RC, Zhao M, Benedictus R. Discussion on the use of the strain energy release rate for fatigue delamination characterization. *Composites Part A: Applied Science and Manufacturing*. 2014;66:65-72.
- [3] Alderliesten RC. How proper similitude can improve our understanding of crack closure and plasticity in fatigue. *International Journal of Fatigue*. 2016;82, Part 2:263-73.
- [4] Pascoe JA, Alderliesten RC, Benedictus R. Towards Understanding Fatigue Disbond Growth via Cyclic Strain Energy. *Procedia Materials Science* 2014;3 (ECF-20):610-5.
- [5] Pascoe JA, Alderliesten RC, Benedictus R. On the relationship between disbond growth and the release of strain energy. *Engineering Fracture Mechanics*. 2015;133:1-13.
- [6] ASTM Standard D5528-01. Standard Test Method for Mode I Interlaminar Fracture Toughness of Unidirectional Fiber-Reinforced Polymer Matrix Composites. US: ASTM International; 2007.
- [7] Hojo M, Nakashima K, Kusaka T, Tanaka M, Adachi T, Fukuoka T, et al. Mode I fatigue delamination of Zanchor-reinforced CF/epoxy laminates. *International Journal of Fatigue*. 2010;32:37-45.
- [8] Allegri G, Wisnom MR, Hallett SR. A new semi-empirical law for variable stress-ratio and mixed-mode fatigue delamination growth. *Composites Part A: Applied Science and Manufacturing*. 2013;48:192-200.
- [9] Stelzer S, Brunner AJ, Argüelles A, Murphy N, Pinter G. Mode I delamination fatigue crack growth in unidirectional fiber reinforced composites: Development of a standardized test procedure. *Composites Science and Technology*. 2012;72:1102-7.
- [10] Murri GB. Evaluation of delamination onset and growth characterization methods under mode I fatigue loading. American Society for Composites, 27th Technical Conference DEStech Publications, Inc.; 2012. p. 601-20.
- [11] Gustafson C-Go, Hojo M. Delamination Fatigue Crack Growth in Unidirectional Graphite/Epoxy Laminates. *Journal of Reinforced Plastics and Composites*. 1987;6:36-52.
- [12] Alderliesten RC, Schijve J, van der Zwaag S. Application of the energy release rate approach for delamination growth in Glare. *Engineering Fracture Mechanics*. 2006;73:697-709.
- [13] Rans C, Alderliesten RC, Benedictus R. Misinterpreting the results: How similitude can improve our understanding of fatigue delamination growth. *Composites Science and Technology*. 2011;71:230-8.
- [14] Jones R, Pitt S, Bunner AJ, Hui D. Application of the Hartman-Schijve equation to represent Mode I and Mode II fatigue delamination growth in composites. *Composite Structures*. 2012;94:1343-51.

- [15] ASTM Standard D6115-97. Standard Test Method for Mode I Fatigue Delamination Growth Onset of Unidirectional Fiber-Reinforced Polymer Matrix Composites. US: ASTM International; 2011.
- [16] Hojo M, Ando T, Tanaka M, Adachi T, Ochiai S, Endo Y. Modes I and II interlaminar fracture toughness and fatigue delamination of CF/epoxy laminates with self-same epoxy interleaf. *International Journal of Fatigue*. 2006;28:1154-65.
- [17] O'Brien TK. Characterization of Delamination Onset and Growth in a Composite Laminate. In: Reifsnider KL, editor. *Damage in Composite Materials*, ASTM STP 775: American Society for Testing and Materials; 1980. p. 140-67.
- [18] O'Brien TK, Murri GB, Salpekar SA. Interlaminar Shear Fracture Toughness and Fatigue Thresholds for Composite Materials. In: Lagace PA, editor. *Composite Materials: Fatigue and Fracture*, Second volume, ASTM STP 1012: American Society for Testing and Materials; 1989. p. 222-50.
- [19] Schon J. A model of fatigue delamination in composites. *Composites Science and Technology*. 2000;60:553-8.
- [20] Wilkins DJ, Eisenmann JR, Camin RA, Margolis WS, Benson RA. Characterizing Delamination Growth in Graphite-Epoxy. In: Reifsnider KL, editor. *Damage in Composite Materials*, ASTM STP 775: American Society for Testing and Materials; 1982. p. 168-83.
- [21] Gregory JR, Spearing SM. Constituent and composite quasi-static and fatigue fracture experiments. *Composites Part A: Applied Science and Manufacturing*. 2005;36:665-74.
- [22] Griffith AA. The Phenomena of Rupture and Flow in Solids. *Philosophical Transactions of the Royal Society of London Series A, Containing Papers of a Mathematical or Physical Character*. 1921;221:163-98.
- [23] Greenhalgh ES. *Failure analysis and fractography of polymer composites*: Woodhead Publishing Limited; 2009.
- [24] Yao L, Alderliesten R, Zhao M, Benedictus R. Bridging effect on mode I fatigue delamination behavior in composite laminates. *Composites Part A: Applied Science and Manufacturing*. 2014;63:103-9.
- [25] Yao L, Alderliesten R, Benedictus R. Interpreting the stress ratio effect on delamination growth in composite laminates using the concept of fatigue fracture toughness. Submitted to *Composites: Part A*. 2015.

3 Energy dissipation in mode II crack growth

The use of laminated composite materials in primary structures is still limited by the occurrence of in-service delaminations. Considering that interlaminar shear is one of the predominant loads experienced by composite structures, understanding the damage mechanisms involved in mode II delaminations is crucial for the development of a damage tolerance philosophy. Therefore, this work examines whether the energy dissipated in the process zone ahead of the crack tip should be accounted for when assessing fatigue delaminations caused by in-plane shear. ENF quasi-static and fatigue tests were performed and the results show that damage propagates ahead of the crack tip in a process zone. Acoustic Emission was used to verify that the process zone dissipates energy which should be accounted for when physically characterizing mode II delamination growth. The extent of the process zone in an ENF specimen cannot be measured by the means of visual observations made from the side of the specimen. Therefore, the definition of a crack tip is not recommended in mode II delamination studies. Instead, an effective crack length that includes the damaged zone ahead of the crack tip should be defined as a first simplifying method in order to correlate the damage extent with the energy dissipated. More studies are necessary to understand and quantify fracture in mode II delamination growth before developing methods to assess it using fracture mechanics.

3.1 Introduction

One of the predominant loads experienced by composite structures is interlaminar shear [1]. While studies addressing in-plane shear delaminations are abundantly available in literature, most of them fail in providing a physical explanation for the behaviour observed in crack extension. In [2, 3], mode II fatigue tests were performed and the data points were fitted by power-laws. No analyses of the fracture surfaces generated during crack extension were presented, hampering the understanding of the physics underlying the phenomenon. In [4], authors assumed the onset of growth in mode II fatigue delaminations when there is a 5% increase in the compliance of the specimen. However, if no growth was observed in the specimen, what is happening when the compliance increases by 5%?

Although in [1, 5] both empirical models and fracture surface analyses were presented, no relations between the damage features on the fracture surface and the curve fit were drawn. Nevertheless, some authors [6, 7] correlated the damage features observed on fracture surfaces with the empirical curve fit models they proposed. However, the use of different similitude parameters (i.e., G_{\max} , ΔG and $\Delta\sqrt{G}$) which are not based on physical principles misleads the explanation of the damage mechanisms encountered.

3.1.1 Problem Statement

There is a lack of fundamental understanding on mode II fatigue delamination. A gap exists between the way we describe the macroscopic behaviour and the micro-mechanisms present in in-plane shear crack extension. Although it has been observed that damage propagates ahead of the main crack tip in a damage zone [8-12], the commonly accepted procedure is to address mode II fatigue delamination phenomenologically. The problem is simplified to the definition of a crack tip, without considering the energy dissipated in a damage zone ahead of that tip. This yields datasets and empirical correlations that do not enable a physical interpretation of the results. Although empirical delamination growth models based on curve fittings may help to provide input for quicker engineering applications, they do not provide an understanding of the physics underlying the observed phenomenon. This understanding is the cornerstone towards developing a reliable physics-based prediction model for delamination growth, reducing the amount of resources spent on extensive test programs to certify aircraft composite structures.

Therefore, this work proposes to scrutinize mode II fatigue delamination and examine experimentally whether and how the energy dissipated in the process zone should be accounted for. In order to do so, the macroscopic delamination growth behaviour is correlated from an energy dissipation perspective with the damage mechanisms observed on the fracture surfaces.

Following the application of the physical SERR G^* for interpreting mode I delamination and disbond growth [13-17], the same parameter is used here to characterize mode II fatigue delaminations. In addition, Scanning Electron Microscopy (SEM) is used to examine the fracture surfaces and Acoustic Emission (AE) is used to verify that energy is dissipated in a process different than the visually observed crack growth.

3.1.2 Hypothesis

Cusps and matrix rollers are examples of typical microscopic features observed on fracture surfaces generated in mode II delaminations. Although an explanation for the formation of matrix rollers is still disputed [10, 18, 19], cusps are known to develop and grow ahead of the crack tip, due to the stress distribution in the resin. Once these cusps coalesce, macroscopic crack growth is observed [8, 9]. In addition, studies have suggested that other features, such as fatigue striations, also propagate ahead of the crack tip in mode II delaminations [10]. The zone in which these micro-cracks develop is referred to as “process zone”.

Because the extent of damage in the process zone depends on the stress distribution ahead of the crack tip, it is not reasonable to estimate that its length is constant during delamination extension. As an illustration, consider the case of crack growth in metals, in which the plastic zone size ahead of the crack tip is not constant, but it increases with the crack length for force controlled conditions. Similarly, the extent of the process zone ahead of the delamination tip is not constant, but varies according to the variation of the stress distribution in the crack front.

Therefore, it is hypothesized that the energy dissipated by these micro-cracks should be accounted for when characterizing mode II fatigue delamination. The determination of the damaged area ahead of the crack tip is fundamental to properly determine the total energy dissipated in delamination growth. Otherwise, both the SERR and the crack growth rate are wrongly estimated, undermining the understanding of the physics of the problem.

3.2 Methodology

3.2.1 Static and fatigue set-up

The End-Notched Flexure (ENF) test [20] was chosen as test method. 3 specimens were tested quasi-statically and 20 specimens were tested under a constant amplitude fatigue loading. The tests were performed at 2 Hertz, once this frequency showed very little vibration in the setup. Both types of tests were performed in a MTS machine equipped with a 10 kN load-cell. Both load and displacement were calibrated and had a relative error of 0.86% and 1%, respectively, in the load-displacement ranges used in the tests. Four specimens were tested at a stress ratio of $R = 0$, four specimens at $R = 0.1$, six specimens at $R = 0.5$ and six specimens at $R = 0.7$. All tests were carried out under displacement controlled conditions. In order to produce a sharp crack tip, all specimens were pre-cracked under a mode II quasi-static loading prior to both fatigue and static tests, as recommended in the ASTM standard [20].

Unidirectional laminates were manufactured with 32 layers of Carbon Fibre Reinforced Epoxy prepreg from the same material batch, M30SC-150-DT 120-34F. The product was cured in an autoclave following the cure cycle recommended by the manufacturer. A 13 μm thick Polytetrafluorethylene (PTFE) film was used in the middle layer as the crack starter. Prior to cutting, the cured laminates were C-scanned to ensure that they were free of defects. In this procedure, a panel with round defects of approximately 1 mm diameter was used as a reference. The specimens were cut from the laminates using a waterjet cutting

machine according to the nominal dimensions shown in Figure 3.1 (a), with a width of 25 mm. The actual test dimensions for precracking, static and fatigue tests are shown in Figure 3.1 (b). Prior to the test, specimens were stored at room temperature and laboratory conditions. All tests were performed at room temperature and laboratory air.

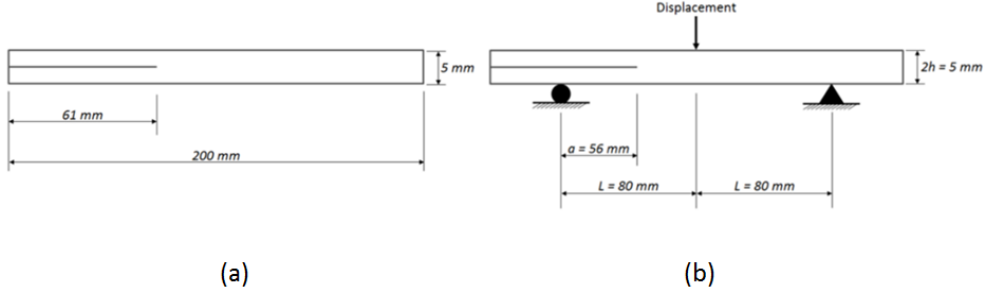


Figure 3.1. Dimensions of the ENF specimens (a) cut from the laminates and (b) tested on the fixture

After a specimen was pre-cracked, the new position of the crack tip was determined by scanning the specimen with an ultrasonic Phased-Array (PA) technique. According to the new position of the crack tip, the sample was repositioned on the test fixture and tested quasi-statically or under constant amplitude fatigue loading, in displacement controlled conditions. The specimens were C-scanned after the fatigue tests, in order to evaluate whether or not the crack front was straight. Finally, some samples were cut and had their fracture surfaces analysed with SEM.

The sides of the specimens were sanded with sandpaper and coated with a layer of white water-based correction fluid to aid in crack detection. Furthermore, vertical pencil lines were drawn on the specimen's side at each 2 mm, approximately, in order to facilitate the detection of crack extension. A camera was positioned close to the specimen and pictures (such as in Figure 3.2) were taken at every certain number seconds.

The crack growth rate, da/dN , is calculated from the measured crack length over the entire test, while the rate of strain energy dissipation, dU/dN , is calculated from the potential strain energy variation throughout the test, as illustrated in Figure 3.3. Considering linear elasticity, the potential strain energy is defined as $U = 1/2 P \delta_{\max}$. However, due to the compliance of the test fixture, a small portion of nonlinearity is observed when the load goes from 0 N to δ_{\min} . In order to account for this nonlinearity, a correction is introduced, such that both δ_{\max} and δ_{\min} are used to calculate an approximated U , as shown in Figure 3.4.

The graphs of a versus N and U versus N are plotted, where a is the crack length and U is the measured potential strain energy of the system. These data points are fitted with a function that produces the best fit to the behaviour presented by the data. For the crack length versus number of cycles, this function is a second order polynomial, while for the potential strain energy versus the number of cycles the fitting method used is the seven point incremental polynomial method [21].

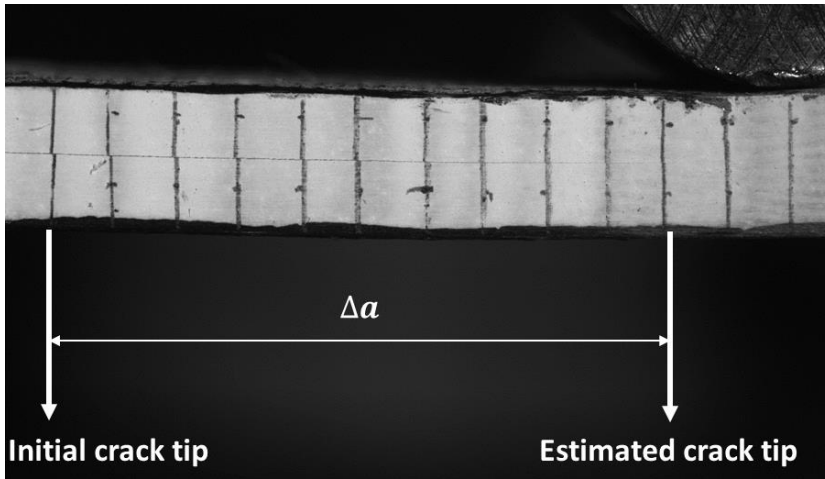


Figure 3.2. Specimen's side coated with white water-based correction fluid

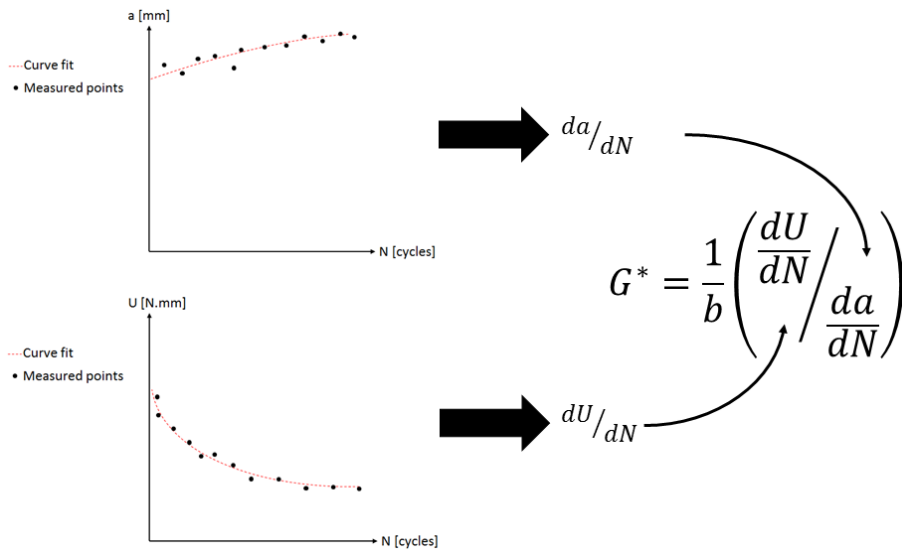


Figure 3.3. Calculation of the crack growth rate da/dN and of the strain energy dissipation rate dU/dN

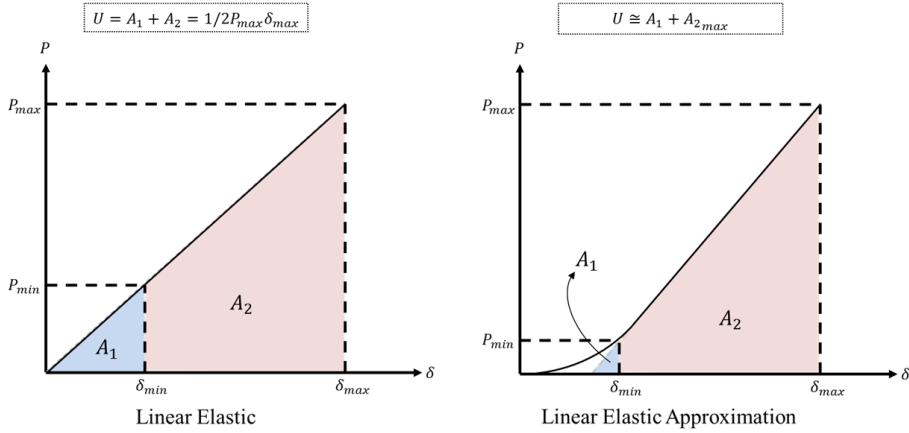


Figure 3.4. Approximation in the calculation of the potential strain energy due to the compliance of the test fixture; P is the load and δ is the displacement

3.2.2 Phased-Array

Following each static test, the new position of the crack tip was estimated by means of Ultrasonic PA measurements. An Olympus Omniscan SX device was used, with a SNW1-0L-WP5 0.005 probe mounted on a 2.25L64-NW1 wedge. The coupling between the probe and the wedge was made with ultrasonic testing oil. The specimen was mounted on two supports and the probe was coated with water-based ultrasonic coupling gel. A grid-paper was bonded to the specimen's side and the probe was moved along the specimen's top surface. The probe emits ultrasound waves. These waves, when interacting with discontinuities, are partially reflected and then detected by the probe. Due to the detected reflections, a bi-dimensional map of the interfaces in the plane section is obtained. Once the reflections indicated what was interpreted as being the crack tip, the estimated position of the tip was marked on the grid-paper.

3.2.3 Acoustic Emission

Three quasi-static tests and three fatigue tests (two at $R = 0$ and one at $R = 0.7$) were monitored with AE. An 8-channel AE system AMSY-6 Vallen Systemè with 4 parametric inputs was used. A wide-band piezoelectric sensor, AE1045S, was clamped to the specimen, as shown in Figure 3.5, using a coupling gel to maximize the conductivity between the sensor and the coupon. The sensor was connected to the system via a preamplifier with gain of 34 dB and band-pass filter 20 – 1200 kHz. A sampling rate of 2 MHz and a threshold of 50 dB_{AE} were used in all tests. Pencil breaks took place before every test in order to check the conductivity and measure the attenuation rate of the signal. Two parametric input channels were used to record load and displacement and to correlate them with the AE hits.

The author emphasizes here that the AE technique is not the subject of study of this thesis. The purpose of employing AE within this study is for supporting the main hypothesis that the process zone, ahead of the crack tip, dissipates energy that should be accounted for when characterizing mode II delamination growth. The AE energy was selected as the characterizing parameter due to its link with energy dissipation due to damage formation

and propagation. Although this link is not straightforward, the AE energy is part of the energy release due to the damage process.

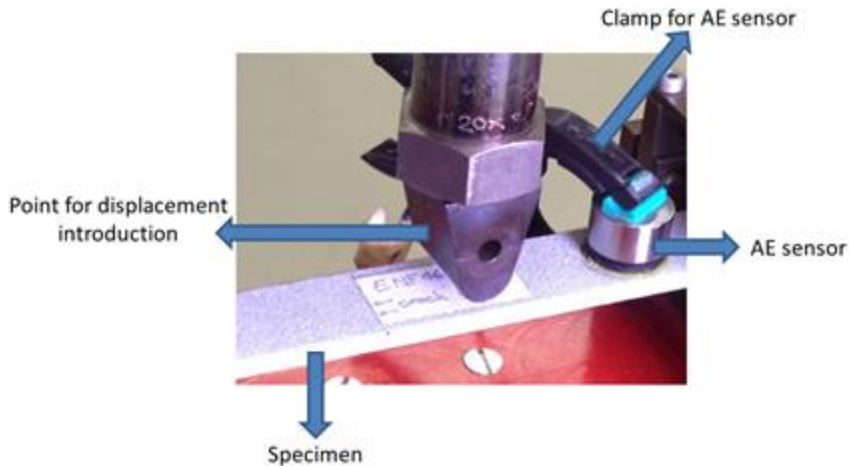


Figure 3.5. Set-up of the AE monitoring system

3.3 Results and Discussion

3.3.1 Phased-Array: estimating the crack tip position

An example of the images obtained with the PA technique is shown in Figure 3.6. The area of the crack in Figure 3.6 (a) can be distinguished, but it is not possible to clearly define a point as being the crack tip. As Figure 3.6 (a) shows, there is a gradient in the reflection, indicated as zone 1 in the picture. In this area, the reflection in the middle of the specimen is weaker, and some reflection due to the bottom surface of the specimen can still be observed. This shows that besides being dependent on the interpretation of the user, the estimation of an exact position for the crack tip is not possible with the used device. Furthermore, some defects cannot be captured with the PA resolution used in the test. Consider Figure 3.6 (b), which shows a PA scan of a specimen prior to any test, in the region where the PTFE insert is present. The PTFE insert cannot be clearly observed because the crack did not open yet and, because of it, there is no air in between the cracked surfaces that is enough to change the acoustic impedance of that area. Therefore, it is possible that micro-cracks and other types of damage are present in an area ahead of zone 1, such as zone 2, for example, but they cannot be detected with the PA resolution used.

For practical reasons, the point in which the reflection in the middle of the specimen apparently ends, defined by the dotted line marking the end of zone 1 in Figure 3.6, was chosen as the crack tip after the performed pre-cracking tests.

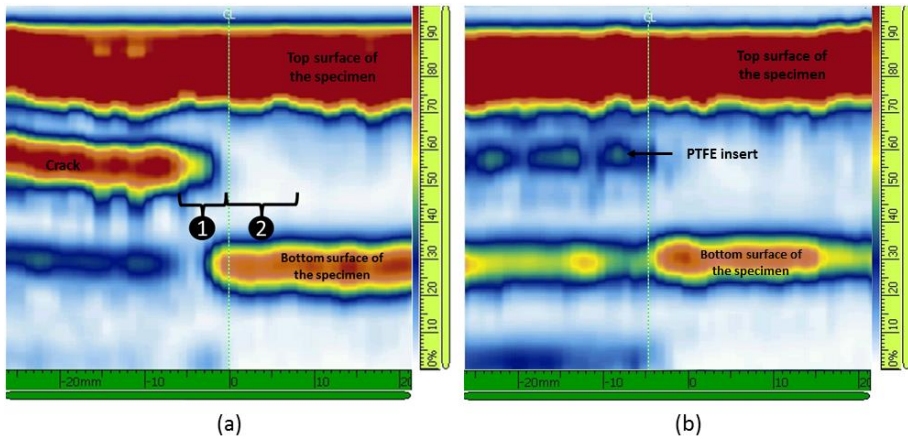


Figure 3.6. Reflection map in the cross-section of ENF specimens. The dashed line shows the centre of the probe; the scale to the right of each map shows the reflection magnitude, red being a strong reflection and white being no reflection– (a) the actual extent of the area designated by 2 is unknown; (b) the PTFE insert cannot be clearly observed

3.3.2 Process zone detection in quasi-static crack-growth

Figure 3.8 shows the relationship between time, applied load and energy of each AE hit for one of the three specimens tested quasi-statically. The energy of each hit was calculated as the integral of the squared AE waveform over its duration. The unit used is *eu*, which corresponds to 10^{-18} J. There is AE activity prior to the observation of the first crack growth from the side of the specimen. Considering that the amount of friction was low [22-25], due to the fact that the tests were static, this activity prior to crack growth can be related to micro-cracking ahead of the crack tip, corresponding to the development of the process zone. The effects of friction are, indeed, present, but these are deemed low. The observation of the fracture surfaces confirm this fact. Figure 3.7 shows the fracture surface of a quasi-static mode II delamination test. The main features observed in this image are well developed cusps and fibre imprints, known to develop ahead of the crack tip, as discussed in Section 3.1.2 of this chapter. These features are basically due to matrix decohesion and failure on the fibre-matrix interface. No debris or deteriorated cusps can be found, as it would be expected in cases of mode II delamination where the amount of friction is considerable [10]. Besides, no significant fibre bridging (other possible source of AE signals) could be observed. Therefore, the AE activity can be logically related to micro-cracking in the process zone.

From an AE perspective, the energy of the hits recorded before any crack growth was observed corresponds to a considerable amount of the total AE energy measured during the whole test. This is determined by adding the energy of each AE hit recorded before crack growth was observed and dividing this value by the summation of the energy of each AE hit recorded during the test. For the specimen *static 01* the energy of the hits before any visible crack growth corresponds to 81% of the total energy measured during the test, while for specimens *static 02* and *static 03* this value is of 23% and 41 %, respectively. This means that, in the tests performed, energy dissipation in the process zone is responsible for at least 20% of the AE energy measured in the whole test.

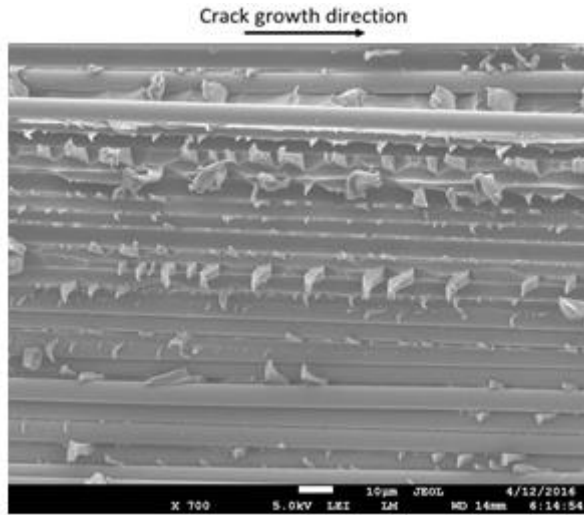


Figure 3.7. Fracture surface of quasi-static mode II delamination specimen

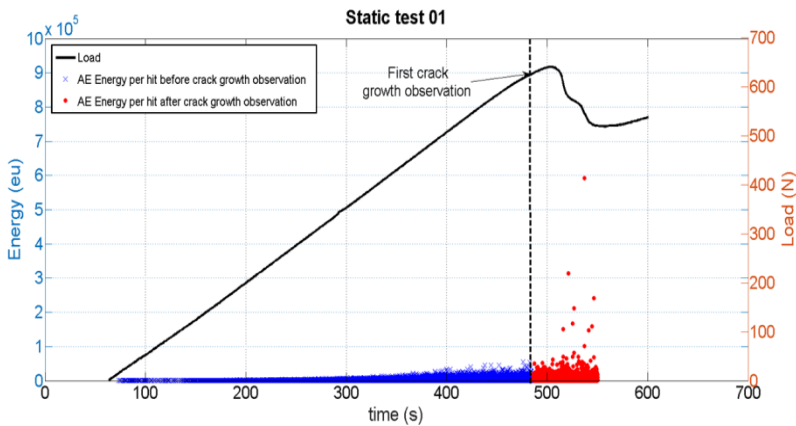


Figure 3.8. Relationship between time, load and energy of the AE hits for specimen *static 01*

Although the measured amount of AE energy before crack growth differs from one specimen to another, the results are evidence of damage formation ahead of the crack tip in mode II quasi-static delaminations. The reader should be aware, though, that the AE sensor records hits. The energy differs for every hit. The author chose to present the energy of the hits as a parameter to relate to energy dissipation, as there is a straightforward comparison between energy dissipation and AE energy activity. In order to strengthen the conclusion that there is significant activity in the specimens before crack growth is observed, the percentages of accumulation of hits before and after the first crack growth observation were also used as a parameter to relate to energy dissipation. For the specimen *static 01* the amount of hits before any visible crack growth corresponds to 76% of the total amount of hits during the test, while for specimens *static 02* and *static 03* this value is of 50% and 70 %, respectively. These facts indicate that using a camera next to the specimen in order to

correlate an amount of crack growth to the energy dissipated by it is not suitable for mode II quasi-static delamination tests.

3.3.3 The similitude problem solved: using the physical SERR G^*

In order to exemplify the problems regarding the choice of a similitude parameter in fatigue delamination, a comparison between different similitude parameters was performed. The measured crack growth rates for the ENF fatigue specimens were plotted against three commonly used similitude parameters. In addition, Mode I Double Cantilevered Beam (DCB) delamination data for the same material, reported in [15], is used for comparison. In Figure 3.9 (a) da/dN is plotted against G_{\max} , while in Figure 3.9 (b) it is plotted against ΔG and in Figure 3.9 (c) against $\Delta\sqrt{G}$. For simplicity, the SERR G was calculated according to the Classical Beam Theory (CBT): Load – Compliance form [26].

One should note that the results of 14 ENF tests are presented. From the 20 fatigue tests performed, 6 could not be analysed properly, due to difficulties in observing the propagation of the crack throughout the test. Due to this fact, these tests were not considered in the present analysis. Therefore, the successful tests, i.e. the ones in which crack propagation could be observed throughout the test, are listed in Table 1.

Table 1. Successful ENF tests

	Successful ENF tests			
	R = 0	R = 0.1	R = 0.5	R = 0.7
Number of specimens tested	3	3	4	4

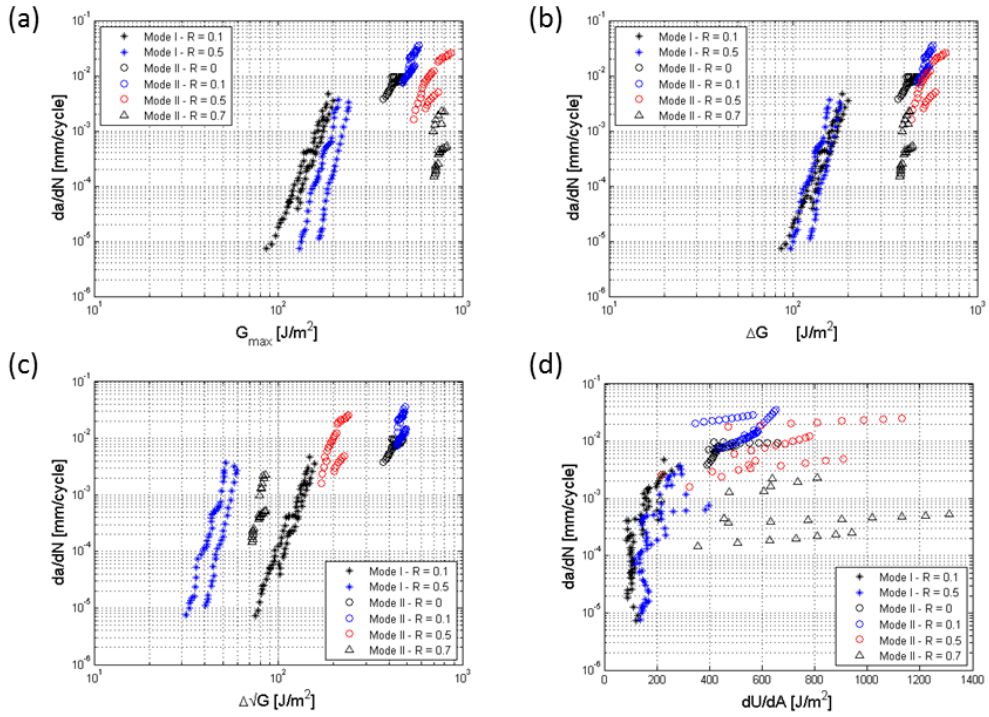


Figure 3.9. Mode II ENF and Mode I DCB fatigue tests – results plotted according to different similitude parameters

It is remarkable that each of the similitude parameters shows different results leading to different interpretations. From Figure 3.9 (a) one could deduce that for crack growth at high stress ratios a higher energy input is necessary. Meanwhile, this trend is completely opposite in Figure 3.9 (c) and fairly constant for the three stress ratios in Figure 3.9 (b). Hence, two questions are raised in this work: which of the parameters properly describes similitude and why?

In order to understand mode II fatigue delamination, it is necessary to use a similitude principle that is based on the physics of the problem and that obeys an energy balance. As discussed in [27], the physical SERR G^* , which is the average SERR over one cycle, is an energy-based parameter that is derived directly from the measured crack growth. G^* is calculated according to Equation 3.1, where b is the width of the sample.

$$G^* = \frac{1}{b} \frac{dU}{da/dN} = \frac{dU}{dA} \quad (3.1)$$

In order to properly characterize mode II fatigue delamination, the measured crack growth rates are plotted against the physical SERR G^* in Figure 3.9 (d). However, Mode II data presented in Figure 3.9 (d) show an amount of scatter that is higher than the one usually reported in literature for fatigue tests of composites. What can a graph with this amount of scatter tell?

In fact, Figure 3.9 (d) can offer valuable information about the physics of mode II fatigue delamination. Micro-cracks are developed ahead of the macro crack tip in the process zone, dissipating energy. By monitoring the sides of ENF specimens, the micro-cracking in the process zone cannot be detected. Only once these micro-cracks coalesce, growth can be observed from the sides of the specimen as a crack jump. This behaviour is shown in Figure 3.10, where from the beginning of the test until 6000 cycles crack growth followed a trend, which is faster than trend 2, due to a sequence of crack jumps. From 6000 cycles onwards, this trend changes and crack growth is slower than in the beginning of the test. This apparent change in crack growth resistance was observed in the majority of the fatigue tests at high stress ratios, several times per test.

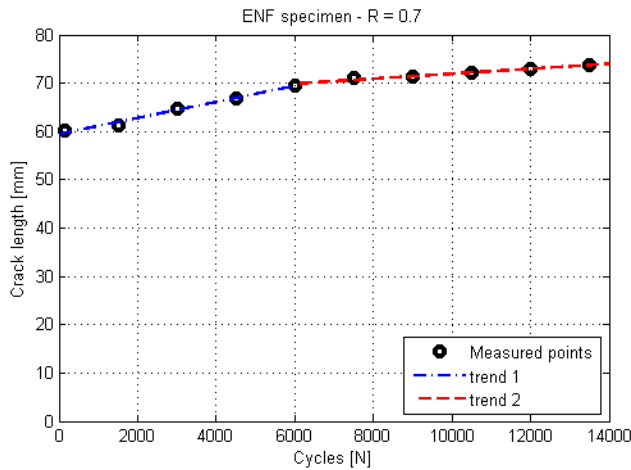


Figure 3.10. Crack length versus number of cycles for an ENF specimen tested at $R = 0.7$

To ensure that this change in crack growth resistance observed at high stress ratios was not a biased interpretation of the researcher measuring the crack length, two researchers measured the crack lengths for other fatigue test specimens monitored by the AE system, in a post-test analysis, separate in space and time from each other. This same behaviour was observed by the two researchers, and the results for one of the specimens, at $R = 0.7$, is presented in Figure 3.11.

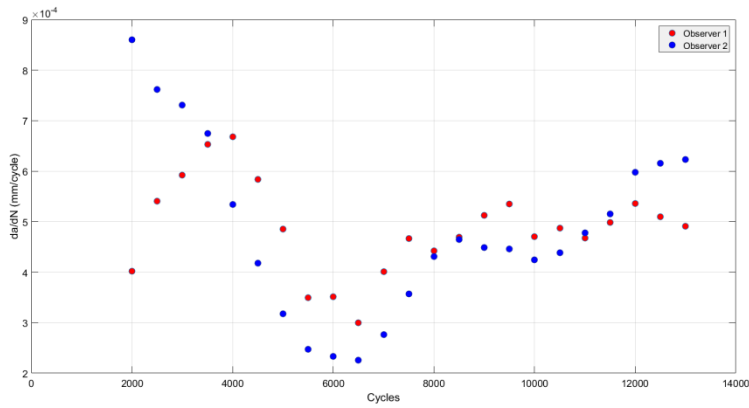


Figure 3.11. Crack growth rate measured by 2 observers for specimen fatigue tested at $R = 0.7$

This change in crack growth rate, seen in Figure 3.11, seems to be a result of micro-cracks formation and coalescence. When micro-cracks are being developed ahead of the main crack tip, the macroscopic crack growth observed from the side of the specimen is slower, such as the one depicted by trend 2 in Figure 3.10. Once these micro-cracks coalesce, the observed crack growth accelerates (such as trend 1 in Figure 3.10), and crack jumps seem to occur. Therefore, should not the results presented in Figure 3.10 and Figure 3.11 start at low da/dN , during the micro-cracking, and then go to a high da/dN , corresponding to when the crack jumps? No, because the specimens were pre-cracked, there was already a process zone formed during the pre-cracking procedure. Therefore, in the beginning of the fatigue loading, a crack jump might be observed, leading to tests that start at a high crack growth rate.

Towards this, AE gives a better insight into the energy dissipation process during the fatigue tests. Two characteristic types of waveforms were recorded in these tests, both shown in Figure 3.12. The first waveform, shown by the orange line, is a typical signal due to coalescence of the micro-cracks in the form of matrix cracking, which will eventually lead to the formation of the main matrix crack, with peak amplitudes in the range of 60 – 75 dB_{AE} . The second waveform, shown by the blue line in Figure 3.12, can be associated with both friction and the formation of the process zone in front of the crack tip, with peak amplitudes in the range of 50 – 60 dB_{AE} [28, 29].

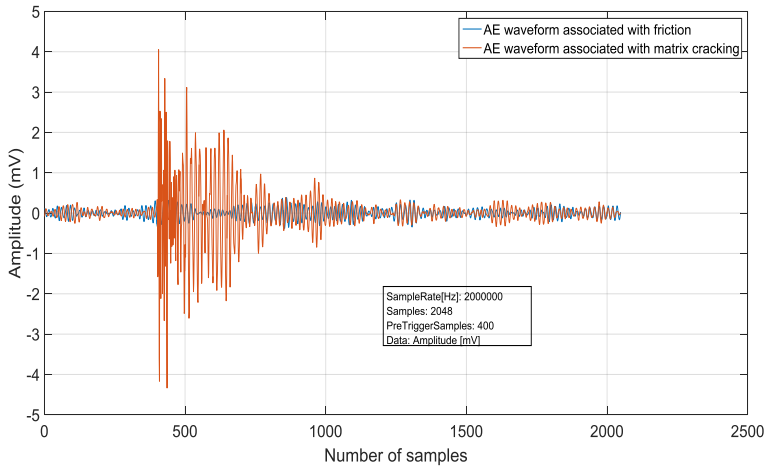


Figure 3.12. Characteristic types of waveforms recorded during the fatigue tests

AE waveforms with peak amplitudes higher than $75 \text{ dB}_{\text{AE}}$ are expected to be generated by fibre-bridging [30]. Therefore, these signals were filtered out of the AE fatigue analysis. The amount of hits exceeding $75 \text{ dB}_{\text{AE}}$ in the performed tests was very limited and it is in good agreement with the observation made by Gutkin and colleagues in [30], in which the AE activity due to fibre-bridging is reported to be mild. Although the test set-up used in [30] was different than the one used in the present work, Gutkin et al. argue to be acceptable to provide range of values for different damage mechanics for known failure mechanisms.

For the specimen for which the crack growth rate is shown in Figure 3.11, the energy of the AE hits was calculated at each 500 cycles, which is the same interval used for crack length monitoring from the sides of the specimen. The result is shown in Figure 3.13 (a). Figure 3.13 (a) and (b) plots the crack growth rate versus the number of cycles and the energy of the AE hits. In F (a), the energy of the total AE hits is presented. In F (b), only the energy of the AE hits for which the waveforms correlate to coalescence of microcracks is presented. The dashed line indicates the trend of the AE hits versus the number of cycles, and it is plotted merely to aid the reader in the interpretation of the results. Surprisingly, in Figure 3.13 (a) the energy measured in the AE hits stays approximately constant during the whole test, not following the trend of change in resistance observed in the crack growth rate. It was expected that, if there was a change in resistance, the energy of the recorded AE hits would also vary in a similar manner. This clearly indicates that, indeed, there is another energy dissipation mechanism acting, which is not currently being considered in the determination of da/dN . The energy of the AE hits related to coalescence was then separated and plotted in Figure 3.13 (b).

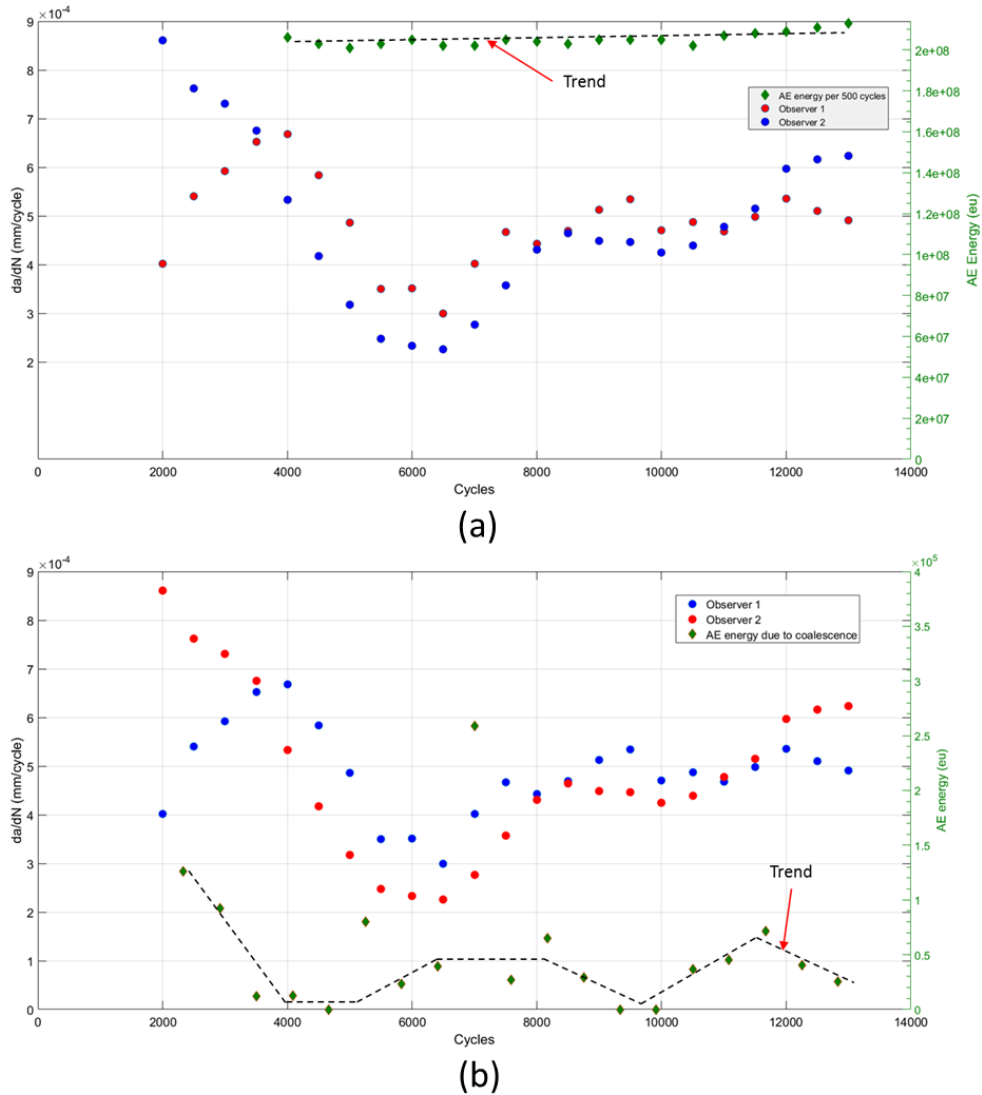


Figure 3.13. Crack growth rate and AE hits energy for specimen fatigue tested at $R = 0.7$; in (a) the energy due to all AE hits is presented, while in (b) just the energy of the AE hits corresponding to coalescence is shown

Remarkably, the energy regarding macroscopic crack growth correlates with the change in resistance in the measured crack growth rates for this specimen. This shows that, monitoring the sides of the specimen, only part of the mechanisms dissipating energy in crack growth are captured. This explains the scatter currently observed for the mode II data in Figure 3.9 (d). According to Equation 3.1, G^* is calculated from measured parameters, namely the crack growth rate and the rate of strain energy dissipation. The decrease in potential strain energy is affected by the compliance change of the specimen, which captures the effect of micro-cracks formation and crack propagation. Micro-cracking is a

physical process that dissipates energy and decreases the stiffness of the specimen, causing the compliance to increase.

Here, a question is raised about whether the load and displacement measured are sensitive enough in order to capture this phenomenon. This topic is further discussed in section 3.3.4 and, for the moment, it is assumed that the measured compliance does capture process zone formation and development. Therefore, the increase in compliance reflects in a change in the potential strain energy of the specimen, which leads to a proper calculation of the rate of strain energy dissipated per cycle, or dU/dN . However, the crack growth rate da/dN is calculated from the measured crack length. The crack length is measured by visual observation, which does not capture the effects of micro-cracking, unless the micro-cracks coalesce and turn into an observable crack jump. Therefore, the crack growth rate is not calculated with taking into account the progression of damage in the process zone. A measured value of energy dissipation is currently correlated with a damage state such as in Figure 3.14 (a), while it should be correlated to the damage state shown in Figure 3.14 (b).

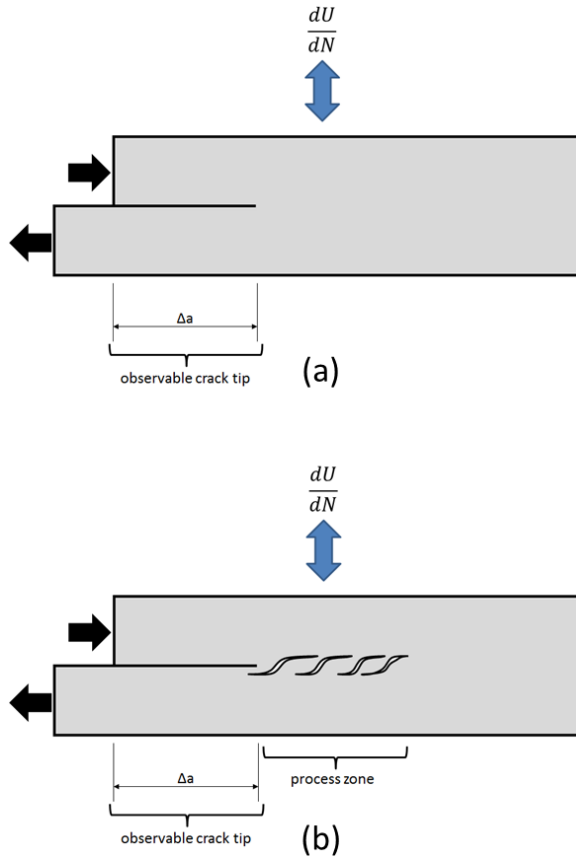


Figure 3.14. Relation between rate of strain energy dissipated and respective damage state considered: in (a) a certain energy dissipation is correlated to an observable crack tip, while this same energy dissipation should be correlated to the observable crack tip + damage in the process zone, shown in (b)

For low stress ratios (i.e., $R = 0$ and $R = 0.1$), this apparent change in the resistance to crack growth, observed in Figure 3.11, was less pronounced or even absent. The damage mechanisms observed for high and low stress ratios differ. Friction is more present between the cracked surfaces at low stress ratios, due to the bigger difference between maximum and minimum displacements in these cases. The direct consequence is that the cracked surfaces slide more against each other. As a result, Figure 3.15 shows that fracture surfaces at $R = 0$ and $R = 0.1$ are brittle, worn out and present a high amount of debris, which show the effect of friction.

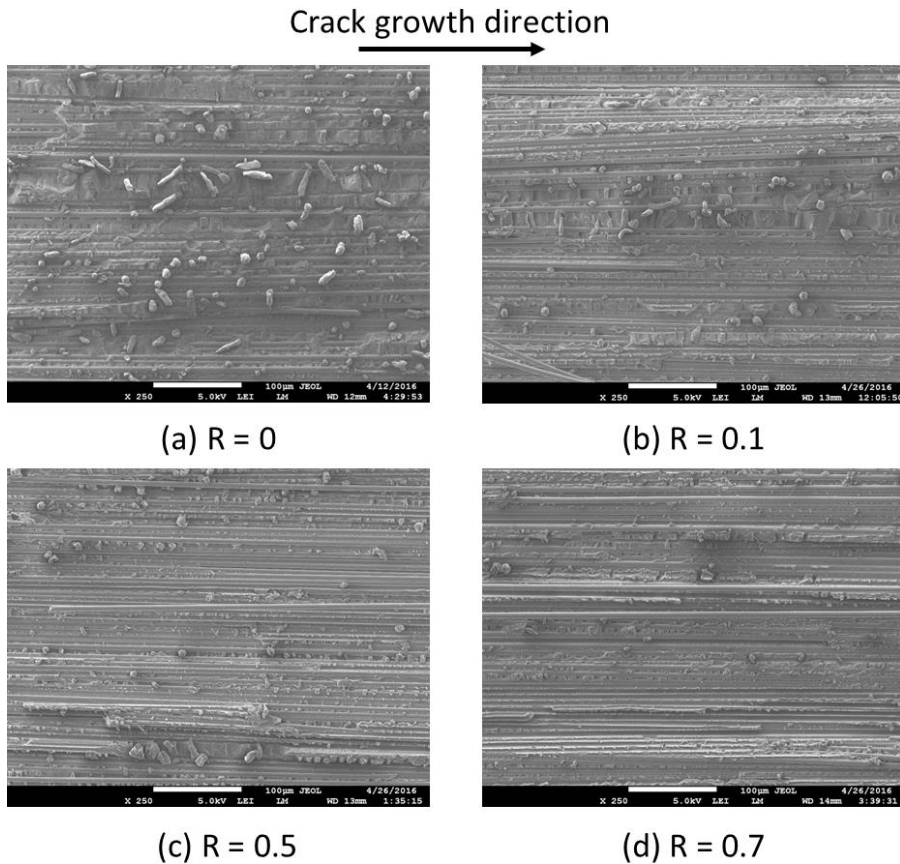


Figure 3.15. Comparison between fracture surfaces generated at different stress ratios

With the increase of the stress ratio, the presence of friction becomes less obvious, as in Figure 3.15 (c) and (d). The dominating damage mechanisms for these cases are deep cracks on the fibre imprints, fatigue striations and cusps, illustrated in Figure 3.16. These features are known to propagate ahead of the crack tip and are less obvious or not present at all at the examined fracture surfaces at $R = 0$ and $R = 0.1$. Friction is easily observed on fracture surfaces at $R = 0$ and $R = 0.1$, while damage mechanisms associated with process zone formation are found on fracture surfaces at $R = 0.5$ and $R = 0.7$. Therefore, this indicates that the AE hits that are not associated with crack coalescence at high stress ratios

are, in fact, associated with the formation of the process zone. Combining the information provided by AE and the fracture surfaces it becomes clear that, for high stress ratios, the energy that is not dissipated on coalescence is mostly dissipated in process zone formation. According to the damage features on the fracture surfaces, it is possible to correlate the AE hits in the range of 50 – 60 dB_{AE} with process zone formation instead of friction, for tests at high stress ratios. In a similar manner, these hits are associated with friction for tests at low stress ratios, due to the damage features their fracture surfaces present. Therefore, the energy dissipated in the process zone is higher on mode II delaminations at high stress ratios.

While only cusps and matrix rollers are likely to develop in the process zone at low stress ratios, cusps and fatigue striations are likely to develop ahead of the crack tip at high stress ratios. Besides, due to features as matrix tearing and plasticity, observed in Figure 3.16 (b), the fracture surfaces are less flat at high stress ratios. This shows, qualitatively, that more fracture area was created for the same crack increment da during fracture when compared with low stress ratios. Therefore, the energy dissipated in the process zone, that is currently not accounted for, increases with the stress ratio. However, one cannot calculate, at the moment, how gradual this increase in energy dissipated in the process zone is with an increase in the stress ratio. In order to better understand this stress ratio dependence, Figure 3.17 presents an illustration in which the behaviour observed in Mode I and Mode II fatigue delamination tests is depicted. This illustration shows qualitatively that the error in the calculation of the energy dissipated in crack growth is bigger at high stress ratios.

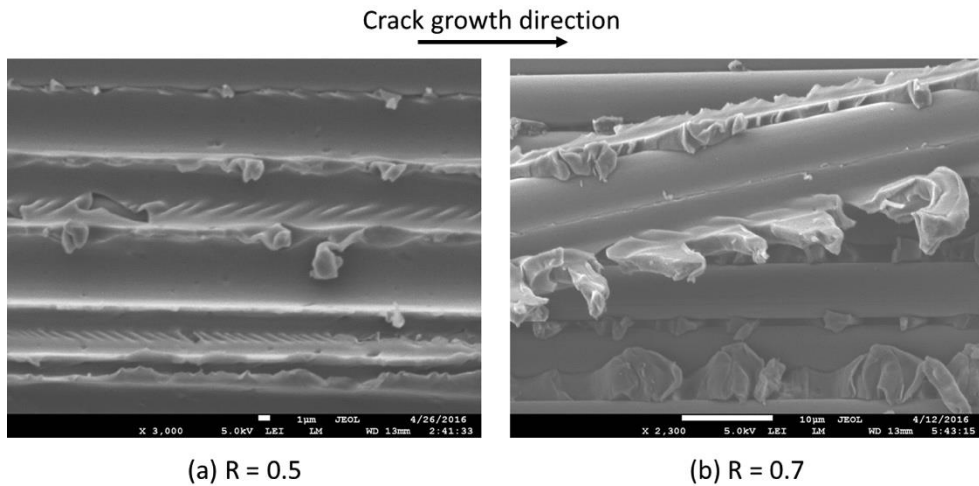


Figure 3.16. (a) cracks on fibre imprint and (b) cusps and matrix flow – typical damage features at high stress ratios

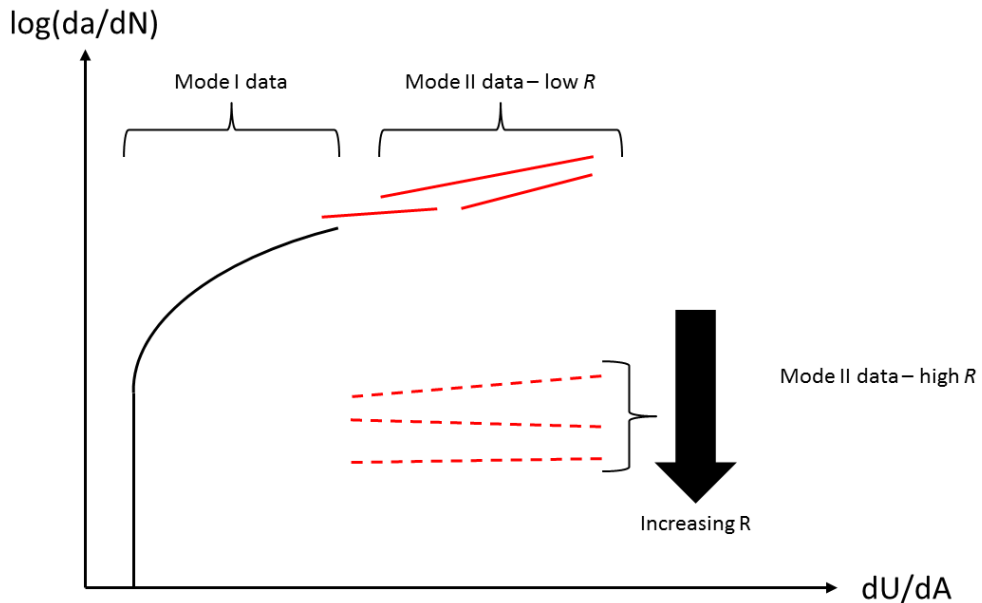


Figure 3.17. Illustration of modes I and II fatigue delamination data

The crack area A that is considered when assessing mode II delamination growth requires a different definition, including not only the crack length but also process zone related damage. This implies that not only the physical SERR G^* , but also any standard fracture mechanics method needs a better definition of the fracture area. The definition of an effective crack length would be necessary. This effective crack length should relate, within the context of energy balance, with the physical crack length. Therefore, before developing methods to assess mode II delamination using fracture mechanics, more research is necessary towards finding a better way to quantify fracture and to define this effective crack length.

3.3.4 Compliance Calibration

A possible manner to capture the effect of micro-cracks formation ahead of the crack tip would be to use a compliance calibration technique in order to derive an effective crack length that captures the process zone. However, although the variation in compliance captures the effects of micro-cracking, it is difficult to calibrate the variation in compliance to a certain amount of damage. In order to perform the calibration, it would be necessary to measure the amount of damage created by a certain loading scenario. This would incur in the aforementioned problem that is necessary, first, to find a better way to quantify fracture.

In addition, Different ways of generating a crack, e.g. by fatigue or quasi-static loading, generate different damage zones ahead of the crack tip. Once the crack grows, the process zone ahead of the crack also extends, but in a rate that is not necessarily the same as the one

of the crack tip. In addition, with the growth of the process zone, the stress distribution in this area will also change and the size of the process zone is not likely to be constant.

Besides, a question was raised in this thesis whether the load and displacement measured are sensitive enough in order to capture the changes due to process zone formation. Previously in this manuscript, this was assumed to be true in order to demonstrate the main hypothesis of this chapter, as well as the dependence of the process zone effects with the stress ratio. However, more research is necessary in order to establish how much energy is dissipated by the process zone and to what extent one can measure it. Because of the aforementioned reasons, predicting micro-cracking becomes troublesome, and a manner to measure accurately the process zone size would be necessary in order to calibrate the compliance of the specimen.

Furthermore, when using the physical SERR G^* to characterize delamination propagation, the crack growth rate da/dN should not be obtained by means of compliance calibration. The strain energy dissipation rate dU/dN is already obtained by the variation in compliance of the specimen. Therefore, obtaining the crack growth rate also by the variation in compliance would result in circular reasoning.

3.4 Conclusions

Damage propagates ahead of the main crack tip in a process zone, which dissipates energy that should be accounted for when characterizing mode II delamination growth. Thus, this work indicates that it is not possible to measure appropriately the extent of the process zone in an ENF specimen from observations made from its side. The size and influence of the process zone in energy dissipation vary with the stress ratio.

A significant amount of evidence shows that the definition of a phenomenological crack tip in mode II delamination studies should not be used. Instead, an effective crack length, which includes the damaged zone ahead of the main crack tip, should be defined. However, more studies are necessary in order to understand and define properly the extent of the process zone in mode II delaminations. Therefore, instead of developing new fracture mechanics models to address mode II delamination problems, efforts should be focused towards quantifying fracture in a better way.

Furthermore, without measuring the real extent of damage, it is not possible to calculate the actual damage growth rate present in mode II fatigue delaminations. Thus, as a direct consequence, it is not possible to use the physical SERR G^* to characterize mode II fatigue delamination, since it depends on an accurate measurement of the damage extent. The utilization of the visually observed crack length as a parameter to calculate the crack growth rate results in its underestimation, which is more pronounced for high values of R .

3.5 References

- [1] O'Brien TK, Murri GB, Salpekar SA. Interlaminar Shear Fracture Toughness and Fatigue Thresholds for Composite Materials. In: Lagace PA, editor. *Composite Materials: Fatigue and Fracture*, Second volume, ASTM STP 1012: American Society for Testing and Materials; 1989. p. 222-50.
- [2] Rans C, Atkinson J, Li C. On the Onset of the Asymptotic Stable Fracture Region in the Mode II Fatigue Delamination Growth Behaviour of Composites. *Journal of Composite Materials*. 2014;0:10-3.
- [3] Cui W, Wisnom M, Jones M. An Experimental and Analytical Study of Delamination of Unidirectional Specimens with Cut Central Plies. *Journal of Reinforced Plastics and Composites*. 1994;13:722 - 39.
- [4] Jagannathan N, Chandra ARA, Manjunatha CM. Onset-of-growth behavior of mode II delamination in a carbon fiber composite under spectrum fatigue loads. *Composite Structures*. 2015;132:477-83.
- [5] O'Brien KT, Johnston WM, Toland GJ. Mode II Interlaminar Fracture Toughness and Fatigue Characterization of a Graphite Epoxy Composite Material. Hampton, Virginia: NASA; 2010.
- [6] Matsuda S, Hojo M, Ochiai S. Mesoscopic fracture mechanism of mode II delamination fatigue crack propagation in interlayer-toughened CFRP. *JSME International Journal Series A: Mechanics and Material Engineering*. 1997;40:423-9.
- [7] Hojo M, Ando T, Tanaka M, Adachi T, Ochiai S, Endo Y. Modes I and II interlaminar fracture toughness and fatigue delamination of CF/epoxy laminates with self-same epoxy interleaf. *International Journal of Fatigue*. 2006;28:1154-65.
- [8] LEE SM. Mode II delamination failure mechanisms of polymer matrix composites. *Journal of Materials Science*. 1997;32:1287-95.
- [9] Lee SM. Mode II Interlaminar Crack Growth Process in Polymer Matrix Composites. *Journal of Reinforced Plastics and Composites*. 1999;18:1254-66.
- [10] Greenhalgh ES. *Failure analysis and fractography of polymer composites*: Woodhead Publishing Limited; 2009.
- [11] Corleto C, Bradley W. Mode II Delamination Fracture Toughness of Unidirectional Graphite/Epoxy Composites. *Composite Materials: Fatigue and Fracture*. 1989;2:201-21.
- [12] O'Brien TK. Composite interlaminar shear fracture toughness, {GIIC}: Shear measurement or sheer myth? In: Bucinell RB, editor. *Composite Materials: Fatigue and Fracture*, 7th Volume, ASTM STP 1330. 1330 ed1998. p. 3-18.
- [13] Pascoe JA, Alderliesten RC, Benedictus R. Towards Understanding Fatigue Disbond Growth via Cyclic Strain Energy. *Procedia Materials Science* 2014;3 (ECF-20):610-5.
- [14] Pascoe JA, Alderliesten RC, Benedictus R. On the relationship between disbond growth and the release of strain energy. *Engineering Fracture Mechanics*. 2015;133:1-13.
- [15] Yao L, Alderliesten R, Benedictus R. Interpreting the stress ratio effect on delamination growth in composite laminates using the concept of fatigue fracture toughness. Submitted to *Composites: Part A*. 2015.
- [16] Yao L, Alderliesten RC, Zhao M, Benedictus R. Discussion on the use of the strain energy release rate for fatigue delamination characterization. *Composites Part A: Applied Science and Manufacturing*. 2014;66:65-72.
- [17] Yao L, Alderliesten R, Zhao M, Benedictus R. Bridging effect on mode I fatigue delamination behavior in composite laminates. *Composites Part A: Applied Science and Manufacturing*. 2014;63:103-9.

- [18] Bürger D. Mixed-Mode Fatigue Disbond on Metallic Bonded Joints. Delft, The Netherlands: Delft University of Technology; 2015.
- [19] Heutling F, Franz HE, Norbakke M, Morlo H, Paulisch D, Czarnecki J, et al. Microfractographic analysis of the delamination growth in fatigue loaded carbon-fibre/thermoset matrix composites. *Mat-wissund Werkstofftechnik*. 1998;29:14.
- [20] ASTM. Standard Test Method for Determination of the Mode II Interlaminar Fracture Toughness of Unidirectional Fiber-Reinforced Polymer Matrix Composites. D7905/D7905M ASTM International; 2014.
- [21] ASTM. Standard Test Method for Measurement of Fatigue Crack Growth Rates. E647-15: ASTM International; 2015.
- [22] Carlsson L, Gillespie J, Pipes R. On the analysis and design of the end notched flexure (ENF) specimen for mode II testing. *Journal of composite materials*. 1986;20:594-604.
- [23] Schuecker C, Davidson BD. Effect of friction on the perceived mode II delamination toughness from three-and four-point bend end-notched flexure tests. *Composite Structures: Theory and Practice*: ASTM International; 2001.
- [24] Russell A, Street K. Factors affecting the interlaminar fracture energy of graphite/epoxy laminates. *Progress in science and Engineering of Composites*. 1982;279-86.
- [25] Blackman B, Kinloch A, Paraschi M. The determination of the mode II adhesive fracture resistance, G_{IIC} , of structural adhesive joints: an effective crack length approach. *Engineering Fracture Mechanics*. 2005;72:877-97.
- [26] Davidson BD, Sun X. Geometry and Data Reduction Recommendations for a Standardized End Notched Flexure Test for Unidirectional Composites. *Journal of ASTM International*. 2006;3:19.
- [27] Amaral L, Yao L, Alderliesten R, Benedictus R. The relation between the strain energy release in fatigue and quasi-static crack growth. *Engineering Fracture Mechanics*. 2015;145:86-97.
- [28] Bar HN, Bhat MR, Murthy CRL. Parametric Analysis of Acoustic Emission Signals for Evaluating Damage in Composites Using a PVDF Film Sensor. *Journal of Nondestructive Evaluation*. 2005;24:121-34.
- [29] Sasikumar T, RajendraBoopathy S, Usha KM, Vasudev ES. Failure strength prediction of unidirectional tensile coupons using acoustic emission peak amplitude and energy parameter with artificial neural networks. *Composites Science and Technology*. 2009;69:1151-5.
- [30] Gutkin R, Green CJ, Vangrattanachai S, Pinho ST, Robinson P, Curtis PT. On acoustic emission for failure investigation in CFRP: Pattern recognition and peak frequency analyses. *Mechanical Systems and Signal Processing*. 2011;25:1393-407.

4 Mixed-Mode fatigue delamination growth

In real structures, delaminations tend to grow under a mix of modes I and II. Although many studies have tried to assess mixed-mode fatigue delamination, little progress was made in understanding the physics behind the problem. Therefore, this work scrutinizes mixed-mode fatigue delamination growth and examines experimentally the damage mechanisms that lead to fracture. To this aim, mixed-mode delamination fatigue tests were performed at different mode mixities, displacement ratios and maximum displacements. Fracture surfaces were analysed after the tests in a Scanning Electron Microscope to gain insight on the damage mechanisms. The physical Strain Energy Release Rate G^ was used as the similitude parameter, enabling the characterization of fatigue mixed-mode delamination propagation. The results obtained show no displacement ratio or maximum displacement dependence.*

4.1 Introduction

In real structures, delaminations tend to grow under a mix of modes I and II [1]. Although studies have tried to assess mixed-mode fatigue delamination, little progress was made in understanding the physics behind the problem. In [2, 3], authors identified a stress ratio dependence in mixed-mode fatigue delamination tests, being the stress ratio defined as the ratio between minimum and maximum load, $R_\sigma = P_{min}/P_{max}$. Meanwhile Zhang et al. [4] showed that the Paris curves shift when tests are performed with different maximum displacements while keeping the stress ratio constant.

None of them presented explanations for these observations. In fact, one should note that the effect of the stress ratio in energy dissipation during fatigue damage growth is a phenomenon controlled by two parameters. These parameters are the cyclic work and the maximum work applied.

This is illustrated in Figure 4.1, which shows 3 different constant amplitude displacement controlled fatigue cycles. Let the displacement ratio be defined as the ratio between minimum and maximum applied displacements, $R_\delta = \delta_{min}/\delta_{max}$. The concept of using the ratio between minimum and maximum displacements is because R_δ is constant in displacement controlled tests. This was also used by Zhang et al. [4]. Loading cycles A and B have different displacement ratios but share the same maximum displacement. Therefore, the energy dissipated in a given increment of crack growth da might be the same for loading cycles A and B. Meanwhile, loading cycles A and C have the same displacement ratio and different maximum displacements, and they dissipate a different amount of energy per crack increment da . Therefore, in order to study the effect of the displacement ratio in energy dissipation, both cyclic energy and maximum work applied, i.e. displacement ratio and maximum displacement, must be considered.

Studies that reported a stress ratio dependence [2, 3] did not report if the maximum work applied was changed when changing the stress ratio. On the other hand, the study in which Zhang et al. [4] observed differences in energy dissipation when changing the maximum displacement was performed only in one displacement ratio. Effectively, no studies were found in which the effects of different displacement ratios and maximum applied work were simultaneously investigated in a range of mode mixities.

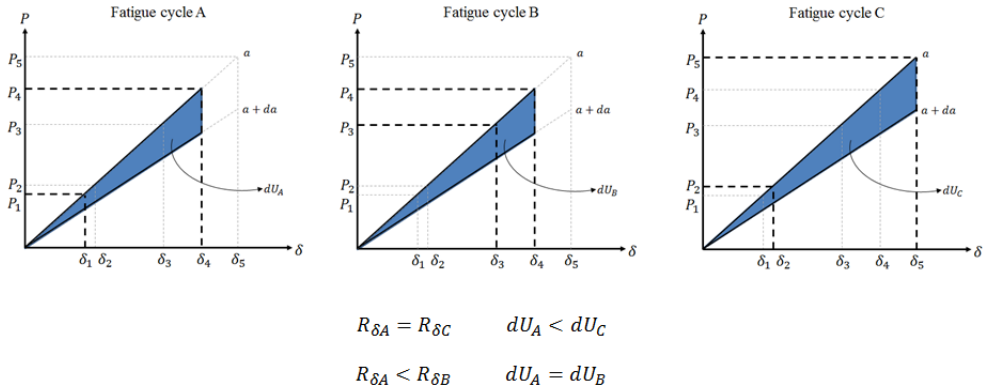


Figure 4.1. Illustration shows that constant amplitude fatigue cycles with different displacement ratios might have the same energy dissipation for a given crack increment da

Moreover, studies available in literature, such as [2-7], often focused on simply obtaining phenomenological power-law relations in order to best fit the data. In some of these studies [2-4], no fracture surfaces were examined, hindering the understanding of the damage mechanisms and the physics of delamination growth. Some authors [5-7], however, report both empirical models and analysis of fracture surfaces. In particular, Asp et al. [7] related the damage mechanisms acting in fracture propagation to the calculated Strain Energy Release Rate (SERR) levels. However, the use of different similitude principles when assessing fatigue delamination misleads the interpretation of the results [8].

4.1.1 Problem Statement and Research Objectives

Mixed-mode fatigue delamination is not well understood. This is demonstrated by the fact that there is no consensus on displacement ratio dependence, the effects of the maximum load applied in the fatigue cycle, or even on the parameter describing similitude.

Furthermore, do damage mechanisms change with a different stress ratio? What different damage features are observed on the fracture surface when the maximum load changes?

The lack of appropriate answers to these questions are evidences of the gap between the way the macroscopic behaviour and the damage mechanisms acting in fracture are described.

Although empirical delamination growth models based on curve fitting may help to provide quicker input for engineering predictions, they do not lead to understanding the physics underlying the observed phenomena. This is a common drawback of assessing problems with phenomenological empirical relations that fit very well the data, but provide no insight on why data behave as such. The fundamental understanding of fatigue delamination growth might shed light on how to interpret and assess damage growth in composites. A better understanding of different types of damage growth in composites could set the path towards a design philosophy that relaxes the current “no growth” approach, resulting in a further weight reduction of aircraft.

Therefore, the aim of this work is to scrutinize mixed-mode fatigue delamination growth and examine experimentally the damage mechanisms that lead to fracture. Through that, this work seeks to understand the effects of different displacement ratios and maximum applied loads on fatigue delamination growth under different mode mixities, and provide physical explanations to it. In addition, the appropriateness of the term “stress ratio effect” for fatigue crack growth is discussed.

Following the use of the physical SERR G^* for interpreting mode I and mode II delamination and disbond growth [9-13], this parameter is employed here to characterize mixed-mode fatigue delamination growth. Besides, Scanning Electron Microscopy (SEM) is used to examine the fracture surfaces and gain insight on the damage mechanisms present at the fracture surfaces.

4.2 Methodology

4.2.1 Relating applied work to energy dissipation

The current thesis uses the physical SERR as the correct approach to describe the similitude in fatigue damage growth. The reasoning, discussed in detail by Alderliesten [14] and summarized here, is that cyclic work is applied when fatigue loading a certain structure. Consider a brittle material system, where plasticity effects are negligible. In a similar manner to what Griffith proposed [15], a single fatigue cycle under displacement controlled conditions can be written in terms of energy

$$U_0 + U_{\uparrow} \rightarrow U_0^* + U_{\downarrow} + U_a \quad (4.1)$$

where U_0 is the monotonic elastic strain energy available at the start of the load cycle, U_{\uparrow} is the work applied by the machine during loading, U_{\downarrow} is the work applied by the specimen during unloading and U_a is the energy dissipated in damage growth. These energies correspond to the areas below the curves illustrated in Figure 4.2.

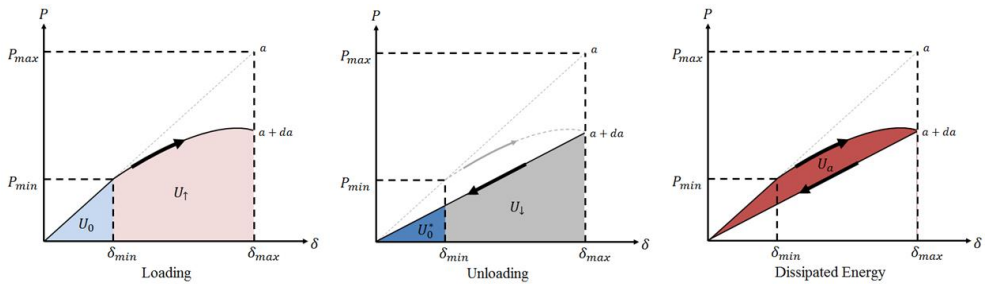


Figure 4.2. Applied work and energy dissipation in a single constant amplitude displacement controlled fatigue cycle

The difference between U_{\uparrow} and U_{\downarrow} is difficult to measure for a single load cycle. An approximate solution is to measure the elastic work applied to the structure at any load cycle $U_{N=i}$, where $U = 1/2 P \delta$, with P and δ the applied force and displacement,

respectively. For the displacement controlled tests performed, the strain energy available will decrease with the number of cycles, such that the variation of the applied work can be easily calculated as dU / dN . Energy dissipation may occur in any load cycle, such that

$$U_0 + U_{\uparrow} \rightarrow U_0^* + U_{\downarrow} + dU / dN \quad (4.2)$$

The energy dissipated per cycle can be written as

$$dU / dN = (dU / dA)(dA / dN) \quad (4.3)$$

Note that the complete load cycle is included in the formulation of Equation (4.2). The stress ratio has a similar effect on dU and da for a given cycle. Hence, Equation (4.3) in which dU / dN and da / dN are plotted against each other may not exhibit a stress ratio effect as observed in Paris-type relationships [14].

The resistance to crack growth, which is the energy dissipated per area of crack created, dU / dA , can be obtained if the strain energy variation and the damage growth rate are measured throughout a test. This is illustrated in Figure 4.3. The reader should note that, according to Equation (4.3), dU / dA is calculated plotting a straight line from the origin of the coordinate system to each data point. The inclination of each of the straight lines obtained between the origin and the data point is $1 / (dU / dA)$. Energy dissipation per area of crack, dU / dA , was observed to increase with an increasing crack growth rate for mode I delaminations [14, 16]. The higher the crack growth rate, the closer to quasi-static fracture the process is. The closer a fracture is to quasi-static, the more energy is dissipated per area, because quasi-static fracture is less energetically efficient than fatigue fracture. This relates to the damage mechanisms observed on the fracture surfaces. With an increase in the crack growth rate, more damage features and different damage mechanisms were encountered on the fracture surface, responsible for the aforementioned increase in energy dissipation [16].

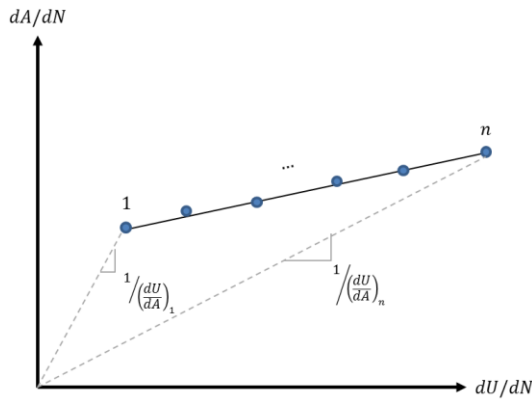


Figure 4.3. Determining the energy dissipated per area of crack created: resistance to crack growth increases with the crack growth rate. In this illustration both axes have linear scales

4.2.2 The Mixed-Mode Bending Test

The Mixed-Mode Bending (MMB) test fixture, schematically illustrated in Figure 4.4 (a), was used to load split specimens at different ratios of Mode I to Mode II loading, where W_g is the centre of gravity of the lever-yoke assembly, cg is the lever length to the centre of gravity and c is the lever length of the MMB test apparatus. The mode mixity, defined as

$$\frac{G_{II}}{G} = \frac{G_{II}}{(G_I + G_{II})} \quad (4.4)$$

is kept constant throughout all tests. In total, 38 specimens were fatigue tested at different stress ratios under constant amplitude loading, displacement controlled conditions. The frequency of the tests was 5 Hertz. Tests were performed at different maximum displacements, in order to understand its effect on energy dissipation in fatigue delamination growth. The test matrix is presented on Table 2.

Table 2. Test Matrix

Number of tests	$(\delta_{max}/\delta_{crit})$	R	(G_{II}/G)
3	0.75	0.1	0.20
2	0.85		
3	0.90		
3	0.75	0.5	
3	0.85		
4	0.90		
2	0.85	0.7	
3	0.85	0.1	0.50
3	0.85	0.5	
3	0.85	0.7	
3	0.88	0.1	0.80
3	0.88	0.5	
3	0.88	0.7	

The results of constant amplitude, displacement controlled Double Cantilever Beam (DCB) and End-Notched Flexure (ENF) fatigue tests for the same material, discussed in [11, 13], are also used at the present work.

4.2.3 Material and specimen preparation

Unidirectional laminates were manufactured with 32 layers of Carbon Fibre Reinforced Epoxy prepreg from the same material batch, M30SC-150-DT 120-34F. The prepreg is manufactured by Delta Tech. The product was cured in an autoclave following the cure

cycle recommended by the manufacturer. A $13\ \mu\text{m}$ thick Polytetrafluorethylene (PTFE) film was placed in the middle layer as the crack starter. The cured laminates were C-scanned to ensure that they were free of defects, using a panel made of the same material with voids of approximately $1\ \text{mm}$ diameter as reference.

$25\ \text{mm}$ wide specimens were cut from the laminates using a waterjet cutting machine according to the dimensions shown in Figure 4.4 (b). End blocks were bonded to the specimens for load introduction following the guidelines given in ASTM Standard D 6671 [17]. A camera was positioned alongside the specimen during the test and crack length measurement was performed in a post-test analysis of the pictures taken, using an open-source image analysis software, ImageJ. The pictures were taken using an Optomotive Velociraptor camera system. To aid in crack detection, the sides of the specimen were sanded and coated with a thin layer of white water-based typewriter correction fluid, and vertical pencil lines were drawn every $15\ \text{mm}$, as shown in Figure 4.5.

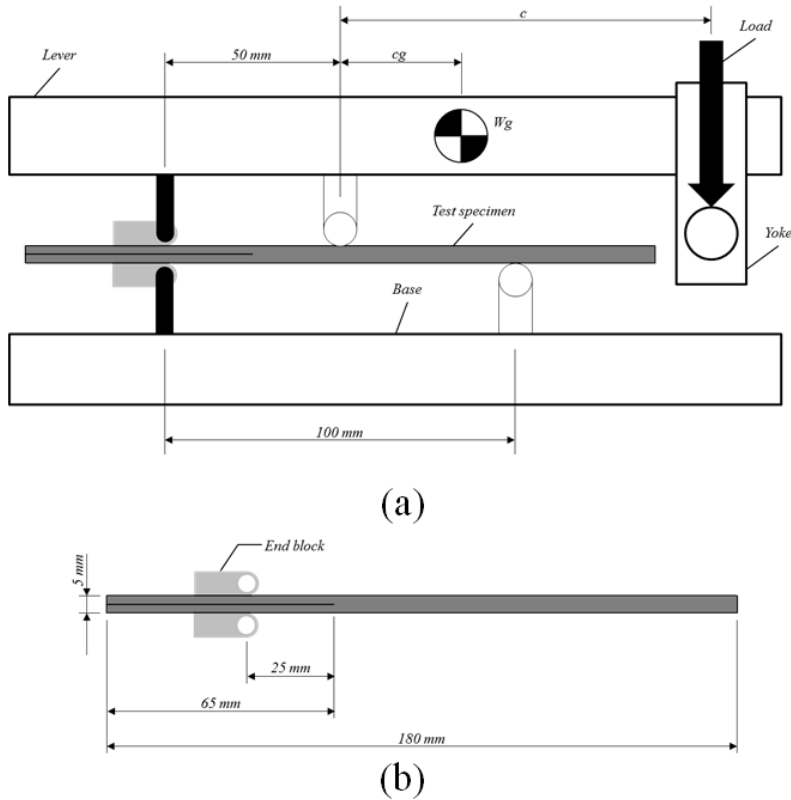


Figure 4.4. (a) MMB test fixture; (b) specimen dimensions

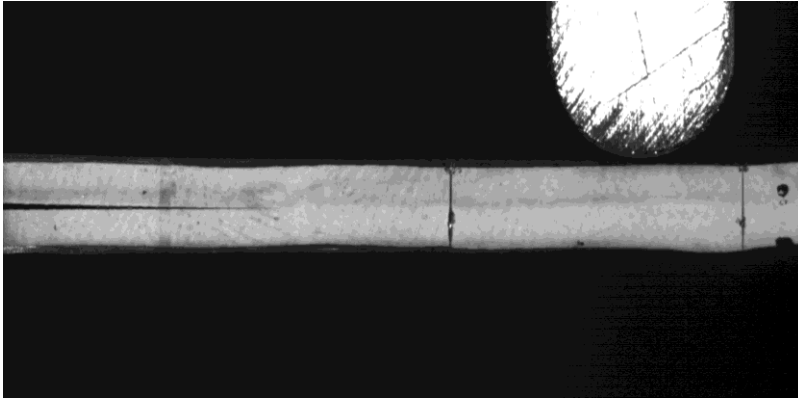


Figure 4.5. Crack detection

All tests were conducted in a MTS machine equipped with a 10 kN load-cell. Both load and displacement were calibrated and had a relative error of 0.86% and 1% , respectively, in the load-displacement ranges used in the tests. The test set-up was designed according to ASTM D6671 [17] and is shown in Figure 4.6. For the analysis performed in this work, which is under displacement controlled conditions, the rate of energy dissipation is calculated through the decrease in the applied work. The weight of the lever is constant, and so is its position for a given mode-mixity. Therefore, the lever weight does not influence in the calculation of the rate of energy dissipation, once this is performed taking the derivative of the decrease in applied work with the number of cycles. When performing a comparison between different mode-mixities, the position of the centre of gravity of the lever did not influence the results. Table 3 shows the material data as obtained by Rodi [18], and the position of the yoke calculated according to the ASTM standard [17]. To gain insight into the damage mechanisms acting during fracture, 13 specimens were analysed in a Scanning Electron Microscope (SEM), after the tests were performed.

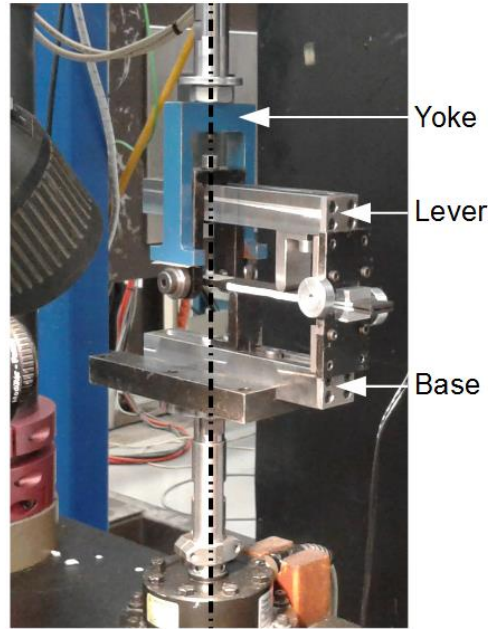


Figure 4.6. MMB apparatus during test

Table 3. (a) Positions on the test fixture; (b) Material data;

G_{II}/G	c (mm)	c_g (mm)
20	90	43
50	40	28
80	27	24

(a)

Material Data	
E_{11} (GPa)	155
E_{22} (GPa)	7.8
G_{12} (GPa)	5.5

(b)

4.2.4 Calculating the physical SERR G^*

The crack growth rate, da/dN , is calculated from the measured crack length throughout the test. Meanwhile, the rate of the average strain energy dissipated per cycle, dU/dN , is calculated from the potential strain energy measured throughout the test. First, the graphs of a versus N and U versus N are plotted, where a is the crack length, U is the potential strain energy of the system and N is the number of cycles. Considering linear elasticity, the potential strain energy is defined as $U = 1/2 P \delta_{\max}$. However, due to the compliance of the test fixture, a small portion of nonlinearity is observed when the load goes from 0 N to δ_{\min} . In order to account for this nonlinearity, a correction is introduced, such that both δ_{\max} and δ_{\min} are used to calculate an approximated U , as shown in Figure 4.7.

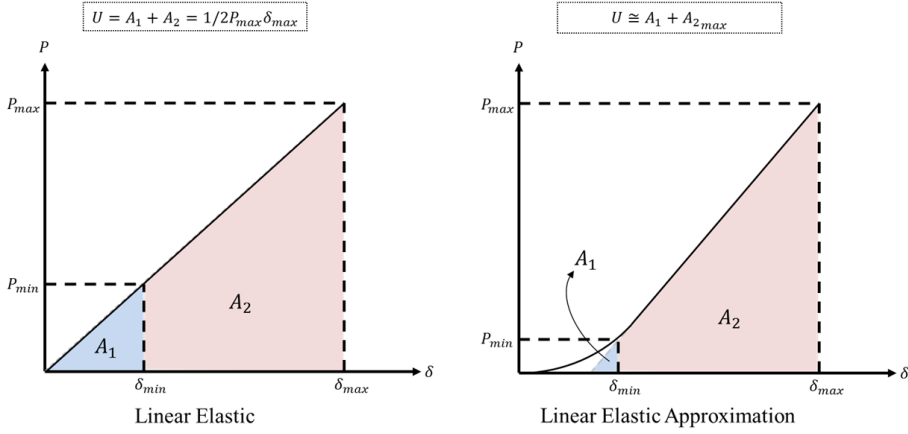


Figure 4.7. Approximation in the calculation of the potential strain energy due to the compliance of the test fixture

The data points obtained are fitted by a seven point incremental polynomial function suggested by ASTM [19], and the rates of crack growth and energy dissipation are calculated from these polynomial fits. Being b the width of the specimen, the physical SERR G^* is then obtained from [13, 20]:

$$G^* = \frac{1}{b} \frac{dU}{dN} = \frac{dU}{dA} \quad (4.5)$$

4.3 Results and Discussion

The results obtained show no displacement ratio or maximum displacement dependence. Furthermore, dU/dA appears to be approximately constant throughout all fatigue tests performed, although tests at 80% of mode II loading seemingly show more scatter at low crack growth rates. The results are presented in Figure 4.8. The correlations between energy dissipation per cycle and damage growth rate are shown in Figure 4.8 (a-c). The energy dissipation per area of crack created is correlated to damage growth rate in Figure 4.8 (d). Although the data is presented on a double logarithmic scale for clarity, each of the results in Figure 4.8 shows linear trends, also if one considers linear plots. Each of these results is discussed in detail hereafter, starting with the behaviour observed in tests at 80% of mode II loading.

When comparing the results for different mode mixities in Figure 4.8, obvious scatter is observed in the results of tests performed at 80% of mode II loading. The first question that is addressed here is: what is the physical explanation for this phenomenon?

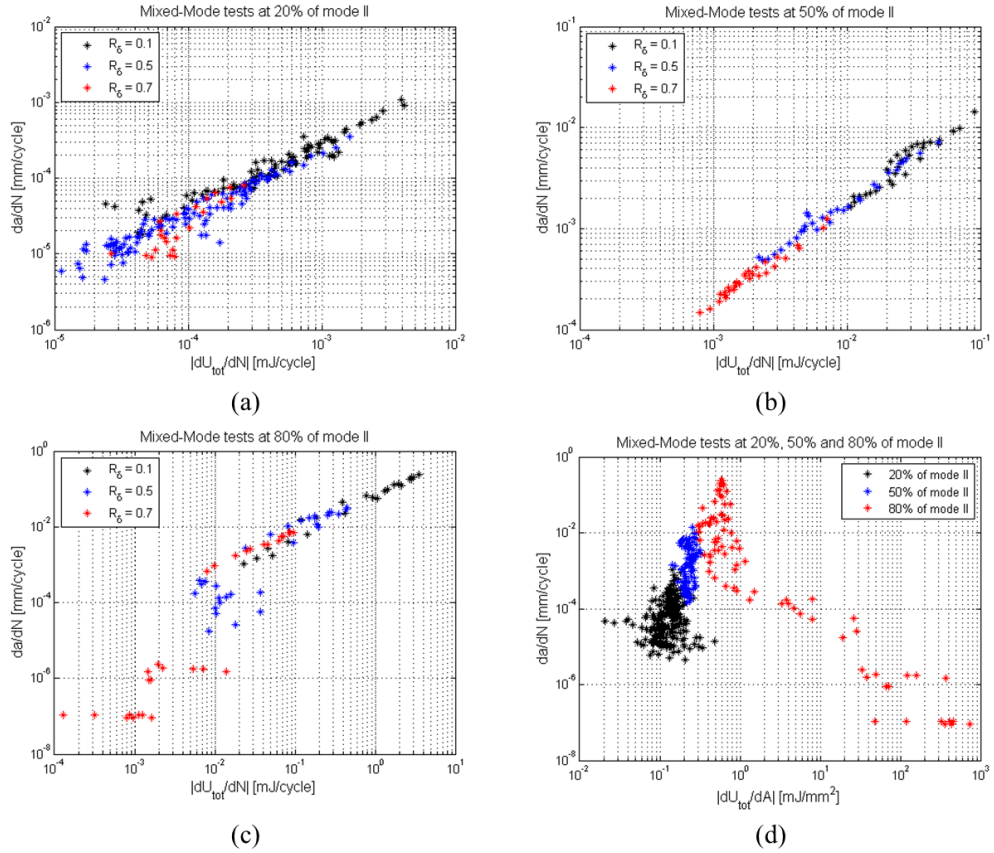


Figure 4.8. Mixed-mode fatigue tests performed at (a) 20% of mode II; (b) 50% of mode II; (c) 80% of mode II; (d) resistance to fatigue crack growth at 20%, 50% and 80% of mode II loading

4.3.1 Process zone effects on mode II dominated fracture

The behaviour observed for low crack growth rates in tests at 80% of mode II loading, shown in Figure 4.8 (c) and (d), is explained by the energy dissipated in the process zone ahead of the physical delamination tip [21]. In mode II delamination extension, a process zone develops with the formation of cusps, striations and microcracks ahead of the crack tip until coalescence is reached and crack growth can be observed from the sides of the specimen [7, 22-25]. These damage mechanisms dissipate a significant amount of energy which is unaccounted for when calculating the crack growth rate da/dN , since the damage in the process zone cannot be visualized and quantified. This causes an error when relating energy dissipation per cycle with crack growth rate. Such an error was shown to be significantly high for tests performed at high displacement ratios [13].

For tests performed at 80% of mode II and high displacement ratios, i.e., $R_\delta = 0.5$ and 0.7 , the same behaviour described for pure mode II fatigue tests in [13] is observed. Figure 4.9 shows the crack length evolution throughout a fatigue test at $R_\delta = 0.5$ and a fracture surface of this test. The zone indicated by the red arrow in Figure 4.9 (a) shows slow crack growth.

Afterwards, the crack grows faster until it is arrested at the location in the specimen underneath the bending load introduction.

The slow crack growth shown in Figure 4.9 (a) is accompanied with the development of the process zone, dissipating substantial strain energy that cannot be correlated to the rate of damage growth, da/dN . On the fracture surfaces corresponding to the areas of process zone development, such as in Figure 4.9 (b), cusps and cracks on the fibre imprints are abundantly observed [13]. Hence, G^* is calculated wrongly for moments when the process zone is developing at expense of crack growth.

Meanwhile, the area with a fast crack growth corresponds to the coalescence of the damage ahead of the crack tip. In this phase, the energy dissipated can be approximately correlated with damage growth, because damage is mainly in the form of visible crack growth due to coalescence of the process zone. However, the measured energy dissipation dU/dN during fast crack growth is correlated to the formation of the entire cracked surface, and not only to the coalescence of the pre-existing damage ahead of the crack. Therefore, this consists on a first approximation, and the reader should be aware that the crack growth rate is, thus, overestimated in this case. To circumvent this problem, more research is necessary in order to understand the energy dissipated per area of crack created in the process zone of mode II dominated delaminations.

Because the physical SERR G^* cannot be calculated when the process zone development dominates damage growth, the crack growth data for these points in tests at $R_\delta = 0.5$ and 0.7 will not be considered in the results. Therefore, moments where process zone is developing, characterized by slow crack growth, such as in Figure 4.9 (a), will be omitted from the results. In a practical manner, this was established such that for tests at 80% of mode II loading, data points in which the crack increment was smaller than 0.1 mm are omitted from now on in this paper. Figure 4.10 shows the correlations between energy dissipation and damage growth for different mode mixities after omitting the points in which process zone effects dominate fracture.

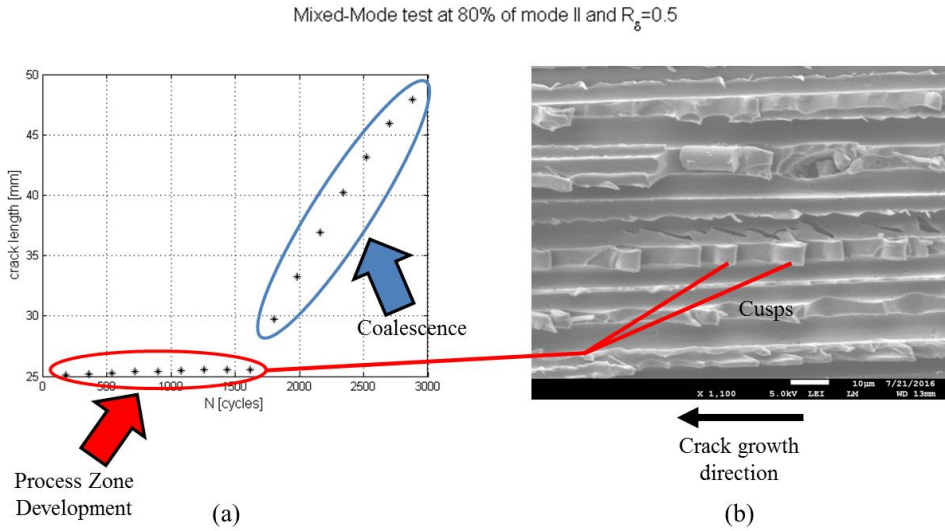


Figure 4.9. (a) Crack length evolution throughout the test shows effects of the process zone; (b) fracture surface of the corresponding fatigue test shows cusps developed

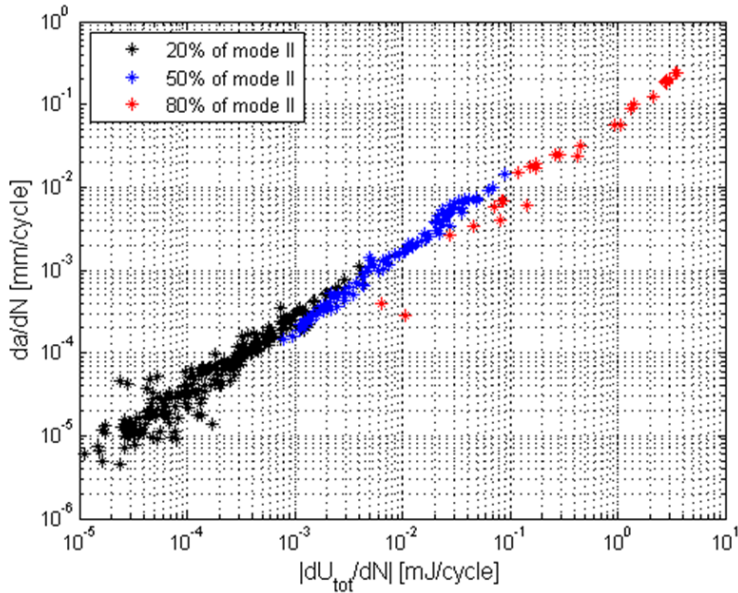


Figure 4.10. Crack growth rate plotted against the energy dissipated per cycle for mixed-mode tests at 20%, 50% and 80% of mode II loading – for 80% of mode II loading, crack increments smaller than 0.1 mm were omitted

For tests performed at 20% and 50% of mode II loading, respectively, a smooth crack growth curve is observed in each of the tests, shown in Figure 4.11 (a) and (c). Figure 4.11 (b) and (d) shows fracture surfaces for these same tests. For the tests performed at 20% of mode II loading, fracture surfaces consist mostly of fibre imprints, brittle cleavage fracture

and ribs, as shown in Figure 4.11 (b). Meanwhile, for tests performed at 50% of mode II loading, the fracture surfaces consist mostly of bare fibres, fibre imprints, more extensive matrix cleavage and some shallow cusps. Features that develop in the process zone, such as striations, deep cracks on the fibre imprints and well-shaped cusps are not dominant on these fracture surfaces like they are on fracture surfaces of tests performed at 80% of mode II, illustrated in Figure 4.9 (b). Therefore, the energy dissipated in the process zone, which is not accounted for in the physical SERR G^* , is taken to be less extensive and to have limited influence in the results for fatigue mixed-mode delamination tests performed at 20% and 50% of mode II loading.

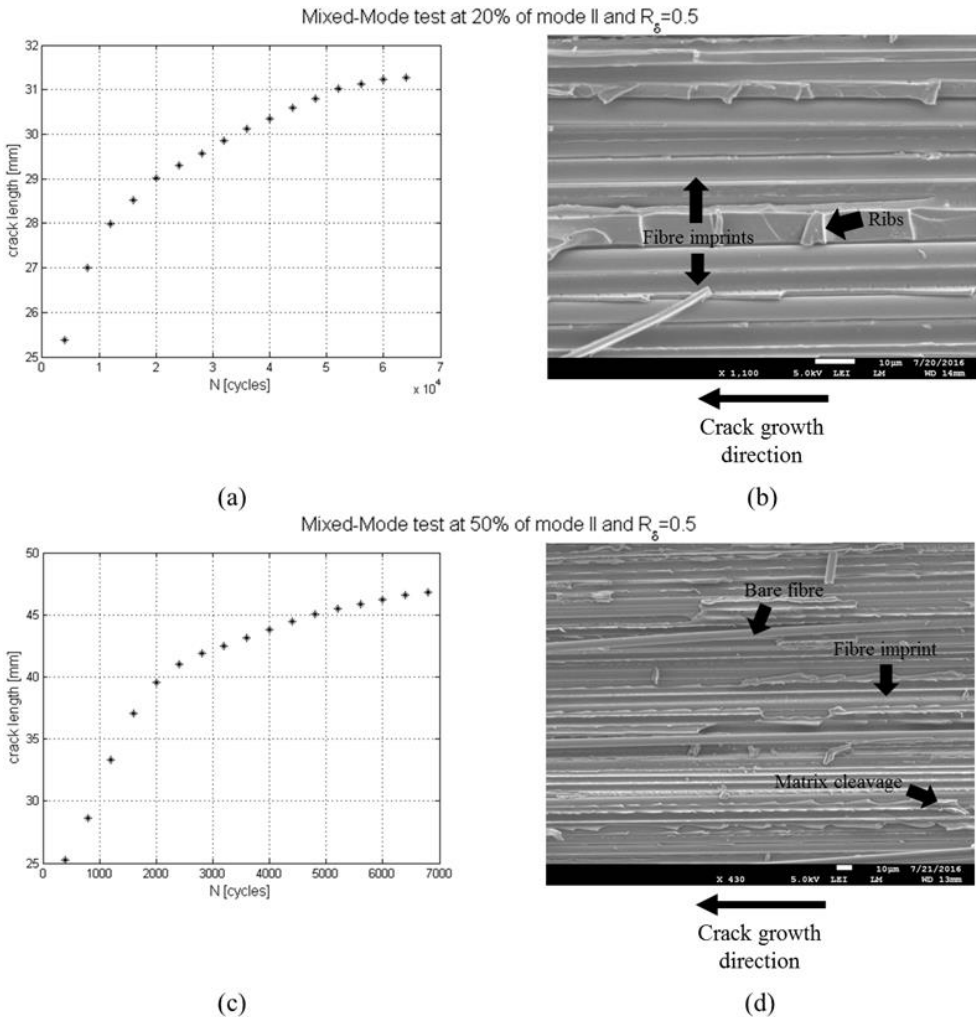


Figure 4.11. (a) crack growth throughout fatigue test at 20 % of mode II and $R_\delta = 0.5$ and (b) respective fracture surface; (c) crack growth throughout fatigue test at 50 % of mode II and $R_\delta = 0.5$ and (d) respective fracture surface;

4.3.2 Effects of applied maximum displacement on delamination growth

Tests at 20% of mode II loading were performed with different maximum displacements and displacement ratios. The results are presented in Figure 4.12 (a-c) and show that damage growth rate and energy dissipation per cycle relate linearly. Although these results are plotted in a logarithmic scale for better visualisation, the reader should note the data relate linearly on a linear scale. This linear relationship aligns with the origin of the coordinate system, which indicates that the energy dissipated per area of crack created dU/dA is approximately constant, regardless of displacement ratio, maximum displacement and crack growth rate.

This behaviour, observed in Figure 4.12 (d), is counterintuitive. More energy is expected to be dissipated per area of crack created at higher crack growth rates, as discussed in chapter 2 of this thesis [16]. However, such an increase in dU/dA is not obvious in mixed-mode. This is due to the fact that for these tests, the damage mechanisms acting in delamination growth were observed to be approximately constant regardless of the applied peak displacement or displacement ratio in the examination of fracture surfaces. New dissipation mechanisms were not observed at higher values of da/dN . The main difference observed on the fracture surfaces was that, at higher crack growth rates, matrix presented higher deformation. However, resin deformation is then limited by matrix plasticity. Plasticity, which is logically expected to increase with the maximum displacement applied, is limited in this brittle material system. Therefore, its effects in energy dissipation are assumed to be negligible.

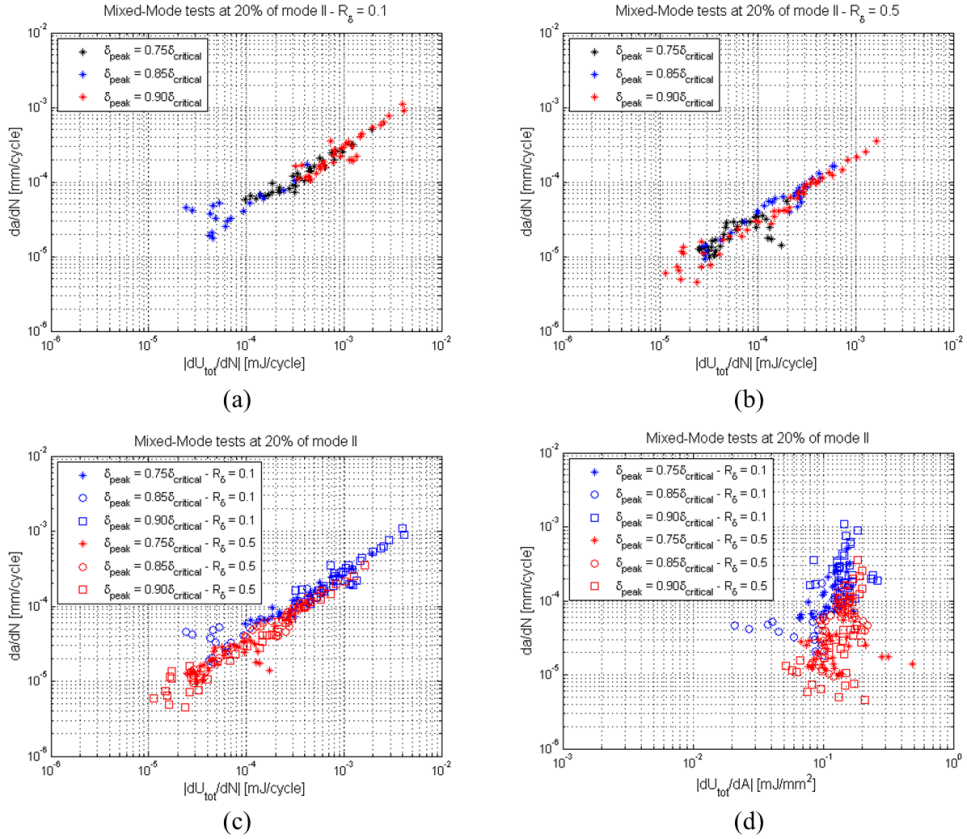


Figure 4.12. Effect of the maximum displacement: (a) tests performed at $R_\delta = 0.1$; (b) tests performed at $R_\delta = 0.5$; (c) all tests performed at 20% of mode II loading; (d) crack growth rate versus energy dissipated per area of crack created for all tests performed at 20% of mode II loading

A higher maximum displacement leads to a higher initial crack growth rate. Figure 4.13 presents fracture surfaces for tests at 20% of mode II under different crack growth rates. More matrix deformation can be observed at a higher crack growth rate, and the fracture surface looks less flat than at a low crack growth rate. This is the main difference between the fracture surfaces in Figure 4.13. However, as discussed above, the low level of plasticity limits the energy consumed by it in delamination growth. Because of this, an increase in dU/dA at higher crack growth rates is not obvious in Figure 4.12 (d), within the present scatter of data.

In addition, for this material system, fatigue fracture at 20% of mode II loading consists basically of fibre pull-out leaving fibre imprints, ribs and some very shallow cusps. No significantly different damage mechanisms were observed at high crack growth rates. The same behaviour is observed for 50% of mode II loading, observed in Figure 4.14. The main difference between the fracture surfaces on Figure 4.14 is also that matrix deformation is more extensive on high crack growth rates, still falling into the case of limited plastic deformation.

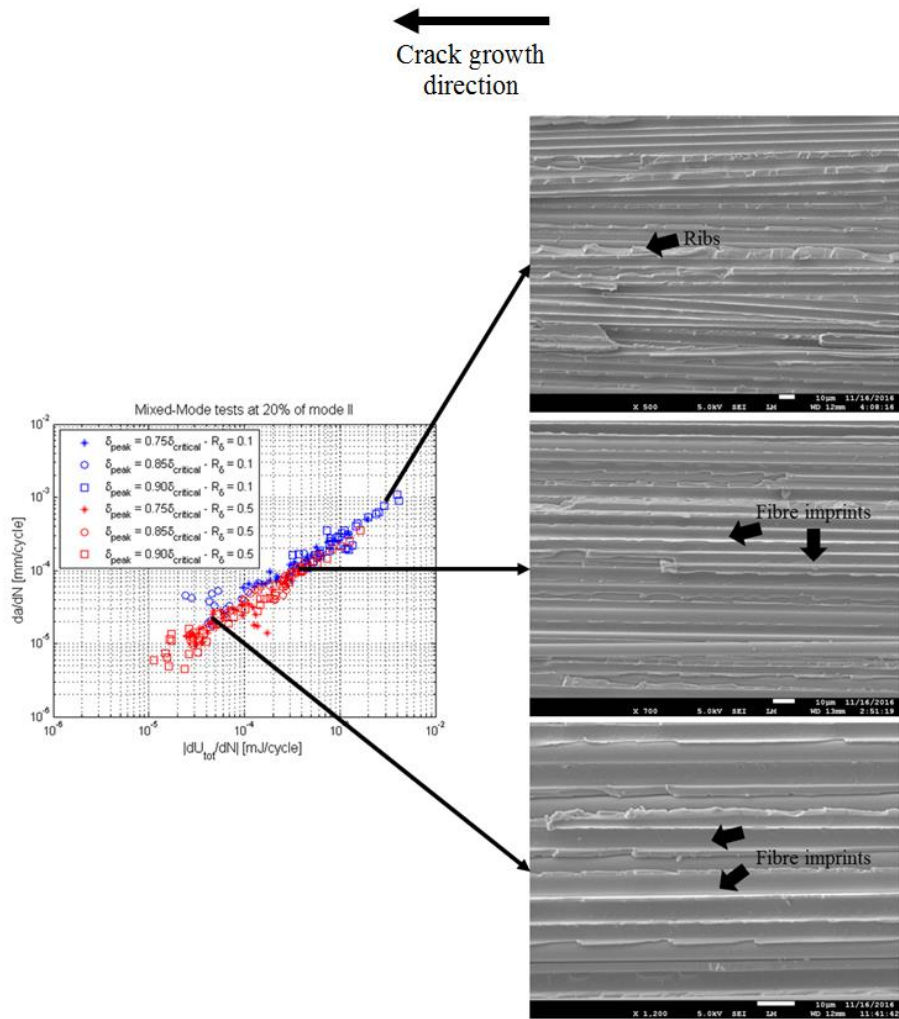


Figure 4.13. Data for 20% of mode II loading. In a higher crack growth rate, more area is created and proportionally more energy is dissipated to do this work, such that dU/dA is constant

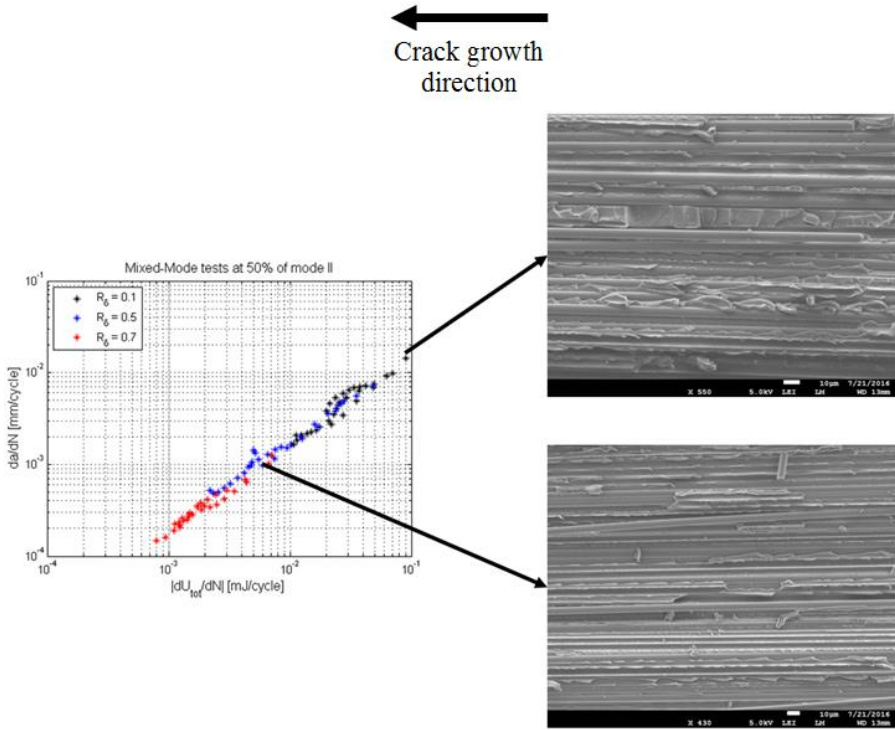


Figure 4.14. Data for 50% of mode II loading. In a higher crack growth rate, more area is created and proportionally more energy is dissipated to do this work, such that dU/dA is constant

4.3.3 Damage mechanisms: the key for understanding energy dissipation in fatigue delamination growth

The results of the present study show that damage mechanisms activated during fatigue loading determine the resistance to delamination growth. Consider Figure 4.15, which shows the results of the MMB fatigue tests performed. The relationship between crack growth rate and energy dissipation per cycle for each mode mixity in Figure 4.15 (a) has a linear relationship. Moreover, each of these linear relationships can be fitted by a straight line going through the origin with a correlation factor R^2 close to 1. This means that for a given mode mixity, the energy dissipated per area of crack created, $G^* = dU/dA$, is approximately constant. The discussion of section 4.3.2. applies to the whole dataset: this approximately constant behaviour of dU/dA is due to the fact that damage mechanisms encountered on the fracture surfaces for each mode mixity were constant independently of the crack growth rate. Nevertheless, it is noteworthy that, for low crack growth rates, the data points seem to deviate from the linear fit for 20% of mode II loading in both Figure 4.15 (a) and (b). This deviation of the experimental data from the linear fit reflects a change in damage mechanisms acting in fracture, and is discussed further at section 4.3.4.

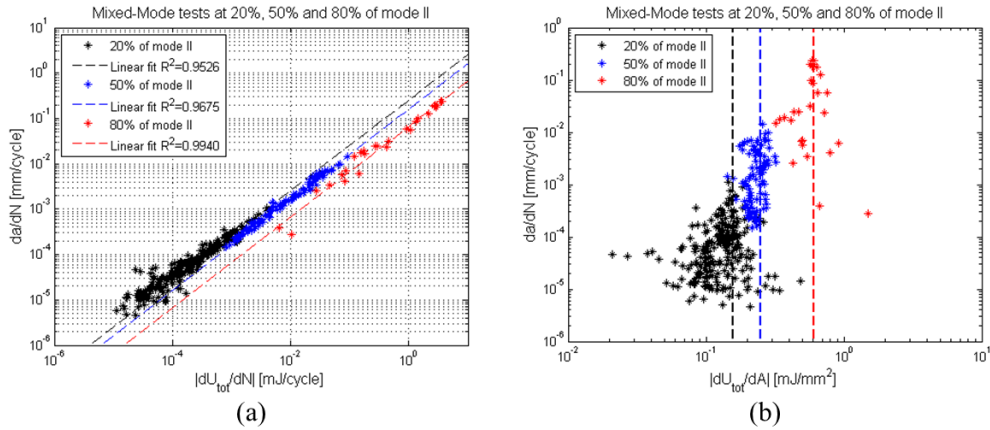


Figure 4.15. (a) relationship between crack growth rate and energy dissipation per cycle fitted with a straight line going through the origin of the coordinate system; (b) relationship between crack growth rate and delamination resistance for each mode mixity

In a similar manner, the relationship between different mode mixities can also be discussed from the perspective of damage mechanisms and energy dissipated in damage growth. Figure 4.15 (b) shows that each different percentage of mode II loading dissipates a different amount of energy per area of crack dU/dA . This occurs because each different mode of loading activates different damage mechanisms, and the energy dissipated to create a crack of area dA depends on the damage mechanisms acting in crack growth.

The trendlines in Figure 4.15 (b) are simply obtained from the inclination of the trendlines fitted to the data in Figure 4.15 (a), taking the width of the specimens into consideration so that the area of fracture is considered. Figure 4.16 (a-c) shows typical damage mechanisms observed on fracture surfaces generated under 20%, 50% and 80% of mode II loading, respectively. For 20% of mode II loading, the main damage mechanisms observed were fibre pull-out, brittle matrix cleavage and the formation of ribs. For 50% of mode II loading more bare fibres are present, suggesting a more extensive interfacial failure. Furthermore, deformation of the matrix during cleavage fracture is more pronounced, ribs are less spaced between themselves and shallow cusps can also be encountered.

Finally, for 80% of mode II loading, cusps and deep cracks on the fibre imprints are the mainly observed features, besides extensive matrix deformation. For each mode of loading, the only obvious change encountered on the fracture surfaces between high and low crack growth rates was in matrix deformation.

This suggests that, for delamination growth in unidirectional composites and a given mode of loading, there might be two main dissipation mechanisms that contribute to a substantial change on the resistance to delamination growth. The first consists of different damage mechanisms that might be activated under different fatigue loading parameters, such as higher maximum displacements. The second factor is the amount of energy dissipated by plasticity during matrix deformation. If the damage mechanisms acting during fracture remain approximately the same and other dissipation mechanisms, such as plasticity, are

negligible, the energy that is dissipated per area of crack created can be approximated to be constant.

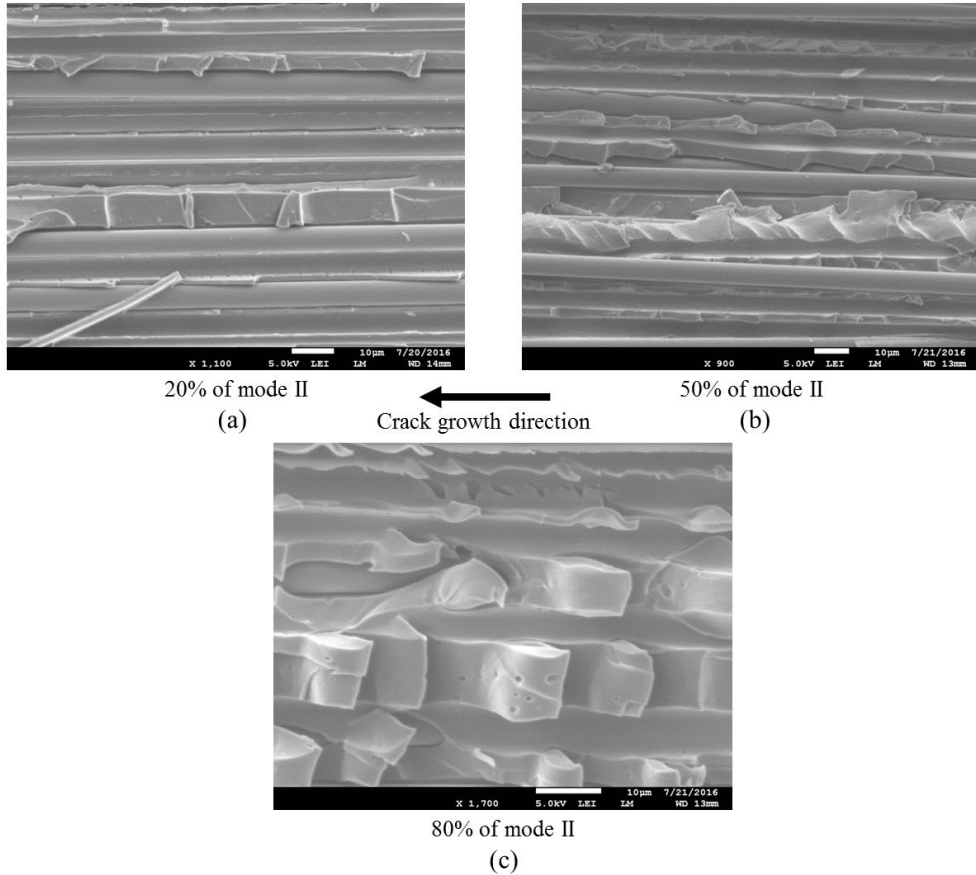


Figure 4.16. Typical damage mechanisms found in fracture surfaces for (a) 20% of mode II loading, (b) 50% of mode II loading and (c) 80% of mode loading

4.3.4 Breakage and pull-out of bridging fibres: changing the damage mechanisms

An example of how different damage mechanisms can change the resistance to delamination growth can be observed in pure mode I DCB fatigue tests performed in the same material system, discussed in [11]. Figure 4.17 shows the correlations between mixed-mode and DCB fatigue tests for the same material. For a better visualization of the results, only the trends of the mixed-mode tests are plotted in Figure 4.17. Figure 4.17 (b) shows that the DCB data, for low crack growth rates, yield similar results to the ones obtained for mixed-mode tests at 20% of mode II loading. At a crack growth rate of approximately 10^{-4} mm/cycle and beyond, however, the DCB data seem to follow a different trend, and the resistance to delamination growth becomes similar to the one obtained for mixed-mode tests at 50% of mode II loading. The explanation behind this change in resistance is in the pull-out and breakage of the bridging fibres.

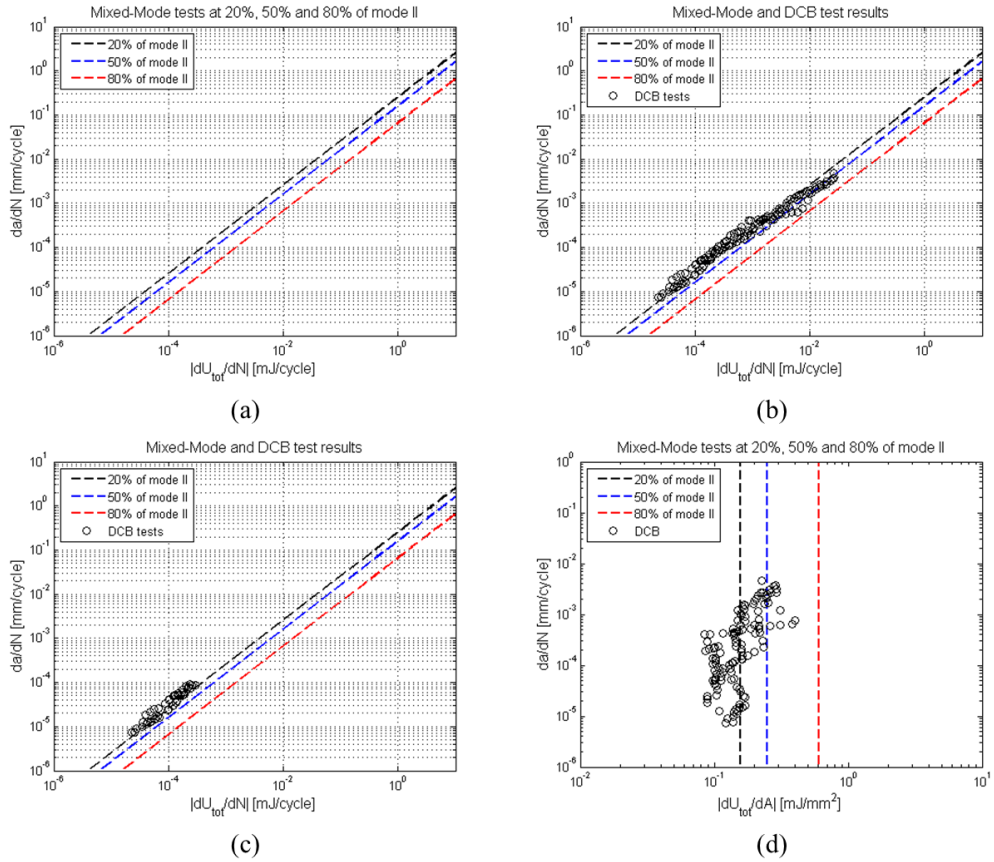


Figure 4.17. Trends obtained for the correlation between energy dissipation per cycle and crack growth rate for (a) mixed-mode tests, (b) mixed-mode and DCB tests and (c) mixed-mode and DCB data without breakage of bridging fibres; (d) correlation between energy dissipation per area and crack growth rate

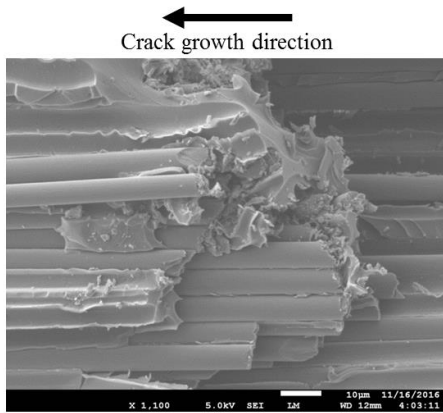
According to what is described by Liaojun et al. [11], at crack growth rates higher than 10^{-4} mm/cycle, a new damage mechanism acts in pure mode I fatigue delamination growth for this material system: the bridging fibres are pulled-out and break, dissipating a significant amount of energy. Figure 4.17 (d) shows that more energy is then released per area of crack created. The pull-out and breakage of bridging fibres, activated at crack growth rates higher than 10^{-4} mm/cycle, increases the resistance of the specimen to delamination growth.

As an example of this effect, Figure 4.17 (c) shows the mixed-mode test trends plotted together with the DCB data not considering the part in which the bridging fibres break. For this case, DCB data have a linear relationship between damage growth rate and energy dissipation per cycle, which is similar to the one for 20% of mode II loading. Similarly, the fracture surfaces for these DCB specimens at crack growth rates smaller than 10^{-4} mm/cycle, discussed in [11, 16], are similar to the ones presented in this work for 20% of mode II loading, which explains the similarity in delamination resistance of these data points.

For mixed-mode tests at 20% of mode II loading, bundles of broken fibres were also observed on the fracture surfaces at high crack growth rates, as shown in Figure 4.18 (a). The pull-out and breakage of these bridging fibres at 20% of mode II loading explain why the data points correlate to a lesser extent with the linear fit at low crack growth rates in Figure 4.15 (a) and (b). This is highlighted in Figure 4.18 (b), which shows that the effect of the breakage of these fibres at 20% of mode II loading becomes dominant at a certain crack growth rate.

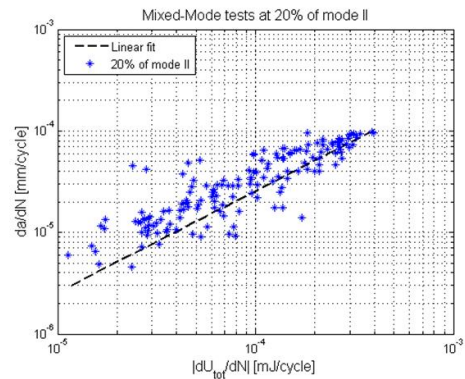
The plot in Figure 4.18 (b) shows mixed-mode data at 20% of mode II loading without the points in which the breakage of bridging fibres occur for pure mode I loading, i.e., crack growth rates higher than 10^{-4} mm/cycle. However, the trend presented in this plot is the one obtained through a linear fit of the data at 20% of mode II loading shown in Figure 4.15 (a), in which crack growth rates higher than 10^{-4} mm/cycle were not excluded. The trend in Figure 4.15 (a) and (b) for 20% of mode II loading fits very well data points at higher crack growth rates. Thus, one can say this linear fit represents the pull-out and breakage of bridging fibres at 20% of mode II loading.

The data points at crack growth rates lower than 10^{-4} mm/cycle, highlighted in Figure 4.18 (b), agree to a lesser extent with the trend obtained in Figure 4.8 (a). At these lower crack growth rates, the pull-out and breakage of bridging fibres is not dominating, and this explains why this linear fit agrees to a lesser extent with data points at crack growth rates smaller than 10^{-4} mm/cycle. This fact indicates that the effect of the pull-out and breakage of these fibres cannot be neglected for mixed-mode tests at 20% of mode II loading. Furthermore, this fact also shows that a change in damage mechanism is responsible for the observed change in the trend of the data.



20% of mode II – $da/dN = 6.7 \times 10^{-4}$ mm/cycle

(a)



(b)

Figure 4.18. (a) bundle of broken fibres at high crack growth ratio – 20% of mode II loading; (b) 20% of mode II loading - test data omitting points in which crack growth rate is higher than 10^{-4} mm/cycle

4.3.5 The “stress ratio effect”

The use of the term “stress ratio effect” to refer to changes in delamination resistance with loading parameters is misleading. In fact, in Paris relationships the appearance of a stress

ratio dependence is not connected to any physical mechanism acting in fracture. Instead, this effect of shifted Paris curves is a consequence of the way data is presented.

Consider the data for 20% of mode II loading at $R_\delta=0.1$ and $R_\delta=0.5$. In order to exemplify that the way we present the data has an effect on the apparent results, Figure 4.19 shows the measured crack growth rates plotted against G_{\max} . The reader can observe that, even if the outlier present on the chart would be disregarded, the curves are clearly shifted for different values of R_δ . Many authors would call this a “stress ratio effect”. However, is this a physical stress ratio effect, or is it an artefact of the way data is presented?

These shifted curves for tests at different values of R_δ were not observed when relating crack growth rate with the physical SERR in Figure 4.12 (c). Furthermore, when analysing the fracture surface, damage mechanisms were approximately constant in tests at 20% of mode II loading under different R_δ . Therefore, there are no physical reasons to call this a stress ratio effect. This behaviour highlights the problems of using similitude parameters, such as G_{\max} , which are not based on the physics of the problem.

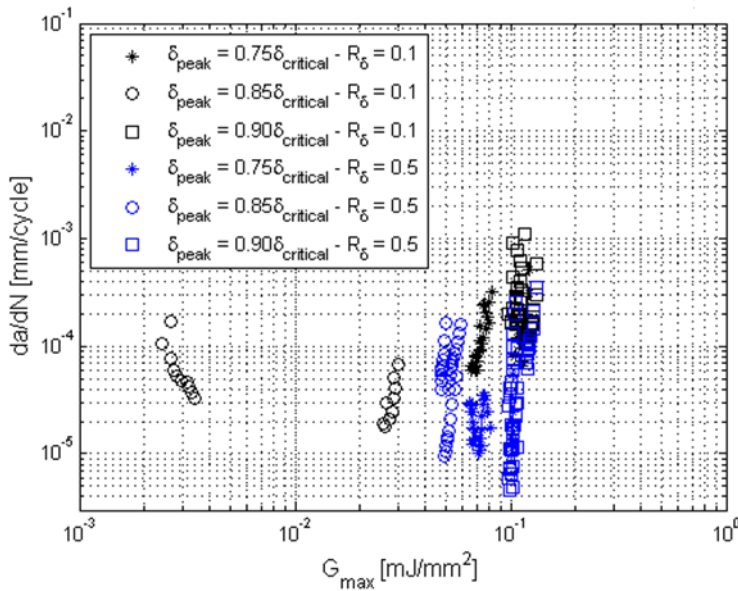


Figure 4.19. Mixed-mode tests performed at 20% of mode II loading – crack growth rate plotted against G_{\max}

Meanwhile, consider Equation (4.3), which describes the macroscopic physics of the problem. Thus, when using the physical SERR, any stress ratio dependence on the relationship between crack growth rate and energy dissipation per cycle must be explained by the physics of damage growth.

Different dissipation mechanisms can be activated by two different loading parameters. The first parameter is the maximum displacement, as the case of the pull-out and breakage of bridging fibres for pure mode I delamination growth. The second parameter is the

displacement ratio, as the case discussed in [13] where the formation and further coalescence of a process zone for pure mode II delamination depend on the amplitude of the fatigue loading. Therefore, even when characterizing fatigue delamination growth with a physics-based equation given by Equation (4.3), one should not bluntly assert that a “stress ratio effect” must or must not be present. First, the relationship between the loading parameters and the dissipation mechanisms they activate in the given material must be known. Once these relationships are known, one can assess whether it is physically plausible to encounter different resistances to delamination under different loading parameters. Moreover, the author reinforces that the term “stress ratio effect” is a misnomer, as discussed elsewhere [26]. The term “stress ratio effect” should not be used. Scientists and engineers should, instead, refer to changes in delamination resistance due to loading parameters.

4.4 Conclusion

Mixed-mode delamination fatigue tests were performed at different mode mixities, displacement ratios and maximum displacements. The physical SERR G^* was used as the similitude parameter, enabling a better understanding of the physics behind the observed phenomena and the characterization of fatigue mixed-mode delamination propagation.

For a given mode mixity, no displacement ratio effect was observed. A higher maximum displacement leads to a higher initial crack growth rate. The energy consumed per area of crack created, however, remains approximately the same. What causes a delamination extension under a specific mode of loading to spend more energy per area of crack created are the different damage mechanisms that might be activated and the energy dissipated by plasticity under certain loading parameters, such as the maximum displacement applied.

For pure mode I loading these mechanisms are the pull-out and breakage of bridging fibres at high crack growth rates. Therefore, the damage features encountered on the fracture surfaces were connected to the energy dissipated on damage growth under fatigue loading. For mode II dominated delamination growth, only an approximation was possible when relating damage created and energy dissipated. This reinforces the necessity of more research into quantifying damage under mode II delamination growth.

Moreover, the term “stress ratio effect” is found to be inappropriate and misleading in case of presenting delamination resistance. With the use of the physical SERR G^* , no dependence with the displacement ratio was found when relating crack growth rate and energy dissipation per cycle. The energy dissipated per area of crack created may change with loading parameters. However, this depends on whether the different loading parameters activate different damage or dissipation mechanisms. Therefore, the existence of a physical stress ratio dependence can only be confirmed for a given material under a certain mode of loading once the relationship between the fatigue loading parameters and the dissipation mechanisms they activate is known.

4.5 References

[1] Reeder JR, Crews J. Redesign of the mixed-mode bending delamination test to reduce nonlinear effects. *Journal of Composites, Technology and Research*. 1992;14:12-9.

- [2] Gustafson C-Go, Hojo M. Delamination Fatigue Crack Growth in Unidirectional Graphite/Epoxy Laminates. *Journal of Reinforced Plastics and Composites*. 1987;6:36-52.
- [3] Jones R, Stelzer S, Brunner AJ. Mode I, II and Mixed Mode I/II delamination growth in composites. *Composite Structures*. 2014;110:317-24.
- [4] Zhang J, Peng L, Zhao L, Fei B. Fatigue delamination growth rates and thresholds of composite laminates under mixed mode loading. *International Journal of Fatigue*. 2012;40:7-15.
- [5] Blanco N, Gamstedt EK, Asp LE, Costa J. Mixed-mode delamination growth in carbon-fibre composite laminates under cyclic loading. *International Journal of Solids and Structures*. 2004;41:4219-35.
- [6] Zhao S, Gadke M, Prinz R. Mixed-Mode Delamination Behavior of Carbon/Epoxy Composites. *Journal of Reinforced Plastics and Composites*. 1995;14:804-26.
- [7] Asp LE, Sjögren A, Greenhalgh ES. Delamination growth and thresholds in a carbon/epoxy composite under fatigue loading. *Journal of Composites, Technology and Research*. 2001;23:55-68.
- [8] Rans C, Alderliesten RC, Benedictus R. Misinterpreting the results: How similitude can improve our understanding of fatigue delamination growth. *Composites Science and Technology*. 2011;71:230-8.
- [9] Pascoe JA, Alderliesten RC, Benedictus R. Towards Understanding Fatigue Disbond Growth via Cyclic Strain Energy. *Procedia Materials Science* 2014;3 (ECF-20):610-5.
- [10] Pascoe JA, Alderliesten RC, Benedictus R. On the relationship between disbond growth and the release of strain energy. *Engineering Fracture Mechanics*. 2015;133:1-13.
- [11] Yao L, Alderliesten R, Benedictus R. Interpreting the stress ratio effect on delamination growth in composite laminates using the concept of fatigue fracture toughness. Submitted to *Composites: Part A*. 2015.
- [12] Yao L, Alderliesten RC, Zhao M, Benedictus R. Discussion on the use of the strain energy release rate for fatigue delamination characterization. *Composites Part A: Applied Science and Manufacturing*. 2014;66:65-72.
- [13] Amaral L, Zarouchas D, Alderliesten R, Benedictus R. Energy dissipation in mode II fatigue crack growth. *Engineering Fracture Mechanics*. 2017;173:41-54.
- [14] Alderliesten RC. How proper similitude can improve our understanding of crack closure and plasticity in fatigue. *International Journal of Fatigue*. 2016;82, Part 2:263-73.
- [15] Griffith AA. The Phenomena of Rupture and Flow in Solids. *Philosophical Transactions of the Royal Society of London Series A, Containing Papers of a Mathematical or Physical Character*. 1921;221:163-98.
- [16] Amaral L, Yao L, Alderliesten R, Benedictus R. The relation between the strain energy release in fatigue and quasi-static crack growth. *Engineering Fracture Mechanics*. 2015;145:86-97.
- [17] ASTM Standard D 6671/ D 6671M-06. Standard Test Method for Mixed Mode I-Mode II Interlaminar Fracture Toughness of Unidirectional Fiber Reinforced Polymer Matrix Composites. US: ASTM International; 2006.
- [18] Rodi R. The residual strength failure sequence in fibre metal laminates: TU Delft, Delft University of Technology; 2012.
- [19] ASTM. Standard Test Method for Measurement of Fatigue Crack Growth Rates. E647-15: ASTM International; 2015.
- [20] Amaral L, Yao L, Alderliesten RC, Benedictus R. Energy based study on quasi-static delamination growth treated as a low cycle fatigue process. In: Siljander A, editor. 34th

Conference and 28th Symposium of the International Committee on Aeronautical Fatigue and Structural Integrity. Helsinki, Finland 2015. p. 240 - 8.

[21] Amaral L, Alderliesten RC, Benedictus R. Towards the Fundamentals of Mode II Fatigue Delamination Growth. 31st Technical Conference of the American Society for Composites. Williamsburg, Virginia, USA 2016.

[22] Corleto C, Bradley W. Mode II Delamination Fracture Toughness of Unidirectional Graphite/Epoxy Composites. *Composite Materials: Fatigue and Fracture*. 1989;2:201-21.

[23] Greenhalgh ES. Failure analysis and fractography of polymer composites: Woodhead Publishing Limited; 2009.

[24] LEE SM. Mode II delamination failure mechanisms of polymer matrix composites. *Journal of Materials Science*. 1997;32:1287-95.

[25] Lee SM. Mode II Interlaminar Crack Growth Process in Polymer Matrix Composites. *Journal of Reinforced Plastics and Composites*. 1999;18:1254-66.

[26] Pascoe JA, Alderliesten RC, Benedictus R. Methods for the prediction of fatigue delamination growth in composites and adhesive bonds - A critical review. *Engineering Fracture Mechanics*. 2013;112-113:72-96.

5 A physics-based relationship for crack growth under different loading modes

In an attempt to understand quasi-static delamination growth under mixed mode loading conditions from a physics-based perspective, this work first evaluated cracking in isotropic materials. The critical Strain Energy Density (SED) approach is adopted, because physically the onset of crack growth is expected to occur when the energy available near the crack tip reaches a critical value.

The main hypothesis of the present paper is that the critical SED for onset of crack growth is constant for a given material, and independent of the loading mode. The relationship derived from this hypothesis therefore relates the physical onset of crack growth and the angle at which that occurs for any opening mode through the SED.

To test this hypothesis, results from literature were taken and shear fracture tests on foam specimens were performed, which both were compared with the derived relationship. The excellent correlation demonstrated the validity of the physics-based relationship, which explains the observed differences between mode I and mode II fracture toughnesses and illustrates why concepts like the Stress Intensity Factor (SIF) alone are insufficient to explain the observations. The developed relationship allows to derive the mode II fracture toughness from mode I fracture toughness tests and the material's mechanical properties.

5.1 Introduction

Quasi-static delaminations are usually characterized by means of the Strain Energy Release Rate (SERR), which is calculated just before the crack propagates and is referred to as the fracture toughness for the onset of delamination growth [1, 2]. However, there is a gap between the macroscopic description of delamination through the SERR and the micromechanisms acting during fracture, as discussed elsewhere [2-4]. Thus, how does the fracture toughness connect with the physics underlying delamination growth? The micromechanisms and the macroscopic behaviour in delamination growth should be connected with a physics-based theory. This would enable a better understanding of this failure mode, which could lead to reliable design rules for the use of composites in aerospace structures.

In order to address this issue, studies available in literature have tried to connect the microscopic damage features with the macroscopic behaviour of damage growth. To this aim, these studies used the SERR and analyses of fracture surfaces to study the effects of resin toughness, resin layer thickness and loading mode in the resistance to delamination [5-10]. A commonly reported result in these studies is that the fracture toughness was observed to be higher for mode II delaminations than for mode I delaminations. The question to be asked at this point is: why? The analytical description of the stresses in the vicinity of the crack tip, such as criterion based on T-stresses [11-13], helps in understanding the problem, but was not able to answer this question yet.

Hibbs and Bradley suggested that the different micromechanisms acting in delamination growth were somehow connected to the difference in the measured fracture toughness for modes I and II. However, they claimed that there must be more to the story [6]. To the present day, a satisfactory answer to this question and the physics connecting delamination growth under different loading modes still have to be addressed.

5.1.1 Motivation

Properly designing composite aircraft structures, reaping all the advantages of their high specific strength and stiffness without overdesigning them, requires a better understanding of delamination. This includes understanding the physics behind delamination growth under different loading modes and how different loading modes relate.

To this aim, uncovering the relationship between the macroscopic resistance to crack propagation and the micromechanisms of delamination is of utmost importance [8].

In addition, once the physics of delamination and the connection between different loading modes are understood, the possibility of calculating fracture toughness data for different loading modes from material properties would dramatically reduce the number of tests necessary to characterize the fracture behaviour of the material. Consider the example in which a physics-based relationship between delamination under modes I and II is clear. Then, only with material properties and mode I fracture toughness data, one would be able to calculate mode II fracture toughness. This would reduce, or even eliminate, the necessity of mode II fracture toughness tests.

5.1.2 Objectives

This study aims to understand quasi-static crack growth from a physics-based perspective, uncovering the fundamental relationship that connects mode I and mode II fracture. This would enable mode II fracture data to be obtained from mode I fracture data and material properties. However, the reader should note that the aim of the present study is not yet to develop an engineering prediction model. Instead, the present study aims at testing the hypotheses presented in Section 5.2 in a broader fashion, using various data sets available in literature.

Therefore, the questions addressed in this chapter are:

- What is the physics-based relationship between mode I and mode II fracture?
- The critical SERR is reported to be higher for mode II than for mode I delamination growth in most cases. What is the physical reason for this?
- How can one estimate mode II fracture toughness from material properties and mode I fracture toughness data?

5.1.3 Methodology

In order to answer the aforementioned questions, the present study scrutinizes quasi-static delamination growth under loading modes I and II. This is accomplished through an analytical description of the stresses and the strain energy concentrated around the crack tip for each case. The starting point of this paper is the analytical treatment of a simpler case, considering mode I and mode II fracture of isotropic, linear elastic, brittle materials. This analysis is followed by the analytical consideration of stresses and strain energy around the crack tip of approximately brittle, orthotropic, linear elastic composite laminates. In order to shed light on the complex mechanisms of mode II delamination growth, rail shear tests were performed in PVC foam specimens, and a qualitative analysis of the delamination process is presented. Finally, the relationship between mode I and mode II fracture is discussed.

5.2 Hypotheses

5.2.1 Fracture and Energy

Fracture, which is decohesion of material, is controlled by energy [14]. When a structure is loaded, potential strain energy is stored in that structure. For a given material, once the strain energy at a certain point of the body reaches a critical value, the onset of fracture occurs. Therefore, fracture is limited by a critical strain energy at which decohesion occurs for a certain material [15, 16]. The critical strain energy for the onset of fracture might be reached by shear stresses, normal stresses or combinations thereof. Therefore, this critical strain energy for the onset of fracture is hypothesized to be independent of the loading mode.

In addition, when analysing crack propagation, instead of considering the stresses at the crack tip, the stresses distributed over a small area around the crack tip will be considered of influence to fracture. This is based on the concept presented in the work of Neuber [17, 18] and also developed later by Lazzarin and colleagues [19, 20], in which stresses distributed around the crack tip are said to provide support to the highly stressed area at the

tip of the crack. Besides, the stress distribution ahead of the crack tip, which changes with the loading mode, was shown to determine the damage mechanisms acting on fracture and observed on the fracture surfaces for ply delaminations [6, 8, 21]. Therefore, in order to account for the damage mechanisms when characterizing the energy dissipated in fracture, the stress distribution around the crack tip must be considered. These hypotheses are thoroughly discussed in further sections of the present work.

5.2.2 Saint-Venant's principle

Following Saint-Venant's principle, only the strain energy stored in the direct vicinity of the crack tip determines the crack increment. The effect of the strain energy stored in areas far away from the crack tip is considered negligible for crack growth.

Therefore, consider the two cracked bodies of the same material, illustrated in Figure 5.1 (a) and (b), loaded under modes I and II, respectively. Now, consider the same arbitrary volume v is used to evaluate the strain energy that causes fracture for both modes I and II, as illustrated in Figure 5.1. The strain energy in this arbitrary volume v due to mode I loading is $w_I(v)$. Similarly, the strain energy in the volume v due to mode II loading is $w_{II}(v)$. Taking into consideration the hypothesis of section 2.1, once the strain energy at a certain point of the body reaches a critical value, the onset of fracture occurs, independently of the loading mode. This is equivalent to saying that $w_I(V) = w_{II}(V)$ at the moment of fracture onset. Logically, if the volume v at which the strain energy is evaluated for both cases in Figure 5.1 is the same, then the critical strain energy per volume that causes the onset of mode I crack growth, s_I , is equal to the critical strain energy per volume that causes the onset of mode II crack growth, s_{II} . Therefore, because of the hypothesis that the strain energy for the onset of fracture is independent of the loading mode, and because the same arbitrary region in the vicinity of the crack tip is being used to compare fracture under any loading mode, the shape and size of this region do not need to be formally defined.

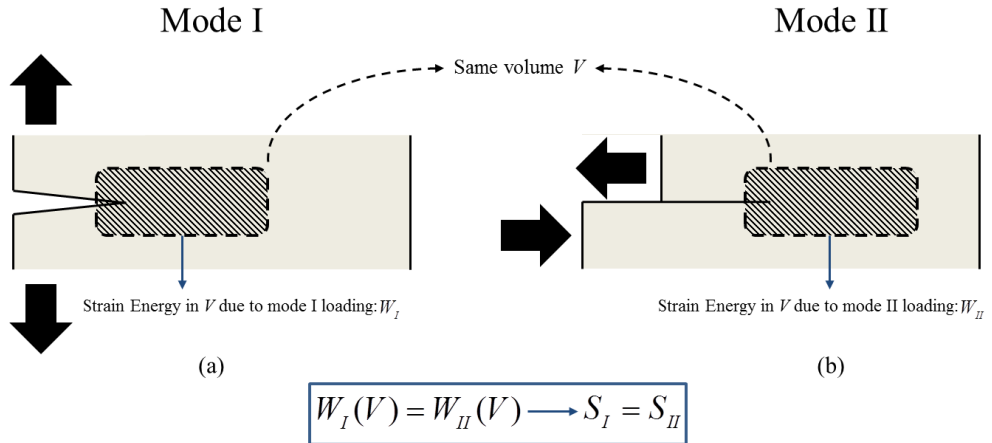


Figure 5.1. (a) cracked body under mode I loading; (b) cracked body under mode II loading. Both cracked bodies are from the same material. The strain energy density S that causes fracture is the same for both loading modes

5.2.3 Pure mode I fracture

Energy dissipation due to other mechanisms besides crack growth such as friction, contact with load introduction structures, fixture compliance and energy dissipation in the process zone ahead of the main crack tip is considered to be small for the onset of mode I fracture. Therefore, the Stress Intensity Factor (SIF) and, consequently, the SERR for the onset of mode I crack growth are considered to include only the effects of energy dissipated in crack increment.

5.3 Rail Shear Tests

In order to understand crack growth under modes I and II and their relationship, the understanding of the formation of a process zone ahead of the crack tip is necessary [4, 21]. According to literature [4, 7, 8, 22, 23], the formation of microcracks in the process zone ahead of the main crack tip and the energy they dissipate on delamination growth are detrimental for mode II crack propagation. Mode I process zones are smaller than mode II process zones, and their effect can be regarded as negligible for delamination extension [7, 8].

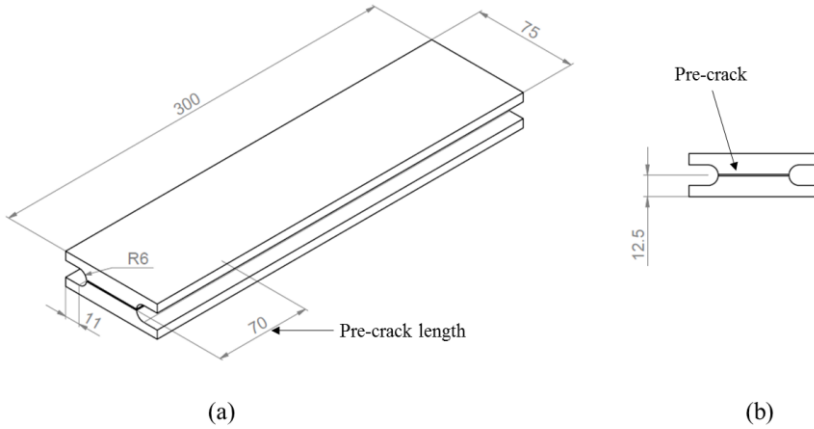
In order to properly observe, at real time, the formation of this process zone, in-situ mode II delamination tests would be necessary. However, the scale and inhomogeneity of mode II delamination makes it very hard to actually observe the phenomenon. Without actual observation the formation of a process zone, common delamination experimental campaigns would hardly shed any light on process zone formation and onset of mode II cracking. Thus, in an attempt to shed light onto the problem of damage mechanisms in mode II delaminations, Greenhalgh and Rogers et al. [24, 25] performed rail shear tests in PVC foam specimens. The shear tested PVC foam yielded a macroscopic fracture surface with morphologies similar to the ones encountered at the microscale in mode II delamination of composites. With the advantage of avoiding the use of a Scanning Electron Microscope (SEM) and enabling naked eye observations of mode II damage mechanisms and process zone formation, the rail shear tests were deemed as a good qualitative representation of mode II delaminations.

Therefore, to better understand mode II process zone formation and support the analyses of the present work, four Divinycell® H-200 PVC foam specimens, identical to the ones used in [24, 25], were tested in a Rail Shear test fixture. The properties of Divinycell® H-200 PVC foam are given in the manufacturer's technical manual [26] and displayed in Table 5.1.

The tests followed the guidelines given by ASTM C-273 [27] and the dimensions of the specimens are shown in Figure 5.2. The chosen cross-section in Figure 5.2 (b) and pre-crack length of 70 mm were the ones that produced cusp-like features on the fracture surfaces of the foam. Specimens with this cross-section were observed to represent mode II delamination fracture surfaces better than the other cross-section geometries proposed in literature, enabling a qualitative investigation of mode II process zone development and cusp formation [24, 25].

Table 5.1. Material properties for Divinycell® H-200 PVC foam [26]

Nominal Density	200 kg/m ³
Tensile Modulus	250 MPa
Shear Modulus	85 MPa

**Figure 5.2. (a) dimensions of the Divinycell H-200 PVC foam specimen; (b) location of the 70 mm long pre-crack created with a saw-cut. All dimensions are in millimetres**

All tests were performed in a hydraulic machine equipped with a 60 kN load cell, using a loading rate of 3 mm/min. A camera was positioned alongside the specimens in order to monitor process zone formation and crack propagation.

5.4 The critical Strain Energy Density

5.4.1 Isotropic Materials

Following the hypotheses that fracture is controlled by energy and that the crack advances when the strain energy around the crack tip reaches a critical value, the strain energy distribution around the crack tip must be determined. To this aim, consider a structure made of an isotropic, linear elastic material under a general three-dimensional stress state. The strain energy stored in an element of volume dV is given by Equation (2.1), where $G = E / 2(1 + \nu)$ is the shear modulus, E is the elastic modulus and ν is Poisson's ratio [28].

$$dW = \left[\frac{1}{2E} (\sigma_x^2 + \sigma_y^2 + \sigma_z^2) - \frac{\nu}{E} (\sigma_x \sigma_y + \sigma_y \sigma_z + \sigma_z \sigma_x) + \frac{1}{2G} (\tau_{xy}^2 + \tau_{xz}^2 + \tau_{yz}^2) \right] dV \quad (5.1)$$

Suppose that this structure has a through-crack that extends in the xz -plane, illustrated in Figure 5.3. The stresses around the crack tip were described by Irwin [29] and are given by

$$\begin{aligned}
\sigma_x &= \frac{K_I}{\sqrt{2\pi r}} \cos(\theta/2) [1 - \sin(\theta/2) \sin(3\theta/2)] - \frac{K_{II}}{\sqrt{2\pi r}} \sin(\theta/2) [2 + \cos(\theta/2) \cos(3\theta/2)] \\
\sigma_y &= \frac{K_I}{\sqrt{2\pi r}} \cos(\theta/2) [1 + \sin(\theta/2) \sin(3\theta/2)] + \frac{K_{II}}{\sqrt{2\pi r}} \sin(\theta/2) \cos(\theta/2) \cos(3\theta/2) \\
\sigma_z &= 2\nu \frac{K_I}{\sqrt{2\pi r}} \cos(\theta/2) - 2\nu \frac{K_{II}}{\sqrt{2\pi r}} \sin(\theta/2) \\
\tau_{xy} &= \frac{K_I}{\sqrt{2\pi r}} \cos(\theta/2) \sin(\theta/2) \cos(3\theta/2) + \frac{K_{II}}{\sqrt{2\pi r}} \cos(\theta/2) [1 - \sin(\theta/2) \sin(3\theta/2)]
\end{aligned} \tag{5.2}$$

with higher order terms in r neglected. K_i stands for the Stress Intensity Factor (SIF), being i the loading mode (I, II or III).

Although the case described is of a crack extension in the xz -plane, the reader should note that any crack is locally under plane strain conditions [29]. Therefore, a stress in the z -direction is considered in this analysis. The reader should be aware that, according to the fracture problem assessed, the stresses presented in Equation (5.2) can be modified to account for a 3D stress state and mode III crack opening.

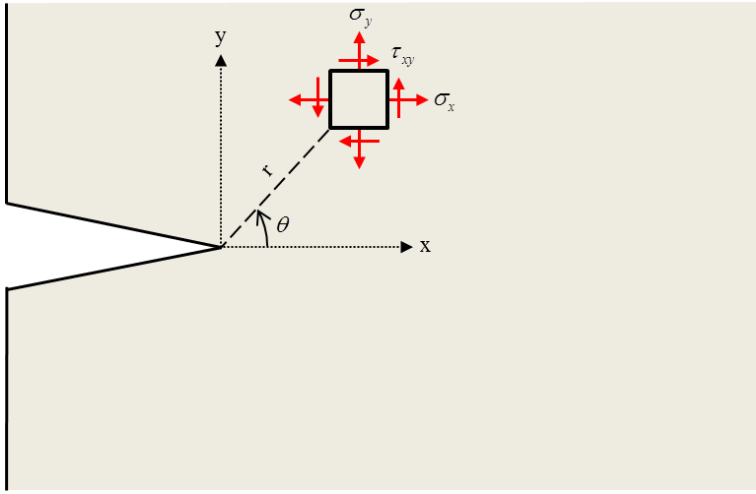


Figure 5.3. Stresses around the tip of a through crack extending on the xy -plane

Substituting the stresses given by Equation (5.2) in Equation (2.1), one obtains the strain energy stored in a volume element dV at any point around the crack tip, which is

$$\frac{dW}{dV} = \frac{1}{\pi r} (a_{11}K_I^2 + 2a_{12}K_IK_{II} + a_{22}K_{II}^2) \tag{5.3}$$

The intensity of the strain energy density field around the crack tip is, then, given by

$$S = a_{11}K_I^2 + 2a_{12}K_IK_{II} + a_{22}K_{II}^2 \tag{5.4}$$

where the coefficients a_{11} , a_{12} and a_{22} are given by

$$\begin{aligned} a_{11} &= \frac{1}{16G} [(3 - 4\nu - \cos \theta)(1 + \cos \theta)] \\ a_{12} &= \frac{1}{16G} 2 \sin \theta [\cos \theta - (1 - 2\nu)] \\ a_{22} &= \frac{1}{16G} [4(1 - \nu)(1 - \cos \theta) + (1 + \cos \theta)(3 \cos \theta - 1)] \end{aligned} \quad (5.5)$$

This concept and the term s , known as Strain Energy Density (SED), were first introduced by Sih and colleagues in a series of investigations on fracture mechanics of brittle materials [15, 16, 30].

For the cases of pure mode I and pure mode II loading, the SED is given by respectively

$$S_I = \frac{K_I^2}{16G} [(3 - 4\nu - \cos \theta)(1 + \cos \theta)] \quad (5.6)$$

$$S_{II} = \frac{K_{II}^2}{16G} [4(1 - \nu)(1 - \cos \theta) + (1 + \cos \theta)(3 \cos \theta - 1)] \quad (5.7)$$

5.4.2 Orthotropic Materials

Consider, once more, a structure with a through-crack that extends on the xz -plane, shown in Figure 5.3. This time the structure is made of a linear elastic, orthotropic material. In this case, the strain energy stored in a volume element dV is

$$\frac{dW}{dV} = \frac{1}{2} \left[\frac{\sigma_x^2}{E_x} + \frac{\sigma_y^2}{E_y} + \frac{\sigma_z^2}{E_z} + \frac{\tau_{xy}^2}{G_{xy}} \right] - \frac{\nu_{xy} \sigma_x \sigma_y}{E_x} - \frac{\nu_{xz} \sigma_x \sigma_z}{E_x} - \frac{\nu_{yz} \sigma_y \sigma_z}{E_y} \quad (5.8)$$

The stresses around the crack tip of orthotropic bodies were described by Sih et al. [30] and are given in the expressions in

$$\begin{aligned} \sigma_x &= \frac{K_I}{\sqrt{2\pi r}} A_I + \frac{K_{II}}{\sqrt{2\pi r}} A_{II} \\ \sigma_y &= \frac{K_I}{\sqrt{2\pi r}} B_I + \frac{K_{II}}{\sqrt{2\pi r}} B_{II} \\ \sigma_z &= \left(\frac{K_I}{\sqrt{2\pi r}} A_I + \frac{K_{II}}{\sqrt{2\pi r}} A_{II} \right) \frac{\nu_{xz} E_z}{E_x} + \left(\frac{K_I}{\sqrt{2\pi r}} B_I + \frac{K_{II}}{\sqrt{2\pi r}} B_{II} \right) \frac{\nu_{yz} E_z}{E_y} \\ \tau_{xy} &= \frac{K_I}{\sqrt{2\pi r}} C_I + \frac{K_{II}}{\sqrt{2\pi r}} C_{II} \end{aligned} \quad (5.9)$$

The coefficients A_i , B_i and C_i , for $i=I$ and II , are given in

$$\begin{aligned}
A_I &= \text{Re} \left\{ \frac{\mu_1 \mu_2}{\mu_1 - \mu_2} \left(\frac{\mu_2}{\sqrt{\cos \theta + \mu_2 \sin \theta}} - \frac{\mu_1}{\sqrt{\cos \theta + \mu_1 \sin \theta}} \right) \right\} \\
A_{II} &= \text{Re} \left\{ \frac{1}{\mu_1 - \mu_2} \left(\frac{\mu_2^2}{\sqrt{\cos \theta + \mu_2 \sin \theta}} - \frac{\mu_1^2}{\sqrt{\cos \theta + \mu_1 \sin \theta}} \right) \right\} \\
B_I &= \text{Re} \left\{ \frac{1}{\mu_1 - \mu_2} \left(\frac{\mu_1}{\sqrt{\cos \theta + \mu_2 \sin \theta}} - \frac{\mu_2}{\sqrt{\cos \theta + \mu_1 \sin \theta}} \right) \right\} \\
B_{II} &= \text{Re} \left\{ \frac{1}{\mu_1 - \mu_2} \left(\frac{1}{\sqrt{\cos \theta + \mu_2 \sin \theta}} - \frac{1}{\sqrt{\cos \theta + \mu_1 \sin \theta}} \right) \right\} \\
C_I &= \text{Re} \left\{ \frac{\mu_1 \mu_2}{\mu_1 - \mu_2} \left(\frac{1}{\sqrt{\cos \theta + \mu_1 \sin \theta}} - \frac{1}{\sqrt{\cos \theta + \mu_2 \sin \theta}} \right) \right\} \\
C_{II} &= \text{Re} \left\{ \frac{1}{\mu_1 - \mu_2} \left(\frac{\mu_1}{\sqrt{\cos \theta + \mu_1 \sin \theta}} - \frac{\mu_2}{\sqrt{\cos \theta + \mu_2 \sin \theta}} \right) \right\}
\end{aligned} \tag{5.10}$$

μ_1 and μ_2 are obtained from each of the conjugate pair of roots of $A_{11}\mu^4 + (2A_{12} + A_{66})\mu^2 + A_{22} = 0$, where the coefficients A_{11} , A_{12} , A_{22} and A_{66} are obtained from the stress-strain relationships in [31]

$$\begin{aligned}
\varepsilon_x &= A_{11}\sigma_x + A_{12}\sigma_y + A_{13}\sigma_z + A_{16}\tau_{xy} \\
\varepsilon_y &= A_{21}\sigma_x + A_{22}\sigma_y + A_{23}\sigma_z + A_{26}\tau_{xy} \\
\varepsilon_x &= A_{61}\sigma_x + A_{62}\sigma_y + A_{63}\sigma_z + A_{66}\tau_{xy}
\end{aligned} \tag{5.11}$$

Substituting the stresses from Equation (5.9) in Equation (5.8), one obtains

$$\frac{dW}{dV} = \frac{1}{2\pi r} (K_I^2 D_1 + K_{II}^2 D_2 + K_I K_{II} D_3) \tag{5.12}$$

Where the SED is $S = K_I^2 D_1 + K_{II}^2 D_2 + K_I K_{II} D_3$ and the coefficients D_i , for $i = 1, 2$ and 3 , are given by

$$\begin{aligned}
D_1 &= \frac{A_I^2}{2E_x} + \frac{B_I^2}{2E_y} + \frac{C_I^2}{2G_{xy}} - \frac{A_I B_I \nu_{xy}}{E_x} - \frac{A_I^2 \nu_{xz}^2 E_z}{2E_x^2} - \frac{B_I^2 \nu_{yz}^2 E_z}{2E_y^2} - \frac{A_I B_I \nu_{xz} \nu_{yz} E_z}{E_x E_y} \\
D_2 &= \frac{A_{II}^2}{2E_x} + \frac{B_{II}^2}{2E_y} + \frac{C_{II}^2}{2G_{xy}} - \frac{A_{II} B_{II} \nu_{xy}}{E_x} - \frac{A_{II}^2 \nu_{xz}^2 E_z}{2E_x^2} - \frac{B_{II}^2 \nu_{yz}^2 E_z}{2E_y^2} - \frac{A_{II} B_{II} \nu_{xz} \nu_{yz} E_z}{E_x E_y} \\
D_3 &= \frac{A_I A_{II}}{E_x} + \frac{B_I B_{II}}{E_y} + \frac{C_I C_{II}}{G_{xy}} - \frac{A_I B_{II} \nu_{xy}}{E_x} - \frac{A_{II} B_I \nu_{xy}}{E_x} - \frac{A_I A_{II} \nu_{xz}^2 E_z}{E_x^2} - \frac{B_I B_{II} \nu_{yz}^2 E_z}{E_y^2} - \frac{A_I B_{II} \nu_{xz} \nu_{yz} E_z}{E_x E_y} - \frac{A_{II} B_I \nu_{xz} \nu_{yz} E_z}{E_x E_y}
\end{aligned} \tag{5.13}$$

A useful application is to use Equation (5.12) to determine the critical SED for delamination growth in orthotropic composite structures. The reader should note, however, that this consists of an approximation. The expressions of the stresses around the crack tip in Equation (5.9) were developed for homogeneous bodies. However, composites are obviously not homogeneous. Hence, the reader should be aware that Equation (5.9) does not give exact solutions for stresses around the crack tip of an orthotropic composite structure. Furthermore, the calculation of SIF's for composites is not straightforward. Therefore, writing Equation (5.12) in terms of the SERR is useful, once the SERR is easier to be determined for composites than the SIF. For orthotropic materials under plane stress the SERR for both mode I and mode II loading are [31]

$$\begin{aligned} G_I &= F_I K_I^2 \\ G_{II} &= F_{II} K_{II}^2 \end{aligned} \quad (5.14)$$

Where

$$F_I = \sqrt{\frac{A_{11}A_{22}}{2}} \left[\sqrt{\frac{A_{22}}{A_{11}}} + \frac{2A_{12} + A_{66}}{2A_{11}} \right]^{1/2} \quad (5.15)$$

$$F_{II} = \frac{A_{11}}{\sqrt{2}} \left[\sqrt{\frac{A_{22}}{A_{11}}} + \frac{2A_{12} + A_{66}}{2A_{11}} \right]^{1/2} \quad (5.16)$$

And the coefficients A_{11} , A_{12} , A_{22} and A_{66} are given in Equation (5.11). Under plane strain conditions, Equations (5.15) and (5.16) should be used with the following substitution

$$A_{ij} = A_{ij} - \frac{A_{i3}A_{j3}}{A_{33}} \quad (5.17)$$

5.4.3 Strain Energy Density and Potential energy in the system

The relationship between the potential energy that goes into the structure and the strain energy density has been discussed by Sih [15]. However, for convenience of the reader, this relationship is summarized in the present section.

Consider a structured loaded under its linear elastic limits. The potential energy per unit volume of an element located at a distance r from the crack tip is P , while the strain energy per unit volume is $U = dW / dV$. If the cracked body is subjected to displacement controlled loading, the strain energy is equal to the negative of the potential energy, such that $P = -U$. However, as $U = dW / dV = S / r$, then

$$P = \frac{-S}{r} \quad (5.18)$$

Crack propagation is assumed to occur in the direction where the potential energy density is maximum, which means

$$\begin{aligned} \frac{\partial P}{\partial \theta} &= 0, \theta = \theta_0 \\ \frac{\partial^2 P}{\partial \theta^2} &< 0, \theta = \theta_0 \end{aligned} \quad (5.19)$$

Rewriting Equation (5.19) in terms of the SED, one obtains a condition for the critical SED, i.e., the SED at which the onset of crack propagation occurs:

$$\begin{aligned}\frac{\partial S}{\partial \theta} &= 0, \theta = \theta_0 \\ \frac{\partial^2 S}{\partial \theta^2} &> 0, \theta = \theta_0\end{aligned}\quad (5.20)$$

Applying the conditions expressed in equation (5.20) to Equation (5.6), the SED is shown to achieve a minimum value at $\theta_0 = 0^\circ$ for a linear elastic, isotropic material under pure mode I loading. In this case, the critical SED is

$$S_{I_{cr}} = \frac{K_{I_{cr}}^2 (1-2\nu)}{4G} \quad (5.21)$$

Similarly, applying the conditions in Equation (5.20) to Equation (5.7), the SED is shown to achieve a minimum value at $\cos(\theta_0) = (1-2\nu) / (4G)$ for a linear elastic, isotropic material under pure mode II loading. The critical SED is, then:

$$S_{II_{cr}} = \frac{K_{II_{cr}}^2 [8(1-\nu) - 4\nu^2]}{48G} \quad (5.22)$$

5.5 Results and Discussion

5.5.1 Brittle Isotropic Materials

Following the discussion in Section 5.2 of the present work, fracture is controlled by energy. When the SED around the crack tip reaches a critical value, crack growth occurs. From the perspective of the material, the energy necessary for the onset of crack growth is independent of the loading mode. Therefore, one can state that the critical SED necessary for the onset of a pure mode I crack is the same as the critical SED necessary for the onset of a pure mode II crack:

$$S_{I_{cr}} = S_{II_{cr}} \quad (5.23)$$

Equation (5.23) presents the relationship between loading modes I and II. Furthermore, using Equations (5.21), (5.22) and (5.23), one obtains a way of determining the mode II SIF from mode I SIF and material data. This concept of determining mode II fracture toughness from mode I fracture toughness and material data, which is a direct consequence of Equation (5.23), will be referred to, from now on, as the critical SED approach. The reader should note, however, that

$$\frac{K_{II_{cr}}}{K_{I_{cr}}} = \left(\frac{12(1-2\nu)}{8-8\nu-4\nu^2} \right)^{1/2} \quad (5.24)$$

is limited to linear elastic, brittle, isotropic materials.

Plotting (5.24) enables to visualize how the critical mode I and mode II SIFs relate according to Poisson's ratio, as given in Figure 5.4. Equation (5.24) shows how pure mode I and pure mode II SIFs relate for linear elastic, brittle, isotropic materials. In order to test whether this relationship can indeed be used for predicting the pure mode II critical SIF or not, Equation (5.24) is applied to different materials reported in literature in the following sections of the present work.

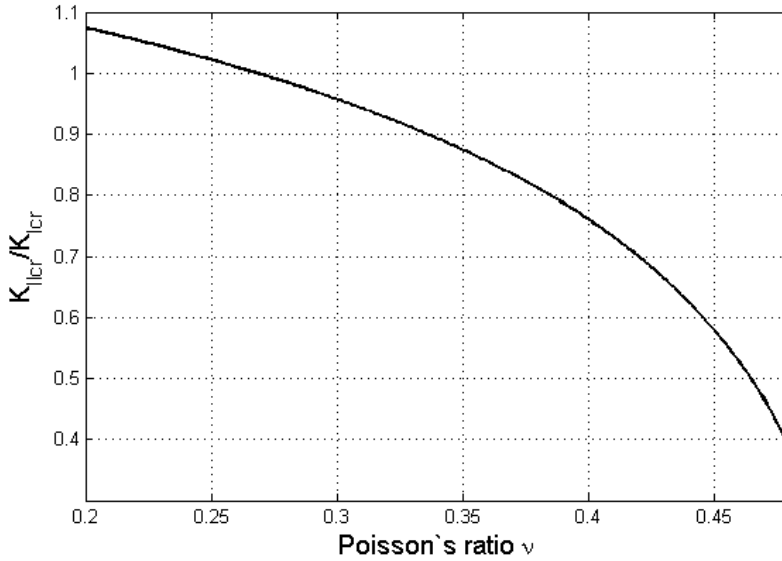


Figure 5.4. Theoretical relationship between K_{IIcr}/K_{Icr} and Poisson's ratio – modes I and II SIF for brittle, linear elastic, isotropic materials

Plexiglass

Erdogan et al. [32, 33] performed a series of fracture mechanics tests on Plexiglass, a brittle, isotropic, linear elastic material. In their experiments, the authors obtained a Poisson's coefficient of $\nu = 0.3447 \pm 0.0254$ and a ratio between the critical SIFs for fracture under pure modes I and II of

$$\left(\frac{K_{IIcr}}{K_{Icr}} \right)_{\text{experiment}} = 0.89 \pm 0.12 \quad (5.25)$$

Using only Poisson's coefficient for Plexiglass in Equation (5.24), one obtains through the critical SED approach that

$$\left(\frac{K_{IIcr}}{K_{Icr}} \right)_{\text{SED}} = 0.88 \pm 0.09 \quad (5.26)$$

The prediction of equation (5.26) is in very good agreement with the experimental result from Erdogan et al. in Equation (5.25). This suggests that, for Plexiglass, the strain energy density distributed around the crack tip controls fracture, and the critical strain energy density for fracture is, indeed, independent of the loading mode.

Rock samples

In order to test the validity of Equation (5.24) for other brittle materials, fracture data from rock samples were obtained from literature and analysed using the critical SED approach. The comparison between experimental data and the prediction via SED is listed in Table 5.2. The Poisson's ratio and $(K_{IIc}/K_{Ic})_{\text{experiment}}$ were obtained from experiments described in literature. $(K_{IIc}/K_{Ic})_{\text{SED}}$ is the prediction obtained through Equation (5.24).

Table 5.2. Comparison of pure modes I and II fracture toughness obtained from experiments described in literature with fracture toughness predicted by the SED

Rock	ν	$(K_{IIc}/K_{Ic})_{\text{experiment}}$	$(K_{IIc}/K_{Ic})_{\text{SED}}$	References for experimental data
Westerly Granite	0.20	≈ 1.10	1.07	[34, 35]
Indiana Limestone	0.32	≈ 1.10	0.93	[35, 36]
Dry snow	0.20	1.10	1.07	[37-39]

The prediction of $(K_{IIc}/K_{Ic})_{\text{SED}}$ seems to be in good agreement with the experimental data obtained from literature. Therefore, one would be able to calculate with good accuracy pure mode II fracture toughness possessing only pure mode I fracture toughness and material data. However, the reader should note that there are limitations when using data from rock samples, once it is notoriously difficult to subject rock specimens to pure traction or shear [38, 40].

In addition, Backers observed a significant variation on the experimentally obtained values of $(K_{IIc}/K_{Ic})_{\text{experiment}}$ described in literature [40]. An example of this variation is shown in Table 5.3. The experimental values of pure mode I and II fracture toughness can vary, among other things, with the rock subtype, grain size, moisture content and type of test method used. The same rock can present different material behaviour, such as plasticity, in case these properties change [38]. A simple example is Poisson's ratio for Indiana Limestone, which is assumed by Ingraffea [35] to be equal to $\nu=0.20$, while Daneshy [36] used $\nu=0.32$. In the results presented in Table 5.2, $\nu=0.32$ was used for being the value of Poisson's ratio that yielded the worst prediction in comparison with the experimental data, in order to show the limitations of the results. This shows that, even with a significant variation in ν , the worst prediction for Indiana Limestone through the SED approach still yields a result that is in relatively good agreement with the experimental data. Furthermore, the critical SED approach developed here is shown to be of valuable use to linear elastic, isotropic, brittle materials. Therefore, scientists and engineers must analyse to what extent the critical SED can be used to characterize the material in question.

Table 5.3. Variation on the experimental results of pure modes I and II fracture toughness found in literature [40]

Rock	$K_{I_{cr}}$ (MPa.m) ^{1/2}	$K_{II_{cr}}$ (MPa.m) ^{1/2}	$(K_{II_{cr}}/K_{I_{cr}})_{\text{experiment}}$
Sandstone	From 0.67 to 2.56	From 0.32 to 4.95	From 0.48 to 1.93
Marble	From 0.46 to 2.25	From 3.33 to 6.36	From 2.83 to 7.23

5.5.2 Orthotropic Composite Laminates

The critical SED approach can be used in order to study delamination growth in orthotropic laminates. Suppose a delamination under pure mode I loading in a linear elastic, orthotropic laminate. The critical SED is given by

$$S_{I_{cr}} = \frac{G_{I_{cr}}}{F_I} D_1(\theta_{0_I}) \quad (5.27)$$

Where D_I is given in Equation (5.13) and it has a minimum value at θ_{0_I} , F_I is obtained from equation (5.15) and $G_{I_{cr}}$ is the critical SERR for the onset of mode I delamination. The latter is typically obtained via a Double Cantilever Beam (DCB) test, described by an ASTM standard [1]. Similarly, for pure mode II loading,

$$S_{II_{cr}} = \frac{G_{II_{cr}}}{F_{II}} D_2(\theta_{0_{II}}) \quad (5.28)$$

Therefore, applying Equations (5.26) and (5.27) to the condition in Equation (5.23), the critical SED approach can be used to characterize the critical SED to fracture in delamination growth. The critical SERR for the onset of mode II delamination can be estimated from material properties and pure mode I delamination tests:

$$G_{II_{cr}} = G_{I_{cr}} \frac{F_{II}}{F_I} \frac{D_1(\theta_{0_I})}{D_2(\theta_{0_{II}})} \quad (5.29)$$

HTA/6376C carbon/epoxy composite

In order to test the critical SED approach in delamination growth of orthotropic composite laminates, data from different sources in literature were obtained and the estimated $G_{II_{cr}}$ was compared to the ones obtained via experiments. Usually, the mode II critical SERR was obtained testing End Notch Flexure specimens, recently described by an ASTM standard [41].

The first composite system analysed was HTA/6376C carbon/epoxy used by Asp et al. in two different studies [42, 43]. The material data given in literature is described in Table 5.4. The specimen lay-up was (012//($\pm 5/04$)S). The sign “//” refers to the plane of the artificial delamination. According to Asp et al., the offaxis angle was introduced to reduce fibre bridging at delamination growth. The specific lay-up was chosen to allow a small off-axis interface angle, while keeping the specimen properties close to those of a unidirectional specimen [43].

Table 5.4. Material data for HTA/6376C carbon/epoxy system

Young's Modulus	$E_x = 146 \text{ GPa}$ and $E_y = E_z = 10.5 \text{ GPa}$
Shear Modulus	$\mathcal{G}_{xy} = \mathcal{G}_{xz} = 5.25 \text{ GPa}$ and $\mathcal{G}_{yz} = 3.48 \text{ GPa}$
Poisson's ratio	$\nu_{xy} = \nu_{xz} = 0.30$ and $\nu_{yz} = 0.51$
SERR	$G_{I_{cr}} = 219.55 \text{ J/m}^2$ and $G_{II_{cr}} = 883.10 \text{ J/m}^2$

Solving Equation (5.28) numerically for the material properties and $G_{I_{cr}}$ given above, the SERR for the onset of pure mode II crack growth is estimated, as well as the angles in which the functions D_1 and D_2 are minimum. The angle in which the function D_1 reaches its minimum is the angle predicted for the first crack propagation under a pure mode I delamination. Similarly, the angle in which the function D_2 reaches its minimum is the angle predicted for the first crack propagation under a pure mode II delamination. The results are shown in Table 5.5.

Table 5.5. Estimation of parameters for the onset of pure modes I and II delaminations

Angle for minimum D_1	Angle for minimum D_2	Estimated $G_{II_{cr}}$
-46.57°	-80.74°	201.75 J/m^2

In order to assess the accuracy of the estimations in Table 5.5, experimentally obtained data is used for comparison. The critical SERR estimated for the onset of mode II crack growth is approximately 23% of the value obtained in ENF experiments performed by Asp and colleagues [42, 43]. This difference in the critical SERR is observed because the value of SERR obtained via ENF experiments does not refer to the onset of crack growth.

What is the SERR obtained via ENF tests giving us?

In mode II delamination growth, a process zone develops with the formation of cusps, striations and microcracks ahead of the crack tip until coalescence is reached and crack growth can be observed from the sides of the specimen [4, 8, 21-23, 43]. Only when coalescence is reached, a drop in the load is observed in the load-displacement history. The maximum load is then used to calculate the value of the critical SERR [4]. This is illustrated in Figure 5.5.

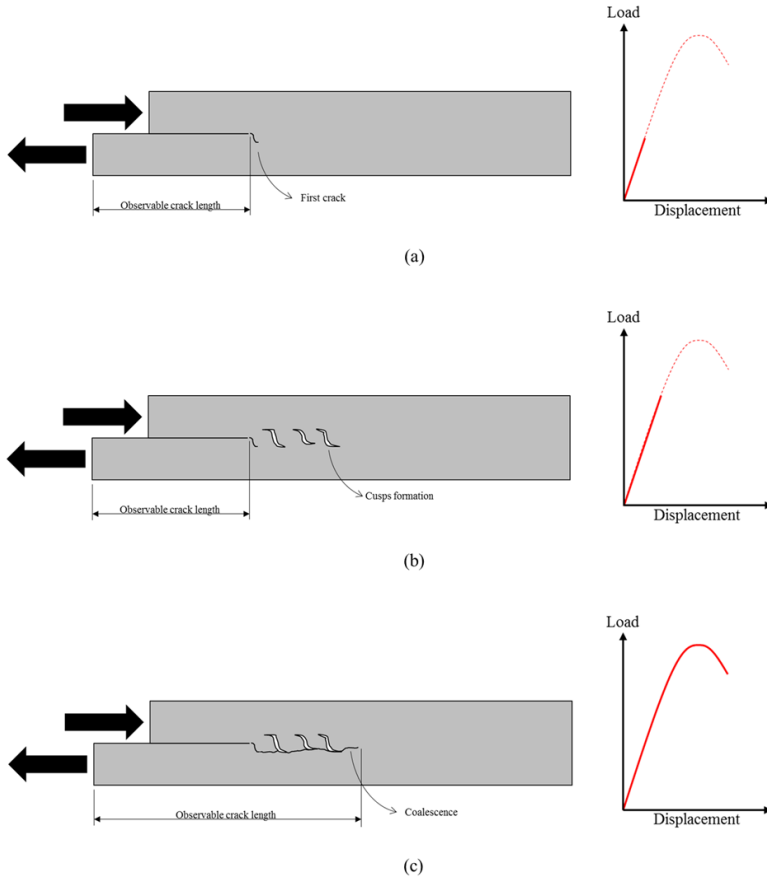


Figure 5.5. Process zone formation in mode II delaminations. (a) first crack occurs before maximum load is achieved, followed by (b) cusps formation and (c) coalescence

Figure 5.5 (a) illustrates that the first crack growth occurs when the load is still below the maximum, and no load drop is observed. This first crack growth cannot be observed by naked eye observation of the sides of the specimen. This is followed by cusps formation (Figure 5.5 (b)) and their subsequent coalescence (Figure 5.5 (c)). Then, a drop in the load is observed. Therefore, the onset of mode II delamination occurs before the specimen reaches its mode II critical SERR determined via ENF tests [4].

The mode I SERR obtained via DCB tests refers to the onset of mode I crack growth, while the mode II SERR obtained via ENF tests refers to the coalescence of microcracks ahead of the crack tip. This is the reason why mode II SERR is usually reported to be higher than mode I SERR. The critical SERR obtained via ENF specimens, which is calculated only after coalescence has happened (Figure 5.5 (c)), is from now on referred to as $(G_{IIc})_{ENF}$. Meanwhile, the critical SERR for the onset of mode II crack growth, determined with the critical SED approach and shown in Figure 5.5 (a), is referred to as $(G_{IIc})_{SED}$. Therefore, if one considers the actual onset of crack growth for modes I and II, i.e., the first cracking, the

onset of a mode I crack growth, at $G_{Ic} = 219.55 \text{ J} / \text{m}^2$, occurs at a higher SERR than the onset of mode II crack growth, at $(G_{IIc})_{SED} = 201.75 \text{ J} / \text{m}^2$. However, why would the first cracks appear at a lower SERR for mode II than for mode I?

The answer to the question above lies in the characteristics of the stress distributions in the vicinity of the crack tip for each loading mode. This question is addressed in detail in Section 5.5.3 of the present work.

For now, another question will be discussed first: how to verify that the onset of mode II crack growth actually occurs at $(G_{IIc})_{SED}$ and not at $(G_{IIc})_{ENF}$? Asp and colleagues did verify that, indeed, the onset of delamination growth occurs before $(G_{IIc})_{ENF}$. They observed the sides of quasi-statically loaded ENF specimens in a SEM. Cracks ahead of the main crack tip were observed even in specimens loaded only until 50% of $(G_{IIc})_{ENF}$ [43]. One of the images Asp et al. obtained in the SEM is reproduced in Figure 5.6 for convenience of the reader.

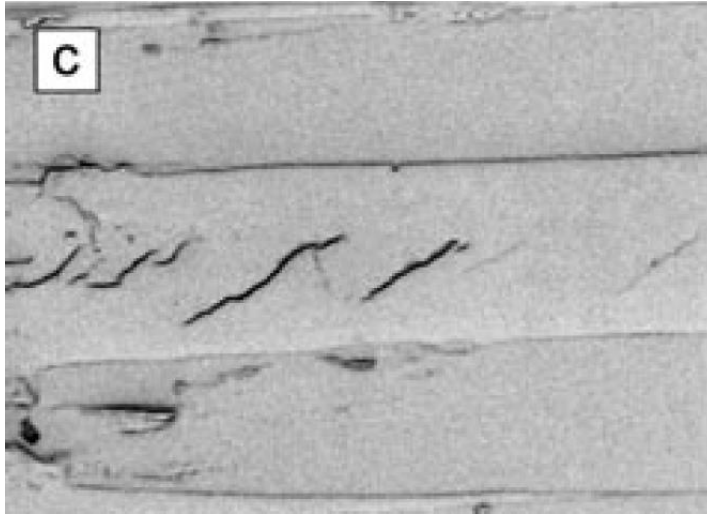


Figure 5.6. Cracks ahead of the main crack tip in an ENF specimen loaded up to 50% of $(G_{IIc})_{ENF}$ (reproduced from [43])

These cracks ahead of the main crack tip were not observed when the specimen was loaded until 25% of $(G_{IIc})_{ENF}$, which is approximately the threshold for the onset of crack propagation determined by means of the critical SED in Equation (5.28). Asp and colleagues did not observe, however, the crack tip itself, and could not tell whether the first crack had already grown when the specimen was loaded up to 25% of $(G_{IIc})_{ENF}$. Thus, the prediction of a first crack occurring in mode II delaminations at $(G_{IIc})_{SED}$ is plausible according to data from literature. However, the actual verification of it would require in-situ mode II delamination tests.

Regarding the angles of the first crack predicted for the onset of both pure mode I and pure mode II delaminations, correlations with experimental data can also be drawn. For the onset

of pure mode I delamination growth, the angle predicted for the first crack to grow was of -46.57° . Khan et al. [44] performed quasi-static mode I delamination tests on DCB specimens of a similar carbon/epoxy composite system inside of a SEM. They observed that the cracks did not propagate straight. Instead, they grew in angle with the x -axis, such that the crack touched the upper or lower fibres of adjacent layers, similarly to the angle of -46.57° predicted by the critical SED approach. This behaviour was also observed by Hibbs and colleagues during in-situ mode I tests [6]. Therefore, the prediction of the angle of the first crack for mode I delaminations seems to be in agreement with literature.

Meanwhile, for the angle of -80.74° predicted for the onset of mode II crack growth, no observations were found in literature. The SEM observations of Asp et al. in [43] focused on the area ahead of the crack tip, where they found that cracks have an angle of approximately 45° with the horizontal. However, Asp et al. did not observe the first crack formed, closer to the initial crack tip, or its angle. Once more, in-situ mode II delamination tests would be necessary in order to observe the angle of the first crack.

In order to circumvent the necessity of in-situ mode II delamination tests, rail shear tests were performed according to the description in section 5.3 of the present work. The idea is to qualitatively compare the results of crack-tip angle and onset of cracking for both rail shear tests and the HTA/6376C carbon/epoxy composite.

Considering the properties of the isotropic foam used in the rail shear tests and approximating the test as yielding a pure mode II loading on the crack tip, Equation (5.22) predicts a first crack at an angle of approximately 90° with the x -axis.

The results presented in Figure 5.7 show that the first crack in the rail shear sample does occur before the maximum load, such as predicted via the critical SED for composite delamination. In addition, a small load drop is observed, highlighted in Figure 5.7 (b), at the moment the first crack occurs. This load drop is small (710 N) when compared to the load range of the test (maximum load of approximately 37.5 kN). When scaling this load drop down to the case of delamination in a carbon/epoxy composite, it might not be observed, once the drop in the load is likely to be within the error of the load cell. Besides, the load drop of 710 N was only observed in rail shear specimens when the sampling rate of the testing machine was set to acquire one data point every 0.009 seconds. When acquiring data points at longer time intervals, the load drop was not obvious.

Given the qualitative similarities between the PVC foam rail shear tests and mode II delamination growth of composites, the rail shear test results indicate that the onset of cracking in mode II delaminations occur, indeed, before the maximum load of the test and before $(G_{II,c})_{ENF}$.

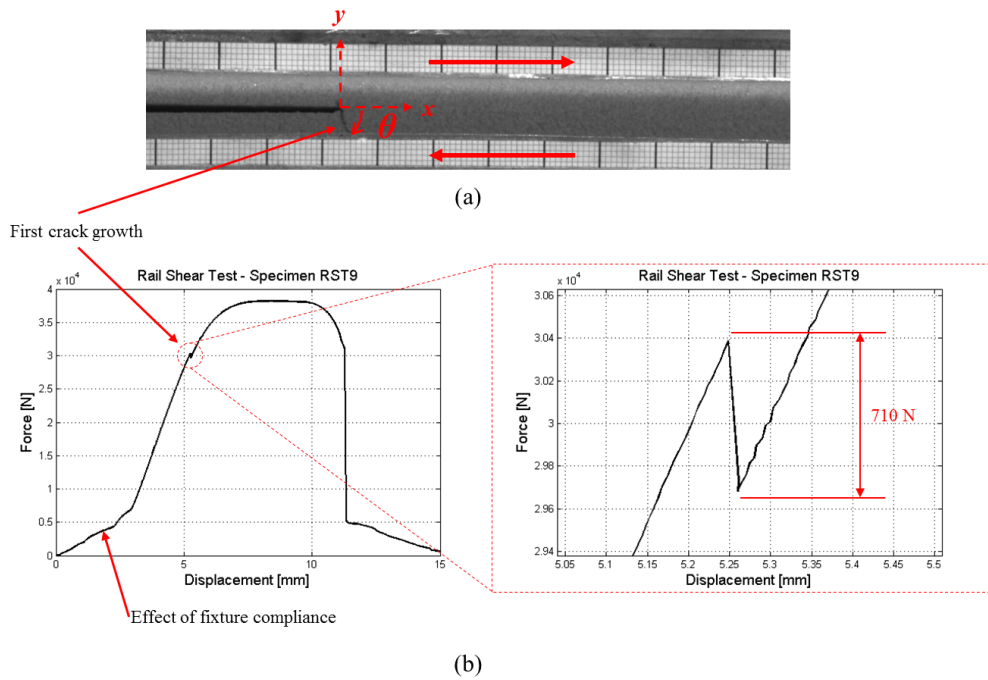


Figure 5.7. Specimen RST9: (a) first crack occurs at $\theta=71^\circ$; (b) a load drop of 710 N is observed when the first crack occurs

The angle of the first crack with the x -axis in the rail shear test is of 71° , smaller than the value of 90° predicted by the critical SED approach. This occurs because of the presence of a mode I component at the crack tip in the foam test, which tends to decrease the angle of the crack with the x -axis. This mode I component is inherent to the rail shear test, as described by the ASTM standard [27], and it tends to increase with damage propagation. This increase in the mode I component with damage growth can be observed in the increased crack opening displacement when damage has developed, shown in detail in Figure 5.8.

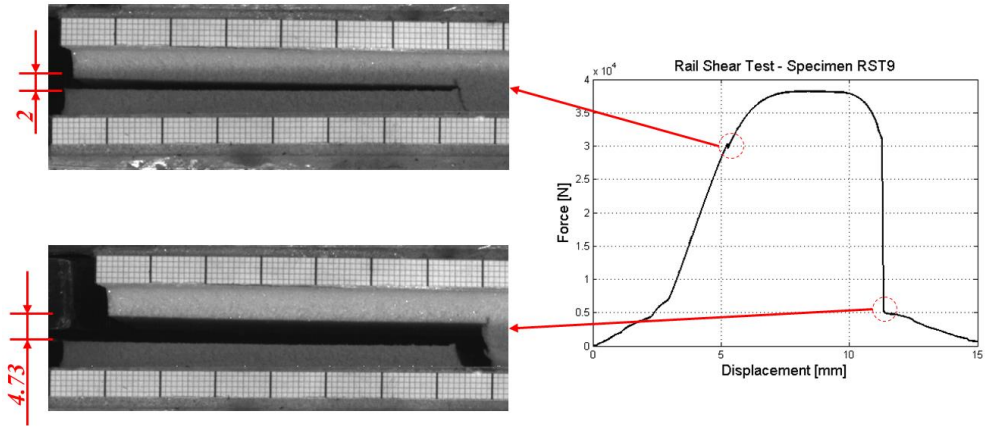


Figure 5.8. Specimen RST9: Effect of mode I component in the rail-shear test

Further in the rail shear test, cracks develop ahead of the main crack tip, and a typical cusp formation can be observed in Figure 5.9. The reader should note that the angle of the cracks ahead of the main crack tip is smaller than the angle of the first crack, as listed in Table 5.6 for every rail shear specimen tested. This is in qualitative agreement with the observations of Asp et al. [43] in which the cracks ahead of the crack tip have an angle of 45° (see Figure 5.6), while the critical SED approach predicts the first crack to be at an angle of -80.74° .

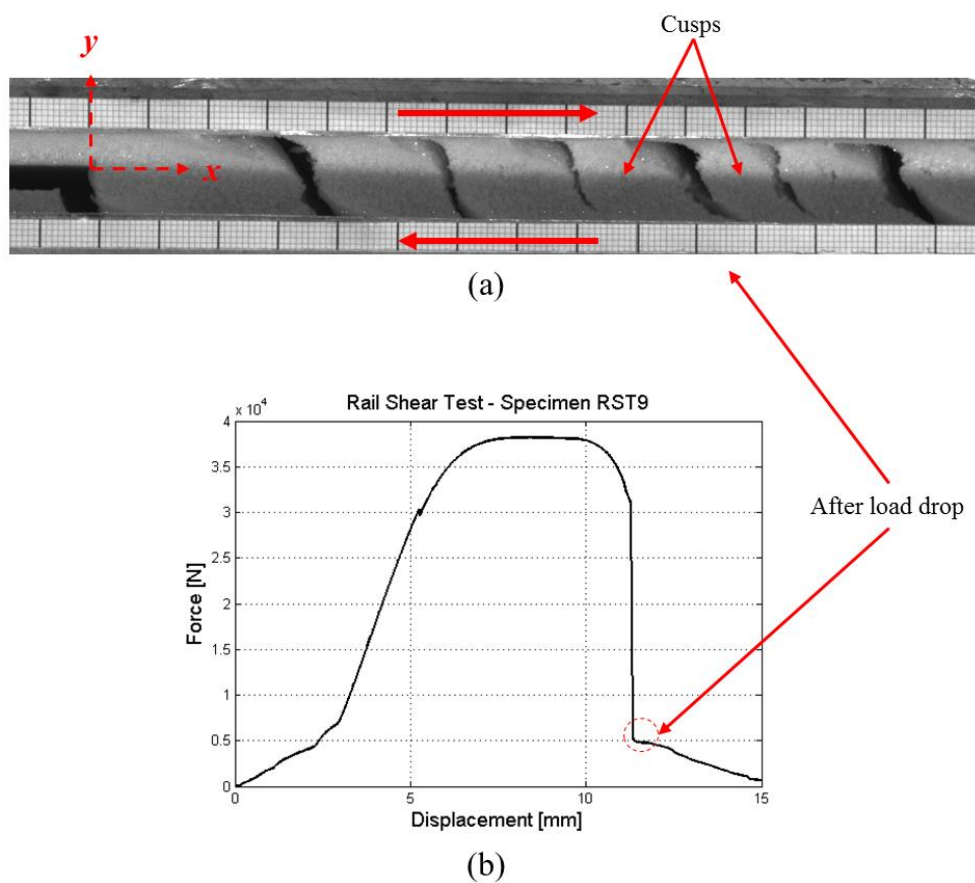


Figure 5.9. (a) Cusps formation after coalescence; (b) load-displacement curve – point after cusps coalescence indicated by red arrow

Table 5.6. Rail Shear test results; θ_0 is the angle of the first crack relative to the x -axis

	θ_0	Cusp angles range	$\frac{P_{\text{onset}}}{P_{\text{maximum}}}$
RST 8	68°	$44^\circ - 55^\circ$	0.59
RST 9	71°	$54^\circ - 69^\circ$	0.79
RST 10	62°	$46^\circ - 56^\circ$	0.67
RST 11	66°	$39^\circ - 56^\circ$	0.68

The critical SED approach predicted the onset of mode II delamination growth to occur at 23% of $(G_{II_c})_{ENF}$, which is approximately 50% of the critical load obtained on the ENF test. Meanwhile, the onset of crack growth in the rail shear tests occurred, on average, at 68% of the critical load. Asp et al. observed cracks ahead of the main crack tip at an angle of approximately 45° with the x -axis, while the rail shear tests yielded cracks ahead of the main crack tip with angles between 39° and 69° .

In addition, no load drops are reported in literature before the maximum load in mode II delamination tests, when the first crack growth is predicted to occur by the critical SED approach. In rail shear tests, a small load drop, considering the load range of the test, was observed when the first crack growth occurred. However, due to this load drop being very small and captured only with a high sampling rate, it is reasonable to assert that it is not observed on carbon/epoxy composite specimens in ENF tests when the onset of delamination growth occurs.

Quantitatively, the results of the rail shear tests do not match perfectly the results of the mode II delamination tests. This is expected, since the rail shear test is only a qualitative approximation to pure mode II ply delamination. From the qualitative perspective, the similarities between pure mode II ply delamination and the rail shear tests of the PVC foam are undeniable. Both show the formation of a process zone ahead of the crack tip, with cracks with a less steep angle with the x -axis than the angle of the first crack predicted by the critical SED approach. Therefore, the SED approach seems to yield valid results for the prediction of the first crack growth in mode II delaminations. Furthermore, this prediction was done using only material properties and mode I fracture toughness data.

However, what is the use of predicting that the first cracking starts at approximately 23% of $(G_{II_c})_{ENF}$ for mode II delaminations?

A first crack occurring for mode II delaminations at 23% of $(G_{II_c})_{ENF}$ implies that composite laminates designed using $(G_{II_c})_{ENF}$ as a basis for quasi-static mode II delamination resistance

might have developed defects ahead of the crack tip although operating at SERR levels below $(G_{II_{cr}})_{ENF}$. In this case, the growth of mode II fatigue cracks is also expected to be faster, since the starting point for the fatigue crack is a laminate in which damage has already developed in the process zone if the structure operated above $(G_{II_{cr}})_{SED}$. Besides, the critical SED approach supplies the designer with a load or SERR level below which, quasi-statically, there is no damage created ahead of the crack tip. This is an important threshold not only for design purposes, but also for performing compliance calibration tests in ENF specimens prior to fracture testing them. If the SERR level is maintained below $(G_{II_{cr}})_{SED}$, the engineer is certain that the compliance calibration procedure did not generate damage ahead of the crack tip. Following the present results, the future studies should aim at validating experimentally $(G_{II_{cr}})_{SED}$ through in-situ experiments and evaluating whether $(G_{II_{cr}})_{SED}$ also works as a threshold for fatigue crack growth.

Other composite material systems

The critical SED approach was also applied to other orthotropic composite laminates for which data is found in literature. The results, listed in Table 5.7, show that the onset of pure mode II delamination growth seems to occur consistently between 24% and 33% of $(G_{II_{cr}})_{ENF}$ for carbon/epoxy composite systems. Finally, data for one glass/epoxy composite system was also used, and $(G_{II_{cr}})_{SED}$ was determined as approximately 10% of $(G_{II_{cr}})_{ENF}$.

The reader should note that the results shown in Table 5.7 are for unidirectional specimens. In case of different lay-ups, the critical SED for onset of fracture will change, because the effective material properties also change (e.g., see Equation (5.29)). Although the onset of delamination is a matrix dominated failure, the SED in the vicinity of the crack tip is the contribution of how the load was distributed from its application points to the crack tip. This load distribution changes once the effective properties of the laminate change.

Table 5.7. Predicted critical SERR for the onset of mode II delamination – other composite material systems

Composite system	$G_{I_{cr}}$	$(G_{II_{cr}})_{ENF}$	$(G_{II_{cr}})_{SED}$	$\frac{(G_{II_{cr}})_{SED}}{(G_{II_{cr}})_{ENF}}$	Reference
IM7/8552	200 J/m ²	800 J/m ²	195 J/m ²	0.24	[45]
G40-800/5260	240 J/m ²	900 J/m ²	237 J/m ²	0.26	[45]
AS4/3501-6	220 J/m ²	650 J/m ²	216 J/m ²	0.33	[45]
Glass/LY556	165 J/m ²	1500 J/m ²	157 J/m ²	0.10	[45]

The critical SED approach enables the estimation of the critical SERR for the onset of pure mode II delamination growth without the necessity of performing ENF fracture toughness tests. In addition, the author understands that for engineering purposes and in order to comply with standards, it is of interest to determine $(G_{II_{cr}})_{ENF}$. Thus, a first estimation of $(G_{II_{cr}})_{ENF}$ is possible, once $(G_{II_{cr}})_{SED}$ seems to be approximately 25% of $(G_{II_{cr}})_{ENF}$ for carbon/epoxy composite systems with a toughened matrix. This is the case for IM7/8552, G40-800/5260 and HTA/6376C. For AS4/3501-6, a carbon/epoxy composite with a brittle matrix, $(G_{II_{cr}})_{SED}$ is 33% of $(G_{II_{cr}})_{ENF}$.

The exact value of $(G_{II_{cr}})_{SED}/(G_{II_{cr}})_{ENF}$ depends on how much the microcracks in the process zone will extend before coalescence is reached. The tougher the resin, the longer will be the process zone and coalescence will be reached much after the occurrence of the first crack [5, 6], decreasing $(G_{II_{cr}})_{SED}/(G_{II_{cr}})_{ENF}$. This explains the variation of $(G_{II_{cr}})_{SED}/(G_{II_{cr}})_{ENF}$ from 0.23 to 0.33 for the carbon/epoxy composites.

For the glass/epoxy composite system Glass/LY556, the value of $(G_{II_{cr}})_{SED}/(G_{II_{cr}})_{ENF}$ decreases to 0.10 because glass fibres are less stiff than carbon fibres. Due to this reduced stiffness of the glass fibres, the constraint to shear deformation in the resin is smaller. Because of this, the process zone increases in volume, causing coalescence to occur later [5, 6] and explaining $(G_{II_{cr}})_{SED}/(G_{II_{cr}})_{ENF} = 0.10$ for Glass/LY556.

Therefore, the relationship between $(G_{II_{cr}})_{SED}$ and $(G_{II_{cr}})_{ENF}$ can be explained by the material properties of the composite systems studied. The exact nature and form of this relationship between material properties and the difference between $(G_{II_{cr}})_{SED}$ and $(G_{II_{cr}})_{ENF}$ is yet to be investigated in future studies. However, the fact that a relationship based on material properties between $(G_{II_{cr}})_{SED}$ and $(G_{II_{cr}})_{ENF}$ exists indicates that the fracture behaviour of the material can be fully characterized with the critical SED approach, performing only mode I fracture toughness tests and having the material properties.

The process to fully characterize the fracture behaviour of the material with the SED approach is illustrated in Figure 5.10. Figure 5.10 (a) shows the current procedure to characterize delamination growth, which involves DCB, ENF and MMB tests. Meanwhile, Figure 5.10 (b) shows the SED approach, for which only DCB fracture tests are necessary in order to characterize delamination onset. Until the moment when $(G_{II_{cr}})_{SED}$ and $(G_{I/III_{cr}})_{SED}$ are obtained, only physics-based relationships are used to obtain the prediction. However, due to engineering purposes, as discussed above, it is interesting to obtain the critical SERR as measured by ENF and MMB tests. To this aim, data from literature and material properties show a relationship between the SERR obtained via the SED approach and the one obtained via standardized tests. However, the exact mathematical form of this relationship is not clear to the present moment.

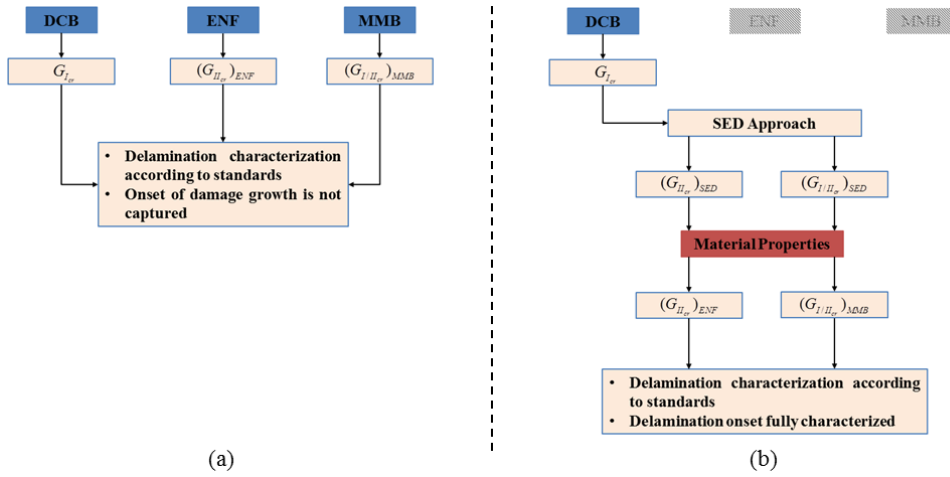


Figure 5.10. Flowchart of the (a) current procedure to characterize fracture; and (b) SED approach – ENF and Mixed-Mode Bending (MMB) tests might not be necessary for fracture characterization

The characterization of mixed-mode fracture follows the same approach, depicted in Equations (5.29) and (5.30) where $s_{I/II_{cr}}$ is the critical SED for mixed-mode fracture at a certain mode mixity. This topic will have to be addressed in detail in future publications.

$$S_{I_{cr}} = S_{I/II_{cr}} \quad (5.30)$$

$$S_{I_{cr}} = K_I^2 D_1 + K_{II}^2 D_2 + K_I K_{II} D_3 \quad (5.31)$$

5.5.3 The fundamental relationship between pure mode I and pure mode II crack growth

The SED necessary for a material to fracture is constant, independently of the loading mode. This hypothesis results on Equation (5.23) and seems to be validated by the ability to predict pure mode II SIF or SERR based only on material properties and pure mode I fracture toughness data.

Equation (5.23) gives a physics-based relationship between mode I and mode II fracture. The critical SED is equal for both loading modes. Therefore, mode I and mode II fracture are intrinsically related. Furthermore, mode I and mode II SIF relate to each other according to the manner the stresses distribute around the crack tip. Using Equation (5.23) as a starting point, for linear elastic, isotropic materials, one obtains Equation (5.24). Similarly, for linear elastic, orthotropic materials, using Equation (5.23) as a starting point, one obtains Equation (5.28). Both Equations (5.24) and (5.28) show that the ratio between mode II and mode I SIF (or SERR) is given by functions that determine how the stresses and, hence, the strain energy, are distributed around the crack tip for each loading mode.

This is shown in Equation (5.32), where $D_1(\theta_0)$ is the stress distribution function for pure mode I delamination and $D_2(\theta_{0II})$ is the stress distribution function for pure mode II delamination. Equation (5.32) gives an insight on why the SERR for the onset of a mode I crack is actually higher than the SERR for the onset of a mode II crack in an orthotropic composite structure: because of the way the stresses are distributed in the vicinity of the crack tip.

$$\frac{G_{IIcr}}{G_{Icr}} = \frac{F_{II}}{F_I} \frac{D_1(\theta_{0I})}{D_2(\theta_{0II})} \quad (5.32)$$

On two different studies, Corleto and Bradley performed finite element simulations in order to understand the differences on the stress distribution of pure mode I and pure mode II delaminations of orthotropic carbon/epoxy specimens [7, 8]. The results of their analyses are reproduced, for convenience of the reader, in Figure 5.11.

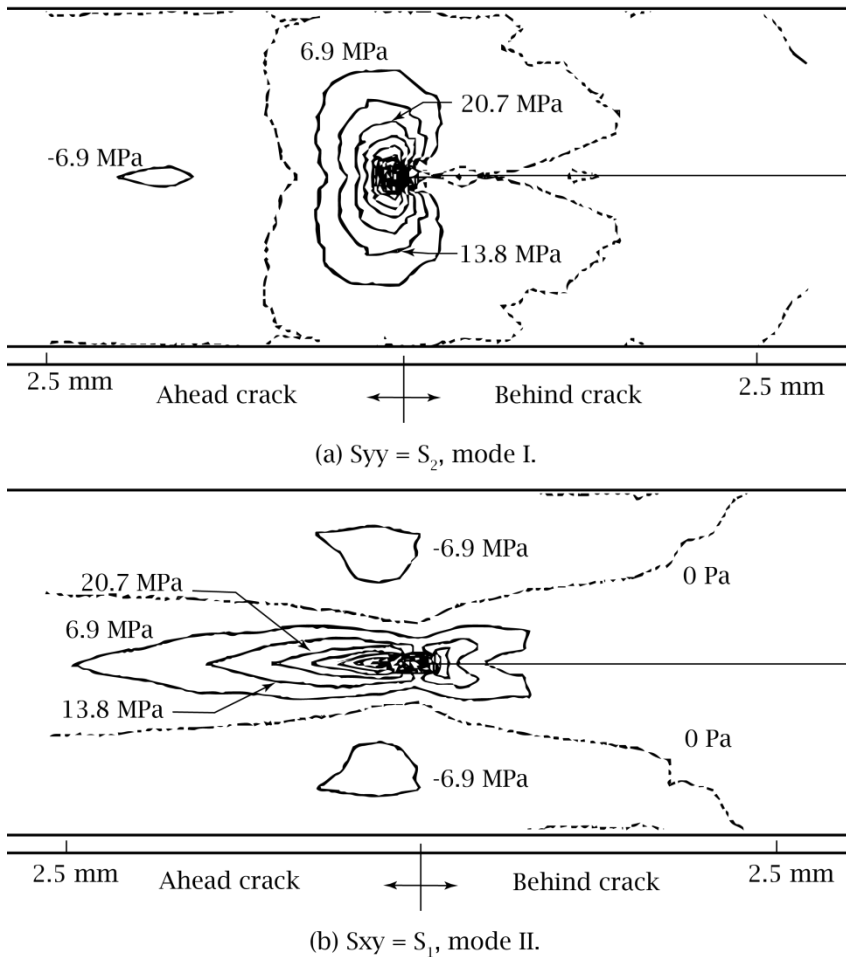


Figure 5.11. Comparison on stress distributions around the crack tip for (a) pure mode I and (b) pure mode II delamination (adapted from [7])

Although the stress levels for both mode I and mode II delamination are very similar, the stress distribution in pure mode II delamination extends for a longer distance in the x -axis than for mode I delaminations, as seen in Figure 5.11. This difference in stress distribution ahead of the crack tip is responsible for the difference in damage mechanisms observed on the fracture surfaces of the specimens, as discussed in [21]. For example, the shear stresses in pure mode II delaminations extend for a longer length, and this explains the large process zone typically encountered on shear delaminations. This process zone gives rise to cusps [21].

The way the stress distributes around the crack tip indicates which damage mechanisms will act in fracture. This gives a hint on why previous studies were not able to relate modes I and II SIF or SERR on a physics-based theory until the present moment: because the SIF or the SERR alone do not completely describe the physics of fracture! This is exemplified

in Figure 5.12 for crack tip stresses in the x -direction. The damage mechanisms acting in fracture are a core part of the crack growth process, and changes in damage mechanisms lead to changes in energy dissipation in crack growth [4, 21]. Therefore, the complete stress functions, with the SIF and the functions that describe the stress distribution, must be used to characterize energy dissipation in fracture. Furthermore, the SIF is a scalar, in an attempt to describe the stress field. With a change in the stress field, the magnitude of the SIF will change. However, how does this change in magnitude of the SIF completely describe the stress field? Hypothetically, one could have two stress fields with a different SIF, but with the same strain energy density in that volume. So, if one wants to relate this change in stress field with a change in the strain energy, this is not possible through the SIF or the SERR alone. The manner of considering the complete stress functions and the contribution of stresses in all directions is through the strain energy density function.

Consider the example of changing the mode of loading for the same material. In this case, the SIF will change. However, the damage mechanisms will also change, and this is accounted for by a change in the functions that say how the stresses distribute in the vicinity of the crack tip, f_1 and f_2 in Figure 5.12, such that the SED will remain constant. This means that the leading parameter in crack initiation is the contribution of the SIF (or SERR) together with the stress functions: the SED is the parameter leading crack initiation!

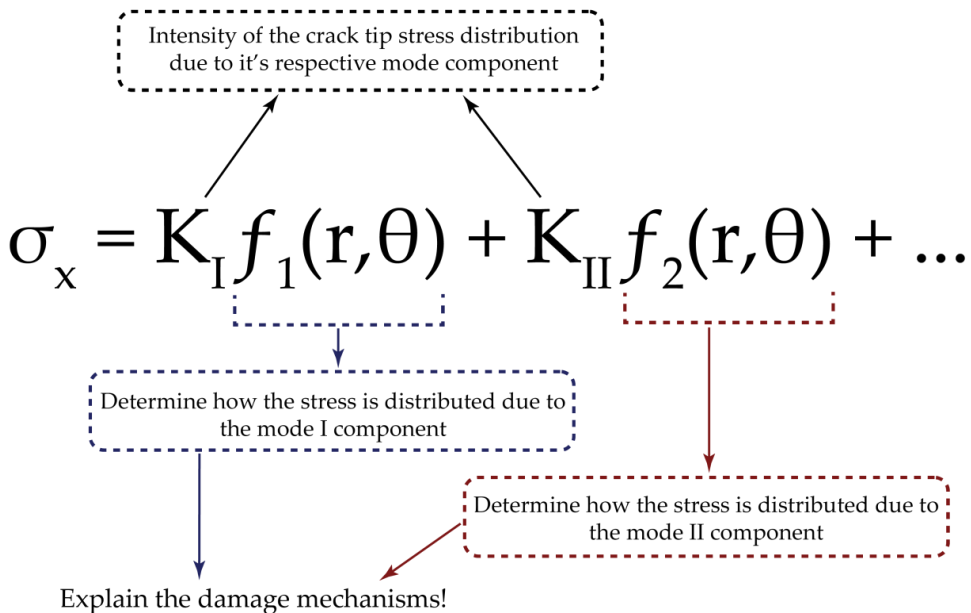


Figure 5.12. Crack-tip stresses in x -direction under a mixed-mode loading. The whole stress function is necessary in order to properly characterize fracture. The stress distribution determines the damage mechanisms activated in fracture. Although only the stresses in x -direction are shown for simplicity, note that stresses in 3 directions are used in the SED approach

5.6 Conclusions

The critical SED approach was proposed for the analysis of fracture propagation in different brittle materials. The onset of crack growth occurs when the strain energy density in the vicinity of the crack tip reaches a critical value. This critical SED for the onset of crack growth is constant, independently of the loading mode, and it gives a physics-based relationship between the different loading modes. The past attempts to relate fracture under different loading modes using the SIF or the SERR failed because these terms are not sufficient to describe the fracture behaviour. The damage mechanisms acting in fracture are a core part of the crack growth process, and changes in damage mechanisms lead to changes in energy dissipation in crack growth. Therefore, the complete stress functions, with the SIF and the functions that describe the stress distribution, must be used to characterize energy dissipation in fracture. The manner of considering the complete stress functions and the contribution of stresses in all directions is through the strain energy density function.

For delamination of composites, mode II fracture toughness, obtained via standardized tests such as the ENF, does not represent the onset of delamination growth. Instead, the mode II SERR measured with the ENF test refers to the point where the microcracks ahead of the main crack tip coalesce. This explains why mode II fracture toughness is reported in literature to be higher than mode I fracture toughness for delamination of composites. Mode II fracture toughness for the actual onset of delamination growth is smaller than mode I fracture toughness for the onset of growth, and can be obtained via the critical SED approach. The SERR for the onset of mode II delamination growth can be used as a threshold for the development of damage in laminated structures under interlaminar shear quasi-static loading.

Furthermore, using the critical SED approach, only material properties and mode I fracture toughness tests are necessary to characterize the delamination behaviour of a composite structure. The SERR for the onset of delamination growth can then be estimated and potentially used as a threshold for the development of damage under quasi-static loading conditions. In addition, using the material properties, the SERR for the onset of delamination growth can be related with the SERR determined via standardized ENF tests.

5.7 References

- [1] ASTM Standard D5528-01. Standard Test Method for Mode I Interlaminar Fracture Toughness of Unidirectional Fiber-Reinforced Polymer Matrix Composites. US: ASTM International; 2007.
- [2] Amaral L, Yao L, Alderliesten R, Benedictus R. The relation between the strain energy release in fatigue and quasi-static crack growth. *Engineering Fracture Mechanics*. 2015;145:86-97.
- [3] Amaral L, Yao L, Alderliesten RC, Benedictus R. Energy based study on quasi-static delamination growth treated as a low cycle fatigue process. In: Siljander A, editor. 34th Conference and 28th Symposium of the International Committee on Aeronautical Fatigue and Structural Integrity. Helsinki, Finland 2015. p. 240 - 8.
- [4] Amaral L, Zarouchas D, Alderliesten R, Benedictus R. Energy dissipation in mode II fatigue crack growth. *Engineering Fracture Mechanics*. 2017;173:41-54.

- [5] Bradley WL, Cohen RN. Matrix deformation and fracture in graphite-reinforced epoxies. Delamination and debonding of materials: ASTM International; 1985.
- [6] Hibbs MF, Bradley WL. Correlations between micromechanical failure processes and the delamination toughness of graphite/epoxy systems. Fractography of Modern Engineering Materials: Composites and Metals: ASTM International; 1987.
- [7] Corleto C, Bradley W, Henriksen M. Correspondence between stress fields and damage zones ahead of crack tip of composites under mode I and mode II delamination. International Conference on Composite Materials, 6 th, and European Conference on Composite Materials, 2 nd, London, England 1987. p. 3.
- [8] Corleto C, Bradley W. Mode II Delamination Fracture Toughness of Unidirectional Graphite/Epoxy Composites. Composite Materials: Fatigue and Fracture. 1989;2:201-21.
- [9] Russell AJ. Micromechanisms of interlaminar fracture and fatigue. Polymer composites. 1987;8:342-51.
- [10] Jordan WM, Bradley WL. Micromechanisms of fracture in toughened graphite-epoxy laminates. Toughened Composites: ASTM International; 1987.
- [11] Ayatollahi M, Pavier M, Smith D. Determination of T-stress from finite element analysis for mode I and mixed mode I/II loading. International journal of fracture. 1998;91:283-98.
- [12] Smith D, Ayatollahi M, Pavier M. On the consequences of T-stress in elastic brittle fracture. Proceedings of the Royal Society of London A: Mathematical, Physical and Engineering Sciences: The Royal Society; 2006. p. 2415-37.
- [13] Ayatollahi M, Hashemi R. Computation of stress intensity factors (KI, KII) and T-stress for cracks reinforced by composite patching. Composite structures. 2007;78:602-9.
- [14] Griffith AA. The Phenomena of Rupture and Flow in Solids. Philosophical Transactions of the Royal Society of London Series A, Containing Papers of a Mathematical or Physical Character. 1921;221:163-98.
- [15] Sih GC. Mechanics of fracture initiation and propagation: surface and volume energy density applied as failure criterion: Springer Science & Business Media; 2012.
- [16] Sih G, Macdonald B. Fracture mechanics applied to engineering problems-strain energy density fracture criterion. Engineering Fracture Mechanics. 1974;6:361-86.
- [17] Neuber H. Theory of stress concentration for shear-strained prismatical bodies with arbitrary nonlinear stress-strain law. Journal of Applied Mechanics. 1961;28:544-50.
- [18] Neuber H. Theoretical calculation of strength at stress concentration. Czechoslovak Journal of Physics B. 1969;19:400-.
- [19] Lazzarin P, Zambardi R. A finite-volume-energy based approach to predict the static and fatigue behavior of components with sharp V-shaped notches. International journal of fracture. 2001;112:275-98.
- [20] Berto F, Lazzarin P. A review of the volume-based strain energy density approach applied to V-notches and welded structures. Theoretical and Applied Fracture Mechanics. 2009;52:183-94.
- [21] Amaral L, Alderliesten R, Benedictus R. Understanding Mixed-Mode Cyclic Fatigue Delamination Growth in unidirectional composites: an experimental approach. Engineering Fracture Mechanics. 2017.
- [22] LEE SM. Mode II delamination failure mechanisms of polymer matrix composites. Journal of Materials Science. 1997;32:1287-95.
- [23] Lee SM. Mode II Interlaminar Crack Growth Process in Polymer Matrix Composites. Journal of Reinforced Plastics and Composites. 1999;18:1254-66.

- [24] Greenhalgh ES. Failure analysis and fractography of polymer composites: Woodhead Publishing Limited; 2009.
- [25] Rogers C, Greenhalgh E, Robinson P. Developing a mode II fracture model for composite laminates. 2008.
- [26] Divinycell H. grade, Technical Manual. Divinycell International AB. 1991.
- [27] C273 A. 273, "Standard Test Method for Shear Properties of Sandwich Core Materials". The American Society for Testing and Materials 2000.
- [28] Boresi AP, Schmidt RJ, Sidebottom OM. Advanced mechanics of materials: Wiley New York; 1993.
- [29] Irwin GR. Analysis of stresses and strains near the end of a crack traversing a plate. {ASME} Journal of Applied Mechanics. 1957;24:361-4.
- [30] Sih GC, Paris PC, Irwin GR. On cracks in rectilinearly anisotropic bodies. International Journal of Fracture Mechanics. 1965;1:189-203.
- [31] Tada H, Paris PC, Irwin GR. The stress analysis of cracks. Handbook, Del Research Corporation. 1973.
- [32] Erdogan F, Tuncel O, Paris P. An experimental investigation of the crack tip stress intensity factors in plates under cylindrical bending. ASME J Basic Eng. 1962;84:542-6.
- [33] Erdogan F, Sih G. On the crack extension in plates under plane loading and transverse shear. Journal of basic engineering. 1963;85:519-27.
- [34] Wong T-F. Micromechanics of faulting in Westerly granite. International journal of rock mechanics and mining sciences & geomechanics abstracts: Elsevier; 1982. p. 49-64.
- [35] Ingraffea AR. Mixed-mode fracture initiation in Indiana limestone and Westerly granite. The 22nd US Symposium on Rock Mechanics (USRMS): American Rock Mechanics Association; 1981.
- [36] Daneshy A. Hydraulic fracture propagation in layered formations. Society of Petroleum Engineers Journal. 1978;18:33-41.
- [37] Van Herwijnen A, Gaume J, Bair EH, Reuter B, Birkeland KW, Schweizer J. Estimating the effective elastic modulus and specific fracture energy of snowpack layers from field experiments. Journal of Glaciology. 2016;62:997-1007.
- [38] Kirchner H, Michot G, Schweizer J. Fracture toughness of snow in shear and tension. Scripta Materialia. 2002;46:425-9.
- [39] McClung D. Dry snow slab quasi-brittle fracture initiation and verification from field tests. Journal of Geophysical Research: Earth Surface. 2009;114.
- [40] Backers T. Fracture toughness determination and micromechanics of rock under mode I and mode II loading: Geoforschungszentrum Potsdam; 2005.
- [41] ASTM. Standard Test Method for Determination of the Mode II Interlaminar Fracture Toughness of Unidirectional Fiber-Reinforced Polymer Matrix Composites. D7905/D7905M ASTM International; 2014.
- [42] Asp L. The effects of moisture and temperature on the interlaminar delamination toughness of a carbon/epoxy composite. Composites Science and Technology. 1998;58:967-77.
- [43] Asp LE, Sjögren A, Greenhalgh ES. Delamination growth and thresholds in a carbon/epoxy composite under fatigue loading. Journal of Composites, Technology and Research. 2001;23:55-68.
- [44] Khan R, Alderliesten R, Badshaha S. EXPERIMENTAL INVESTIGATION OF THE MICROSCOPIC DAMAGE DEVELOPMENT AT MODE I FATIGUE DELAMINATION TIPS IN CARBON/EPOXY LAMINATES. 2016.

[45] Kaddour A, Hinton M, Smith P, Li S. Mechanical properties and details of composite laminates for the test cases used in the third world-wide failure exercise. *Journal of Composite Materials*. 2013;47:2427-42.

6 Conclusions and recommendations

6.1 Conclusions

The present chapter summarizes the main conclusions of this thesis.

6.1.1 Quasi-static and fatigue delamination growth

Quasi-static data can be consistently treated as low-cycle fatigue. A real physical SERR can be obtained from a da/dN versus dU/dN plot, for both quasi-static and fatigue loading conditions. Therefore, using the same parameter to characterise fatigue and quasi-static crack extensions allows a straightforward comparison between the two loading cases, based on energy dissipation and damage mechanisms. The actual strain energy dissipated in crack growth depends on the damage mechanisms acting in fracture and not on the loading condition (static or fatigue loading). The values of the SERR for fatigue and quasi-static loading conditions can be linked. The lower limit is given by fatigue loading at low da/dN values, which present the lowest SERR and, consequently, the smoother fracture surfaces. As the crack growth rate increases, the damage mechanism starts to change, and more energy is dissipated in fracture. The upper limit is given by quasi-static fracture, which presents the largest SERR due to matrix cleavage and fibre breakage.

6.1.2 The influence of process zone in mode II strain energy dissipation

Damage propagates ahead of the main crack tip in a process zone, which dissipates energy that should be accounted for when characterizing mode II delamination growth. It is currently not possible to measure appropriately the extent of the process zone in an ENF specimen from observations made from its side. The size and influence of the process zone in energy dissipation vary with the stress ratio. Therefore, the definition of a crack tip should not be used in mode II delamination growth. More studies are necessary in order to quantify the damage ahead of the crack tip and then define an effective crack length that can be used to characterize mode II delamination growth. Instead of developing new fracture mechanics models to address mode II delamination problems, efforts should be focused towards quantifying fracture in a better way.

Furthermore, without measuring the real extent of damage, it is not possible to calculate the actual damage growth rate present in mode II fatigue delaminations. The direct consequence is that it is not possible to use the physical SERR G^* to characterize mode II fatigue delamination. The utilization of the visually observed crack length as a parameter to calculate the crack growth rate results in its underestimation, which is more pronounced for high values of R .

6.1.3 Effect of mode mixities and loading parameters in energy dissipation

With the use of the physical SERR G^* , no dependence with the displacement ratio was found when relating crack growth rate and energy dissipation per cycle under a given mode

mixture. The energy consumed per area of crack created remains approximately constant. What causes a delamination extension under a specific loading mode to consume more energy per area of crack created are the different damage and dissipation mechanisms that might be activated under certain loading parameters. Therefore, the existence of a physical stress (or displacement) ratio dependence can only be confirmed for a given material under a certain mode of loading once the relationship between the fatigue loading parameters and the dissipation mechanisms they activate is known.

6.1.4 A physics-based relationship between different fracture modes

The onset of crack growth occurs when the strain energy density in the vicinity of the crack tip reaches a critical value. This critical SED for the onset of crack growth is constant, independently of the loading mode, and it gives a physics-based relationship between the different loading modes.

The past attempts to relate fracture under different loading modes using the SIF or the SERR failed because these terms are not sufficient to describe the fracture behaviour. Changes in the damage mechanisms acting in fracture lead to changes in energy dissipation in crack growth and must be taken into account. Therefore, the complete stress functions, with the SIF and the functions that describe the stress distribution, must be used to characterize energy dissipation in fracture. The concept of considering the complete stress functions and the contribution of stresses in all directions is through the SED function.

For delamination of composites, mode II fracture toughness, obtained via standardized tests such as the ENF, does not represent the onset of delamination growth. Instead, the mode II SERR measured with the ENF test refers to the point where the microcracks ahead of the main crack tip coalesce. This explains why mode II fracture toughness is reported in literature to be higher than mode I fracture toughness for delamination of composites. Mode II fracture toughness for the actual onset of delamination growth is smaller than mode I fracture toughness and can be obtained via the critical SED approach. The SERR for the onset of mode II delamination growth can be used as a threshold for the development of damage in laminated structures under interlaminar quasi-static shear loading. Using the critical SED approach, only material properties and mode I fracture toughness tests are necessary to approximate the delamination behaviour of a composite structure.

6.1.5 General conclusions

The results presented in this thesis show that characterizing delamination growth with the actual amount of strain energy dissipated in crack growth can lead to a better understanding of the physics behind fracture. This approach to delamination growth allowed a varied amount of phenomena to be explained. The relationship between quasi-static and fatigue crack growth, parameters that influence energy dissipation and the uncovering of a physics-based relationship between different loading modes were made possible through the

consideration of strain energy dissipation in delamination growth. Therefore, the use of an energy-based approach to characterize delamination growth is considered to be successful.

Nevertheless, in order for a characterization of delamination growth through this energy-based approach to be complete, more research is necessary on the topic of mode II delaminations. Particularly, the definition of a crack tip in such problems is misleading and may yield wrong conclusions. Therefore, future research should be focused towards quantifying properly the actual amount of damage generated in delamination growth.

6.2 Recommendations

The present thesis sets the path towards a physics-based prediction model for delamination of unidirectional composites. However, the road towards this final goal is long. Many questions were raised and discussed through chapters 2 to 6, and these must be carefully addressed. Therefore, some recommendations regarding future research are outlined here.

A phenomenological description of a crack tip is not suitable for addressing mode II delamination growth problems. Therefore, damage created under fatigue or quasi-static loading needs to be properly quantified. The zones of damage ahead of the main crack tip need to be considered and the rate of damage growth needs to be quantified appropriately. In order to achieve this goal, it might be necessary to scrutinize what dissipation mechanisms are acting during damage creation and propagation and how much energy they are dissipating. Once the damage growth rate is quantified, this can be related with the energy dissipation rate, enabling the full characterization of mode II and mixed-mode delamination growth.

Once delamination growth has been fully characterized, a reliable prediction model can be sought based on the uncovered physics of the problem. In order to do so, the relationship between the energy available for crack growth, dU/dN , and the strain energy input in the system U , should be well understood. The parameters that affect the relationship between dU/dN and U might point towards the mathematical relationship for a prediction model.

In addition, the SERR at which the very first crack occurs in the material was calculated with the SED approach. Research is necessary towards understanding if this value of SERR can be used as a threshold also for fatigue loading under different loading modes (I, II and I/II). This would be useful for designers to estimate a load level in which damage is not propagated in the structure.

Epilogue

“I have heard of ancient cultures they used to leave monuments and landmarks in areas where the dark became light. Stones of remembrance at the locations of warzones they survived. And it is not that the journey was not difficult to chaotic. It is not that death did not stain the ground with the blood of their loved ones. It is the fact that in spite of all the trials, there was a light at the end of the tunnel. There was a miracle in the midst of the madness. There was hope in the chaos.”

During the time of my PhD research, I had my best years. However, throughout my life, *“I have seen my share of dark places. I have felt trapped in discouragement, disappointment, decisions I regret. Trapped in what felt like an ocean of hopelessness. But when the waves had down calmed, and the quakes of life’s disaster stopped, I found myself underneath the rubble: still breathing. Somehow stronger, wiser and more refined.”* So this thesis is my stone of remembrance, of monuments and miracles I have seen, definitely not only during my PhD, but throughout my life. Because in the end, all things work together.

Parts of the text were adapted from *Lecrae ATWT: Chapter 4*, available on YouTube.

Lucas Amaral

Delft, 16/10/2018

Acknowledgements

First, and most important, I need to thank God. I believe He has made me capable to go through this PhD journey. Many times have I seen His care with me. Besides, I would also like to thank God for the wonderful people he has put around me during this journey.

There is a saying that states *“if you want to go fast, go alone, but if you want to go far, go together”*. I do not believe in it. Actually, I do not think it is possible to go anywhere at all if you are alone. Sometimes we may not realize, but we are surrounded by great, generous and kind people. And they make a difference in our day!

Therefore, I would like to thank each and everyone of you people that made such a difference in my journey: Big Adrián, Small Adrián, Andrei, Andy, Aubryn, Bernhard, Calvin, Chirag, Chunsen, Chelsea, Daniel, Derek, Dimitrios, Fabricio, Freek, Giacomo, Gillian, Hans, Huajie, Ilias, Ilhan, Irene, Jos, Julian, Konstantin, Lei, Liaojun, Marcello, Marcias, Maria, Maria Pia, Maro, Mayank, Michiel, Michiel, Morteza, Niels, Nikos, Otto, Pedro, Ping, Roger, Romina, Sofia, Sotiris, Tian, Vassilis, Vincent, Vincentius, Wandong, Zahid, and also all you new people that I do not know the names ☺. A special thanks to the “boobs office”. Nick, Leila, Eirini, Nicolas and Cornelis. Thank you so much for making my days so much fun!! You guys are special! I will never forget you! Walker, thank you for spending so much time hearing my love-life complaints and making me laugh even in the most difficult days! Genevieve, thank you for bearing my horrible jokes and still be my friend!

Thank you Rob Leonard, for helping me so many times with practical advices. In addition, I cannot forget the amazing team of technicians. They definitely made my work possible! Bart, Bob, Ed, Frans, Fred, Johan, Lijing, Marianne and Misja. Thank you! A special thanks to Gertjan, Cees and Berthil, who many times made an extra effort just to help me.

Thank you René Alderliesten, for supporting me all the time. I know how hard it can be to deal with me sometimes. Thank you for your patience and guidance. Thank you professor Rinze, for believing in my work and supporting me in every moment I needed.

Gemma: I will never be able to thank you for everything you did for me. You always wanted to make sure both my work and my personal life were in good shape! You are awesome.

During these 4 years, I have had people outside TU Delft also playing a very important role in my life. Henk Polinder and family, Niek Tramper, Gerrit, Carey Walters and everyone

from the International Christian Fellowship Delft. Henk, Kate and Laura Jansen: you have become my family in the Netherlands. I will never be able to thank you or pay you back for everything you have done for me. Bobby Jansen, Henk van Koppen, Bas and Deborah: thank you for your true friendship, for the beers, coffee and dinners we had, football matches we watched and played, and for being there for me. Viviam, Viviane, Rodolfo and Ana Clara, I am very glad I could share some moments during my PhD with you. Guilherme, Fernanda Machado, Fernanda Soares Leite and Renan: although you were across the ocean, you have made me happy and you have supported me.

I obviously cannot forget my family: Robinson, Elisa, Thais and Pedro. You have been my everything from day one. I could not have done it without you.

Last but not least important, I would like to thank everyone that somehow supported me with advices, prayers, conversations and messages. I cannot name you all here, but be sure: I am very thankful!

We do not go anywhere without good people next to us!

Lucas Amaral

Curriculum Vitae

The author was born in São Bernardo do Campo, Brazil, on the 22nd of May 1990. In 2008 he enrolled in the Science and Technology Bachelor programme at Universidade Federal do ABC – UFABC, Brazil. In 2011 the author graduated and received his bachelor of Science and Technology degree. After that, the author enrolled for the Aerospace Engineering programme at UFABC.

Due to the excellent academic performance, the author was invited to follow a Master's degree in Mechanical Engineering concurrently to his Aerospace Engineering degree. He obtained his title of Aerospace Engineer on September 2013 and, shortly after, received his title of Master of Science in Mechanical Engineering on February 2014.

From June 2013 to February 2014, the author worked as a Finite Element Engineer for Applus IDIADA in São Paulo, Brazil. During this period he worked as a contractor for General Electric – Oil & Gas, performing stress analyses of subsea structures.

In April 2014 the author started the PhD research project that resulted in this thesis. The author performed this research project at TU Delft, faculty of Aerospace Engineering, under supervision of Dr Ir R.C. Alderliesten as promotor and Prof Dr Ir R. Benedictus as co-promotor.

List of Publications

Journal Papers

Amaral L, Alderliesten RC, Benedictus R. *Towards a physics-based relationship for delamination growth under different loading modes*. Engineering Fracture Mechanics. 2018;195:222-41.

Amaral L, Alderliesten R, Benedictus R. *Understanding mixed-mode cyclic fatigue delamination growth in unidirectional composites: An experimental approach*. Engineering Fracture Mechanics. 2017;180:161-78.

Amaral L, Zarouchas D, Alderliesten R, Benedictus R. *Energy dissipation in mode II fatigue crack growth*. Engineering Fracture Mechanics. 2017;173:41-54.

Amaral L, Yao L, Alderliesten R, Benedictus R. *The relation between the strain energy release in fatigue and quasi-static crack growth*. Engineering Fracture Mechanics. 2015;145:86-97.

Conference Papers

Amaral L, Alderliesten RC, Benedictus R. *Towards the Fundamentals of Mode II Fatigue Delamination Growth*. 31st Technical Conference of the American Society for Composites. Williamsburg, Virginia, USA2016.

Amaral L, Yao L, Alderliesten RC, Benedictus R. *Energy based study on quasi-static delamination growth treated as a low cycle fatigue process*. In: Siljander A, editor. 34th Conference and 28th Symposium of the International Committee on Aeronautical Fatigue and Structural Integrity. Helsinki, Finland2015. p. 240 - 8.